Doctoral Dissertation

Mold-less microneedle fabrication for pre-loading drug

Harit Pitakjakpipop

Supervisor: Professor Kazuaki Matsumura

Graduate School of Advanced Science and Technology
Japan Advanced Institute of Science and Technology
Materials Science

March 2022

Referee-in-chief:

Professor Dr. Kazuaki Matsumura

Japan Advanced Institute of Science and Technology

Referees:

Professor Dr. Yuzuru Takamura

Japan Advanced Institute of Science and Technology

Professor Dr. Toshiaki Taniike

Japan Advanced Institute of Science and Technology

Associate Professor Dr. Eijiro Miyako

Japan Advanced Institute of Science and Technology

Associate Professor Pakorn Opaprakasit

Sirindhorn International Institute of Technology, Thammasat University

Abstract

The microneedle technology gets high attention in transdermal drug delivery systems (TDDS) research due to the limitations in the oral and parenteral drug delivery systems. Herein, the photolithography microneedle fabrication method, mold-less, has been employed to overcome the limitation of other fabrication methods. It takes less than 5 minutes for each fabrication process that includes adjusting the length and shape of microneedle by varying the time for UV irradiation and the pattern micro-windows on the photomask that is suitable to produce for industrial scale. Four-point star-shaped microneedles are fabricated via a photolithography process, and sulfobetaine (SPB) monomer is combined with dextran-glycidyl methacrylate/acrylic acid (Dex-GMA/AAc) to form the hydrogel network. The toxicity study shows that the Dex-GMA/AAc/SPB polymer can be considered as extremely biocompatible. The microneedle itself exhibits high drug loading capacity, high-efficiency drug release, and inhibits protein aggregation. The acrylated epoxidized soybean oil (AESO) sheet, microneedle substrate, shows a clear and flexible property and non-absorb drug during the drug loading process; when the microneedle patch is applied on the skin, it also curves along the surface that demonstrating its ability to be easy to apply to any body part. A pre-drug loading platform is designed for the advanced features of the microneedles that provide an effective option for administering therapeutic drugs.

The rhodamine B drug loading and releasing models show that the microneedle can load drug up to 8μg on one microneedle patch and release up to 80% of loading in 6h, with only 41 needles. The microneedle has the potential for chemical drug delivery due to its propensity for greater loading and releasing efficiency in microneedle applications. The Dextran-FITC diffusion represented that the molecular drug weight lower than 10 kDa can absorb/diffuse into the center of the microneedle. The Dextran-FITC showed a fast release and diffusion into the artificial skin in a short period.

Abstract

The protein delivery shows some limitation of protein loading and releasing at low pH, but at pH 7.4, protein releases show higher efficiency suitable for transdermal drug delivery, owing to the presence of pH 7.4 in the interstitial fluid. The Lactate dehydrogenase (LDH) enzyme activity study illustrates that the poly-SPB side chains in the Dex-GMA/SPB/AAc hydrogel inhibit protein aggregation while loading enzyme into the microneedle according to having a higher enzyme kinetic activity than Dex-GMA/AAc hydrogel that do not have the poly-SPB side chains even under external stress, releases the proteins in their native state (without activity loss). A ThT assay determining the fibril formation in human insulin indicates that the human insulin-loaded Dex-GMA/AAc and Dex-GMA/SPB/AAc effectively suppress the formation of fibrils in human insulin under the dry condition and high-temperature condition that presented only 25% and 20% aggregation, respectively. The combination of hydrogel microneedle and poly-SPB side chains has a potential for biopharmaceutical transdermal drug delivery, especially protein base drug that increases the efficiency bioavailability.

Keywords: microneedles, photolithography, transdermal drug delivery, zwitterionic polymers, protein aggregation

Contents

List of Figures

Chapter 1

General Introduction

1.1 Transdermal drug delivery

For thousands of years, people have applied materials on the skin for treatment that was the basic therapeutic knowledge for the modern era of transdermal delivery. Recently, transdermal delivery has become a priority option for oral delivery and hypodermic injection. Prausnitz et al. [1]categorized three generations of the transdermal delivery system from the first time introduced to the medical system. The first-generation transdermal delivery must have low molecular weight, lipophilic and low-dose drug. The second-generation transdermal delivery systems enhance the treatment by using different devices such as the iontophoresis machines and the non-cavitational ultrasound probes aim to control the rates of drug diffusion. The third-generation delivery systems overcome the drug passing of stratum corneum layer barrier problems that allow delivering macromolecules, including therapeutic proteins and vaccines. The devices such as microneedles, thermal ablation, microdermabrasion, electroporation and cavitational ultrasound have been developed in this field.[1] The microneedle platform represents an attractive alternative to other methods; it is easy to self-administer and shows a high administered drug that reaches the systemic circulation (bioavailability).[2]

1.1.1 Skin layer

The human skin is the largest organ in the human body which 2-3 mm thickness —the systemic circulation and outward flow of water, electrolytes and various substances. Human skin comprises two layers. An epithelium, called the epidermis, is the outermost layer, and the underneath layer, called the dermis, is connective tissue. The stratum corneum is located in the outermost layer of the epidermis and has about 10-30 μm. The stratum corneum behaves as the primary barrier between the body and the environment consists of about 20 layers of corneocytes. An extracellular matrix is located between the epidermis and dermis (Figure 1.1). The dermis thickness varies from 500–2000 μm depending on the part of the body that lies below the epidermis. It is composed of fibroblasts, elastic fibers and collagens, filled in a ground substance composed of gelatinous proteoglycans and glycoproteins[3]. Extracellular fluid (ECF) means all body fluid outside the cells. The main component of the ECF is the interstitial fluid (ISF). For this situation, the microneedle for drug delivery can dissolve or extract the drug by the interstitial fluid below the stratum corneum and diffuse into the blood body circulation.

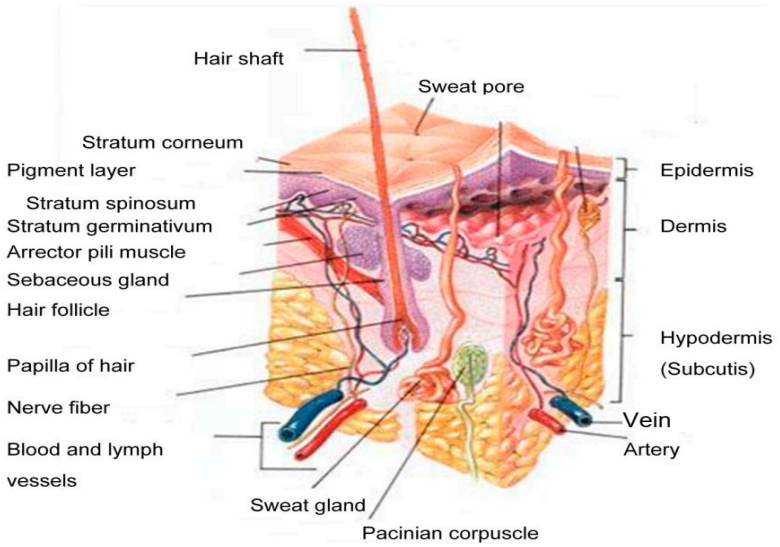

Figure 1.1 Schematic illustration of the human skin layer[4].

1.2 Microneedle

1.2.1 Microneedle technology

Microneedles (MNs) technology has been improving the efficiency of transdermal drug delivery. MNs can penetrate the stratum corneum layer but do not reach the nerve system[5][6] and creates microchannels; hence the drug is administered directly into the epidermis or dermis layer, which enhances skin permeability, allowing the macromolecular drugs to enter into the systemic blood circulation.[7][8][9] In biomedical research, various materials are used to prepare MNs, including metals, silicon, and polymers, with the height of the needle ranging between 300-1,500 μm, and the base width between 100-500 μm[10][11] intended to delivery drug or diagnose. MNs have received widespread attention owing to their properties, such as painlessness, short time of skin trauma, possible self-administration, lack of bleeding, and high bioavailability.[12] In contrast, the other delivery methods have the risk of potential degradation associated with the gastrointestinal tract or first-pass liver effects.[13][14]

Recently, the properties and functions of microneedles have been receiving great attention from researchers worldwide, as seen by the increasing number of research articles in the field. Figure. 2a illustrates the increasing number of publications for overall microneedle research. In comparison, Figure 2b is emphasizing on the high output research on microneedle drug delivery only. The microneedle research areas include; sensors, medical devices, tissue adhesion[15], and diagnostic[16][17].

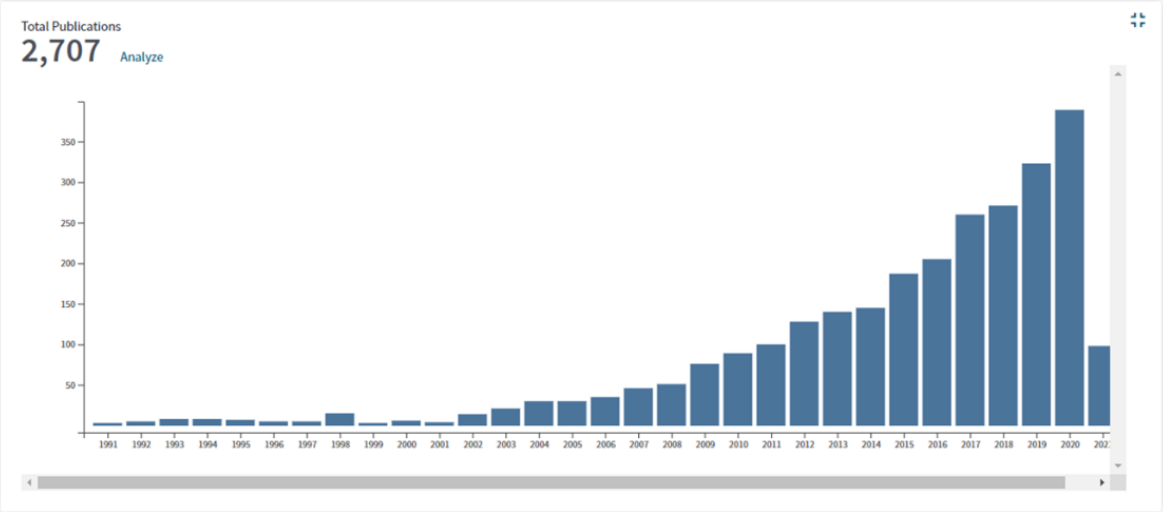

Figure 1.2 Comparison of the number of publications related to research (Data collected from title search in Web of Science, Thomson Reuters on April 2021).

1.2.2 Microneedle materials

1.2.2.1 Metal microneedle

The metal microneedles were fabricated by laser cutting process on the thin stainless steel sheets[18][19] and sterilized in a steam autoclave before use. The advantage of the metal microneedle is that its mechanical property is the strongest among all microneedle materials. The metal microneedle patch (Figure 1.3) was inserted, with drug-coating, into the skin to create the microchannels to increase the skin permeability. In this case, the drug should rapidly dissolve from the needle because the metal microneedle should be removed as soon as possible to prevent the toxicity of the metal.

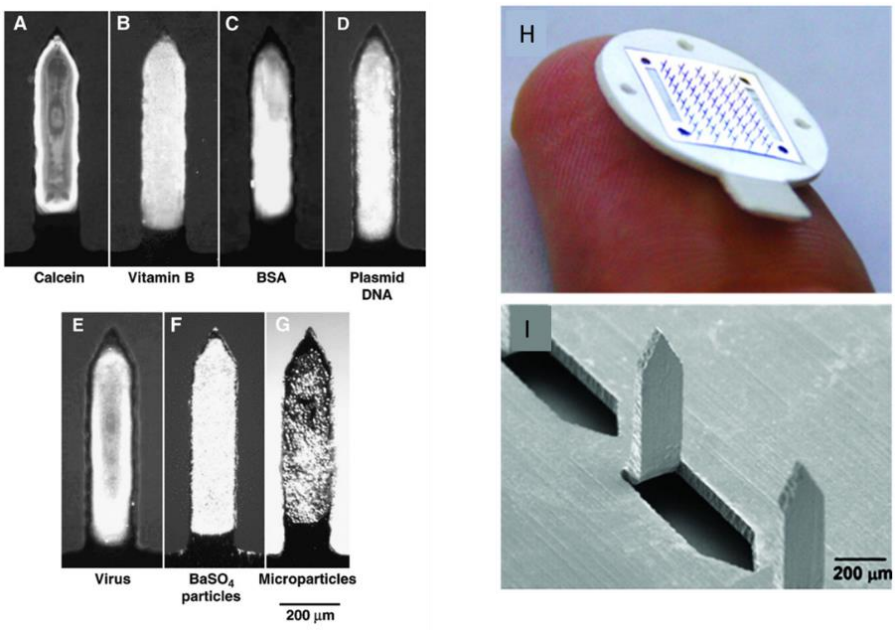

Figure 1.3 Single microneedles coated with different (A-G) types of drugs, (H-I) illustrate the microneedle patch and close up picture top view[18][19]

1.2.2.2 Silicon microneedle

The silicon microneedle has a similar function as the metal microneedle, but the silicon microneedle process requires a cleanroom for fabrication. The silicon wafer was modified by a deep reactive ion etching process, consisting of anisotropic and anisotropic dry etching or dry etching, which depends on the design. Figure 1.4a illustrates that this fabrication technique creates the small-size cylinder shape microneedle array, and figure 1.4b shows the microfluid microneedle (hollow) device that can bypass the drug epidermis layer. However, silicon or ceramic microneedle has lower toxicity than metal microneedle, but it requires a clean room, an expensive, time-consuming process.

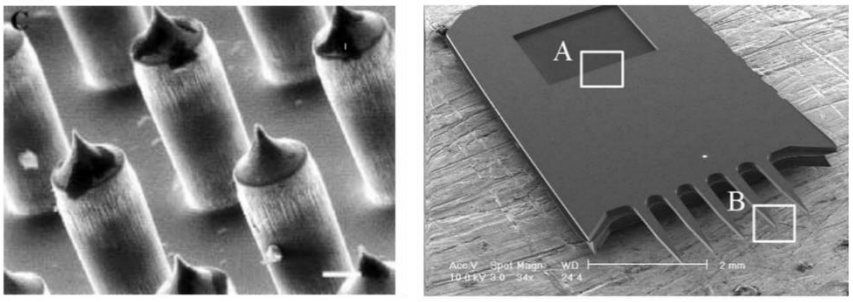

(a) (b)

Figure 1.4 (a) cylinder silicon microneedles (bar=20 μm) [20], (b) a microfluid microneedle[21]

1.2.2.3 Polymeric microneedle

The polymeric microneedle has gained more attention than other materials mentioned above due to its characteristics; (1) biocompatible, devoid of the immune response, (2) strong enough to penetrate stratum corneum layer, (3) controllable drug release, and (4) protecting drug damage or denature during the fabrication process (5) easy to fabricate. A wide range of polymer performance has been used for the structure of microneedle or drug cargo. The function of polymeric microneedle delivery can be categorized into three groups; dissolvable, bio-degradable, and swellable. For drug delivery, dissolvable and degradable have been more often developed because the interstitial fluid will dissolve and extract to the blood circulation. In comparison, the swelling microneedle has developed to extract the interstitial fluid for diagnostic and delivery in the same microneedle.

1.3 Fabrication methods

There are two main strategies of MNs fabrication: mold-based fabrication and mold-less fabrication. The mold-based fabrication gives the exact shape of microneedle and shielding drug cargos. Some limitations of this technique are time-consuming, inflexible to change the MNs structure, need for extra pieces of equipment, and unsuitable for mass production. The most common mold-based process that has been used involves polydimethylsiloxane (PDMS) casting for micro-molding[22][23][24][25]. Briefly, starting with fabricating a female mold from the master template by pouring PDMS to the master microneedle, the PDMS female mold was peeled carefully once after PDMS solidifies. Micro-molds are filled with polymer (ingredient) solutions using vacuum and centrifugal force to allow all cavities to fill with the solution. The polymer solution is solidified by air drying or UV irradiation, followed by removing the microneedle array from the mold (Figure 1.5). This method has only academic significance as it can be applied in only small-scale preparation [23][26], because it is time-consuming and requires a sterilization room to process.

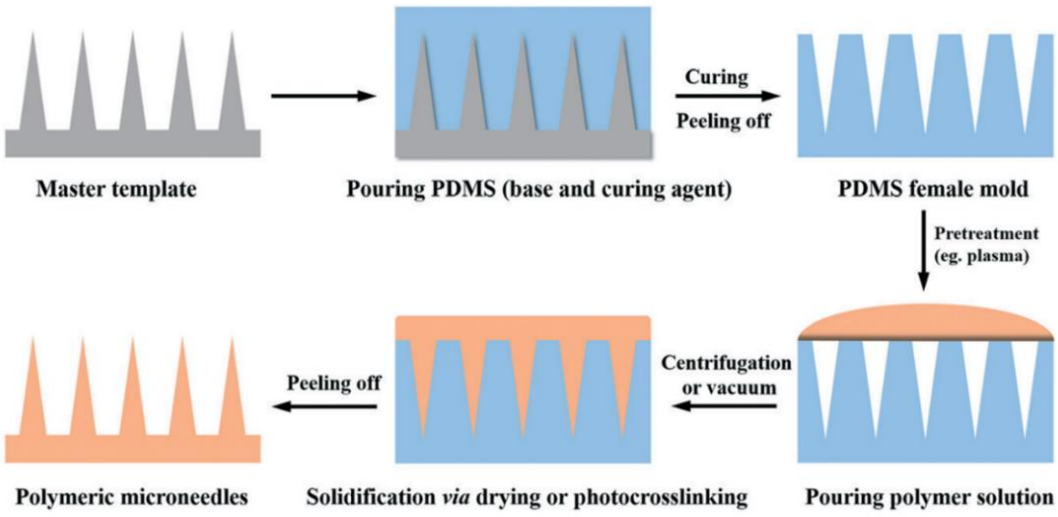

Figure 1.5 Schematic illustration of polymeric microneedle fabrication via PDMS micro-molding[25]

On the other hand, mold-less fabrication such as drawing lithography, photolithography, and droplet-borne air blowing are suitable for the various structure of microneedle and allows tenability of height, base-width, and shape[17][27]. The 3D printing microneedle [28] allows the fabrication of complicated structures but is unsuitable for large-scale production due to the expensive materials required, time-consuming, and the requirement of a high-resolution 3D printer.[15][29]

Drawing lithography

The drawing lithography method is suitable for polymers which have high viscosity. The process is performed in the range of melting temperature (T_m) to the glass transition temperature (T_g), such that during cooling down T_g the amorphous portion of polymer slowly change from the glassy liquid into the solid-state since the rearrangement occurs. In the fabrication process, the 2 identical circular plates are placed on the glassy liquid polymer (Figure 6). The polymer then adheres to the surface of circular plates; the glassy liquid gets elongated while moving apart of circular plates on decreasing temperature. The microneedle becomes narrow and solidifies around $_g$ before isolating between the upper and the lower plate. Although this method can create an ultrahigh-aspect ratio microneedle, however, it does not provide microneedles with accurate size, requires a stable condition to fabricate, and only cone-shape microneedle fabrication is possible.

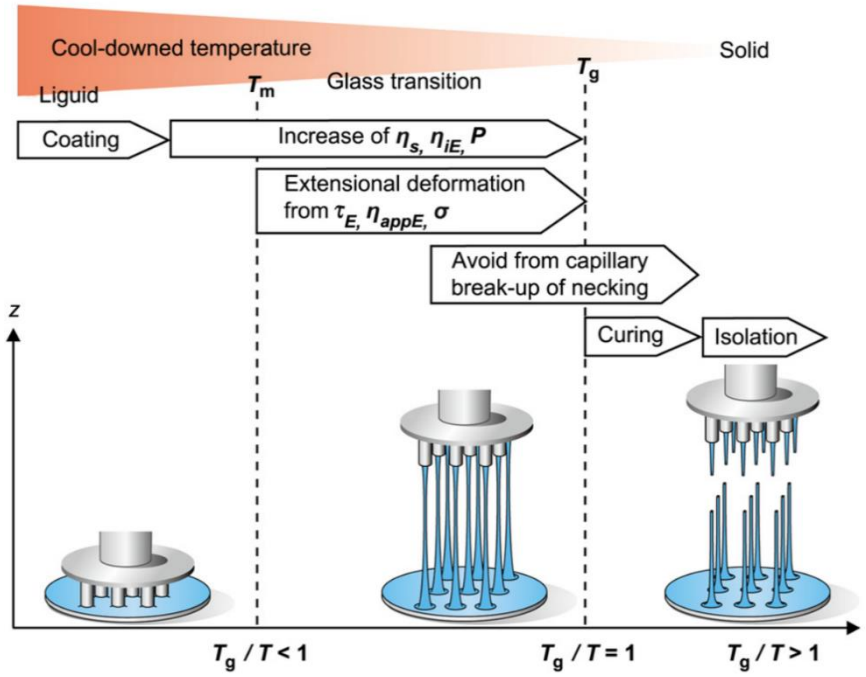

Figure 1.6 Drawing lithography fabrication process[30]

Droplet-borne air blowing

The droplet-borne air blowing process also uses two plates positioned face-to-face and then moving apart like the downing lithography, but it is applied air blowing to polymer droplets for solidification without heat or UV irradiation. In Figure 1.7, the polymer solution was dispensed, dropping for the base structure and following the drug-loaded polymer on the top. The top plate, which has the same dispensing drops were moved to contact the lower plate. The plates were pulled apart gradually while the air was blowing. The liquid polymer became solid in a couple of mins, and the microneedle array was separated. The droplet-borne air blowing was commonly applied for the dissolvable microneedle compatible with chemical drugs and proteins, but it requires a specific machine for dropping polymer and sterilization room to process.

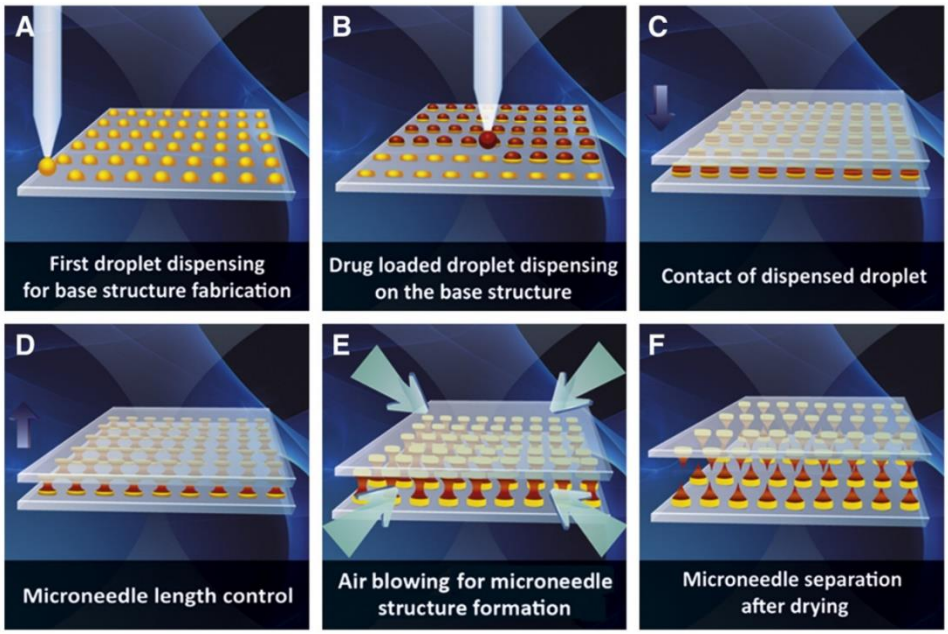

Figure 1.7 Schematic illustration of dissolving microneedle fabrication via droplet-born air blowing method [31]

The 3D printing microneedle

Recently, 3D printers have provided a high resolution and have been developed for different purposes. It has been widely used for functional materials and microstructure fabrication. The researchers have designed different patterns and methods to fabricate microneedles to meet the specific functions. The 3D resin printers have been synthesized for many purposes, and many of them have been approved by the Food and Drug Administration, USA (FDA). Figure 1.8 illustrates the process of microneedle fabrication for the basic design [29]. The UV projector has generated the image projected to the mirror and reflected the resin bath to solidify microneedle layer to layer by photopolymerization. Figure 1.9 (A-F) shows the basic cone-shaped microneedle in different aspect ratios fabricated for the low-cost printer [29]. In contrast, figure (H-I) illustrates sophisticated microneedles printed for a high-resolution 3D printer for enhanced tissue Adhesion[15].

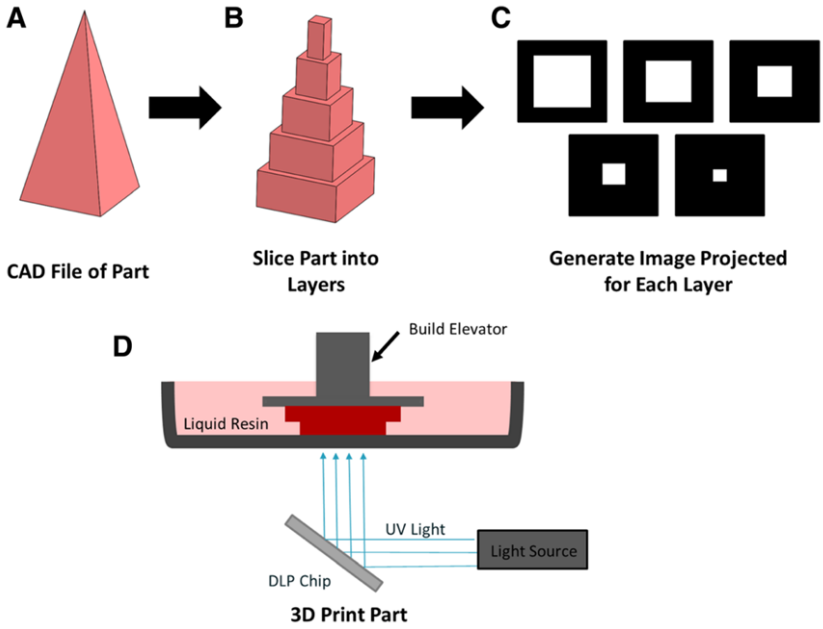

Figure 1.8 A stereolithographic 3D printer produces parts one layer at a time by photopolymerization[29]

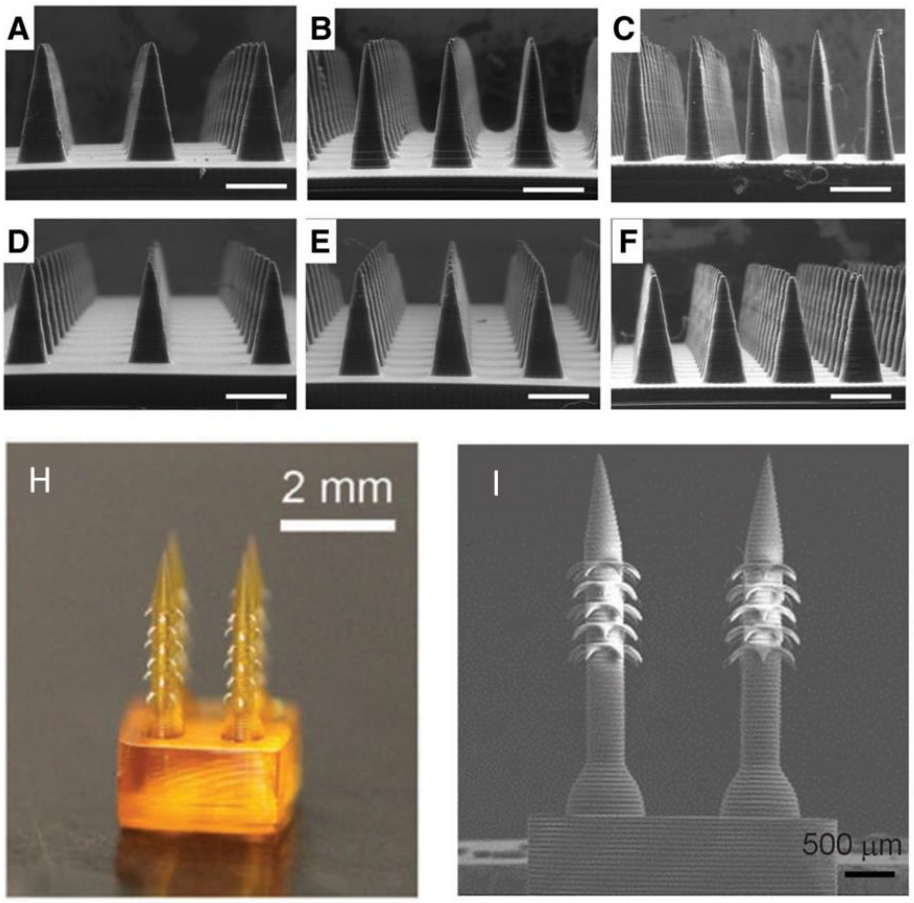

Figure 1.9 The 3D imprinted microneedle (A-F) The SEM images of the cone-shape microneedle, H) digital camera, and I) SEM images[15]

Photolithography

The photolithography microneedle fabrication overcomes the limitations of 3D printing; this method reduces the time consumed and the need for expensive instruments. Photolithography using photomasks was used to fabricate polymeric microneedles in a single step[32]. The ultraviolet (UV) light dose was developed to batch presented a photoinitiator to form crosslinked polymeric 3D hydrogel microneedle structures (figure 1.10). During UV irradiation, the photoinitiator generates the free radicals that propagate the rapid polymerization reaction UV, and the light refracts at the noncured and photocured hydrogel (figure 10). Therefore, the 3D microneedle shapes will depend on high-intensity light propagation. Therefore, a short fabrication offers greater suitability of scaling up commercially for industrial purposes[33]. Some research using inclined/rotated UV lithography[33] or micro lensed UV lithography[34] was also applied to this method to enhance the UV light beam and intensity. The inclined/rotated and micro-lensed methods were created and only a circular cone, whereas the multi-blade photomasks patterns can fabricate microneedle with the wings shape.

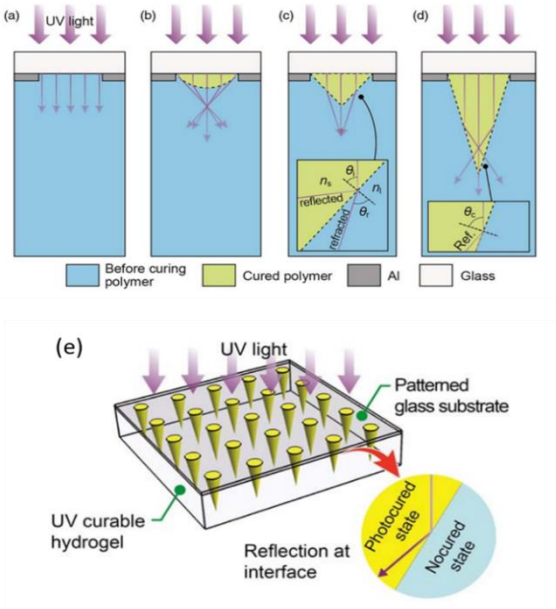

Figure 1.10 Schematic illustration (a-e) of the mechanism photopolymerization of self-focusing 3D lithography in PEGDA resin bath[32]

Most research used a polyethylene glycol diacrylate (PEGDA) [33] [32] [35] as a polymer resin that can produce the solid microneedles with a simple cone-shape or complicated 3D snake teeth (snake fang) [35] features without inclined/rotated and micro-lensed UV exposure, which the mechanical properties of the microneedles were depended on polymer-based resin.

The snake fang microneedle (Figure 1.11) is the most complicated microneedle shape classified as the solid microneedle. The 3D structure microneedle design depends on multi-blade patterns (Figure 1.11C). The increasing number of blade patterns will increase the number of microchannels on the side of the microneedle slope. Figure 1.12 shows the simulation of hydrodynamics of liquid drug delivery that the drug solution will supply from the PDMS drug reservoir.

However, this device shows several advances in the fabrication process and delivery system, but this fabrication process is time-consuming and many steps fabrication; therefore, it is not suitable for scaling up commercially for industrial applications.

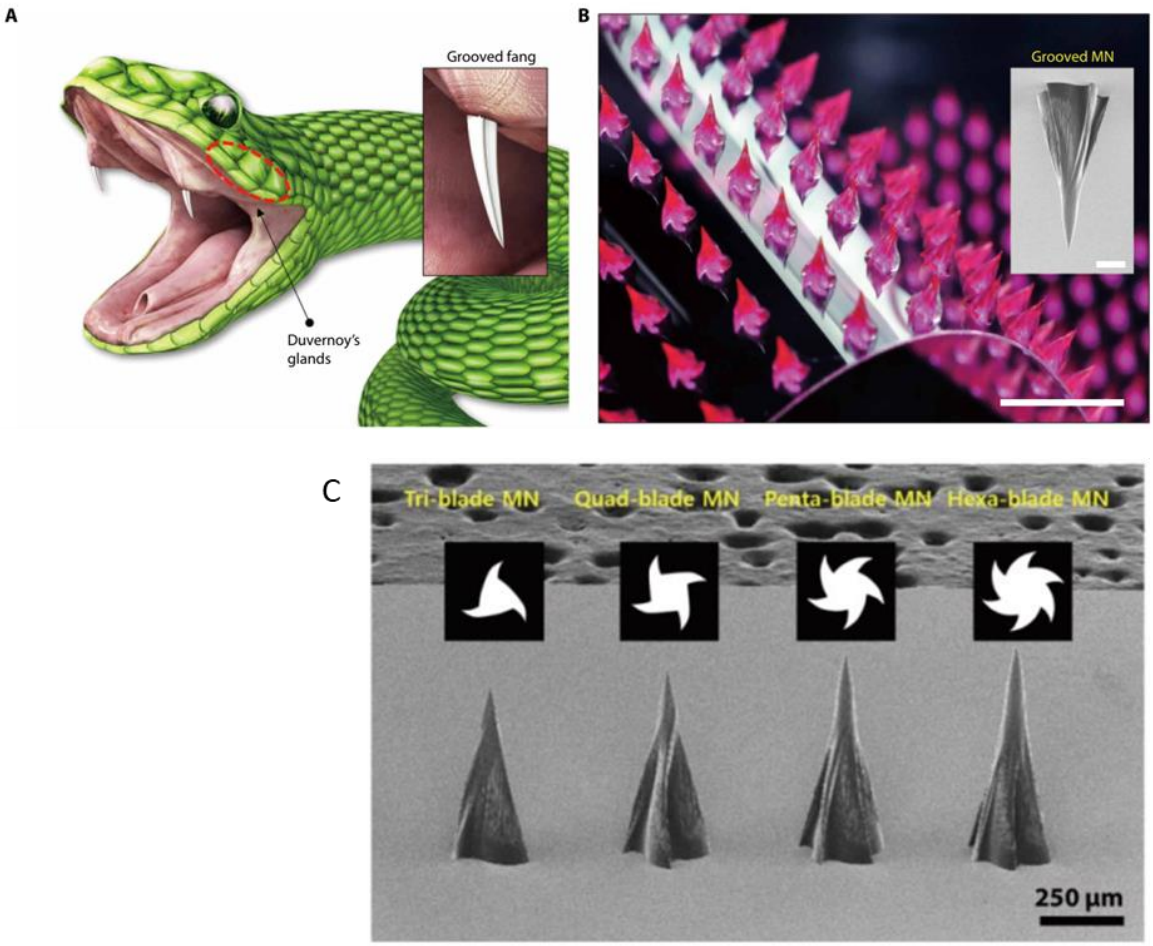

Figure 1.11 Design of the snake fang–inspired stamping patch. A) the venom delivery system of the rear-fanged snake B) Photograph of the snake fang–inspired MN array, C) photomasks with multi-blade patterns under the optimized UV exposure condition [35]

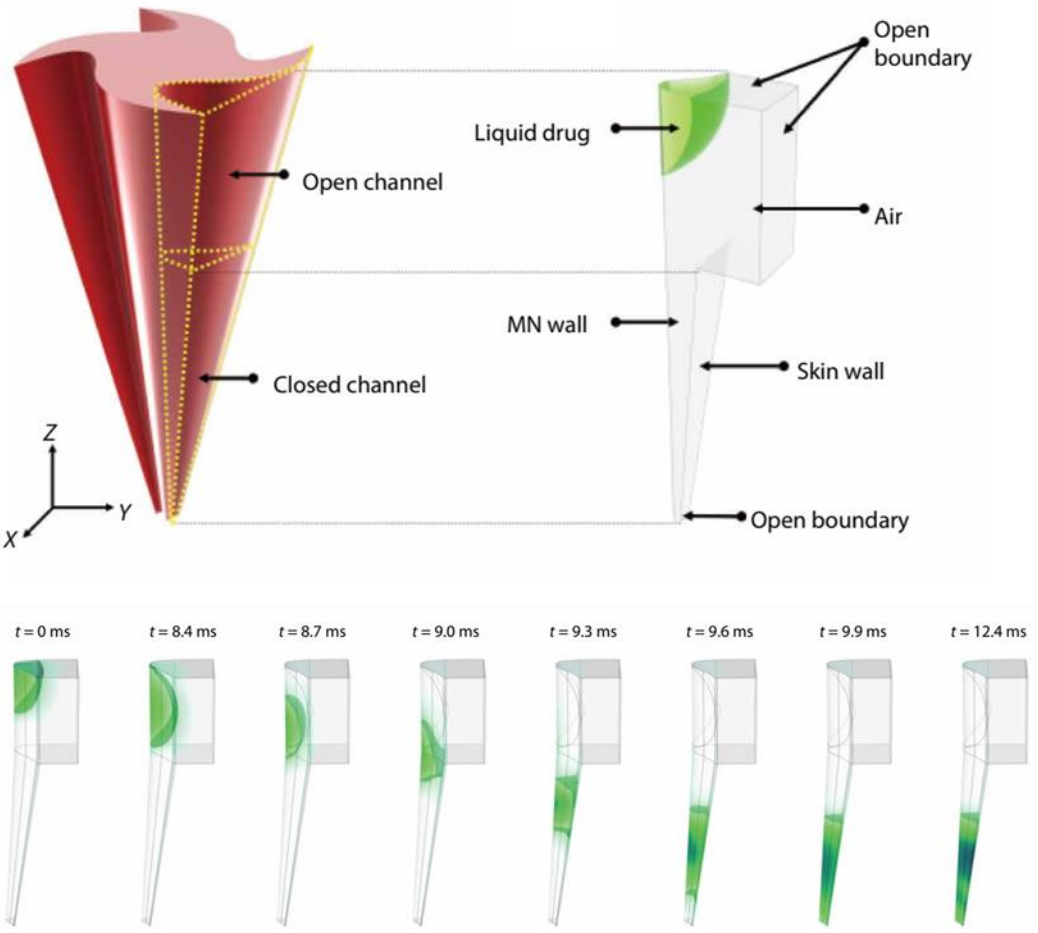

Figure 1.12 Simulation of the hydrodynamics of liquid drug delivery [35]

Herein, we developed the photolithography (mold-less) technique; a micro-windows mask was prepared from a thin aluminum film on a glass slide and create the pattern by evaporating the aluminum layer with a high-resolution low-energy laser. UV irradiates to the micro-photomask perpendicularly to the polymer resin in the bath container, creates the conical path, and develops the 3D microneedle structure. In this study, we also developed the biocompatible photo-crosslinkable polymer from the dextran base polymer.

Our study developed the low-cost microneedle set up using only one UV LED (380-400) nm as a light source and projected UV light upward that different from other research (Figure 1.13).

In addition, we synthesized the Dex-GMA/SPB/AAc, biocompatible polymer resin, that be able to cure by UV 380-400 nm. The cured polymer (dry) can swell water or biological liquid into the microneedle and become a hydrogel. This microneedle has many outstanding properties that overcome other methods and materials; 1) we can choose any drug for loading into the microneedle before using a cancer drug, insulin, antibody, antigen vaccine. 2) we can vary the dosage by adjusting the concentration of the original drug while loading; thus, we can minimize the drug usage and drug denaturation. 3) It is possible to process mass-scale production due to the short time fabrication; in this study, the fabrication and washing process is less than 5 min for a single microneedle patch and the low price of fabrication set up.

Figure 1.14 illustrates a concept of the novel microneedle for drug delivery. Figure 1.14a shows the drug is tapped in the polymer network of the dry microneedle. The drying state microneedle is strong enough to penetrate the stratum corneum skin layer and absorb the liquid from the epidermis layer. The swollen microneedle (Figure 1.14b) balances the drug concentration in hydrogel and out by releasing the drug to the reservoir. After completing delivery, the microneedle patch will be removed move out of the skin.

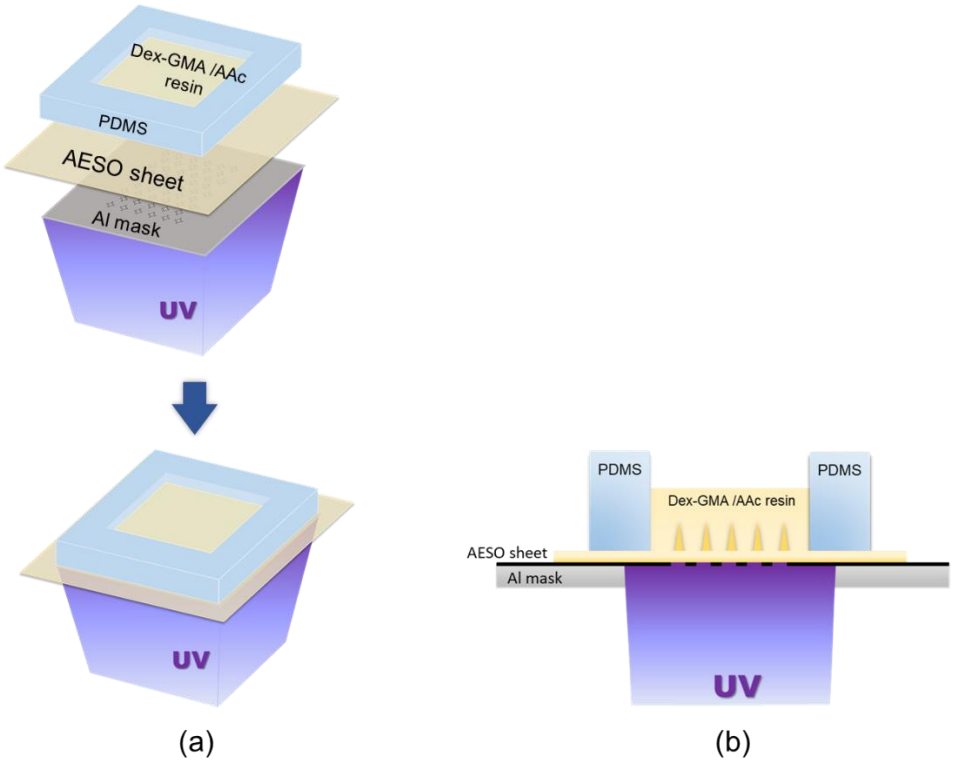

Figure 1.13 (a) Schematic illustration of mold-free fabrication set installation, (b) side view cross-section set up.

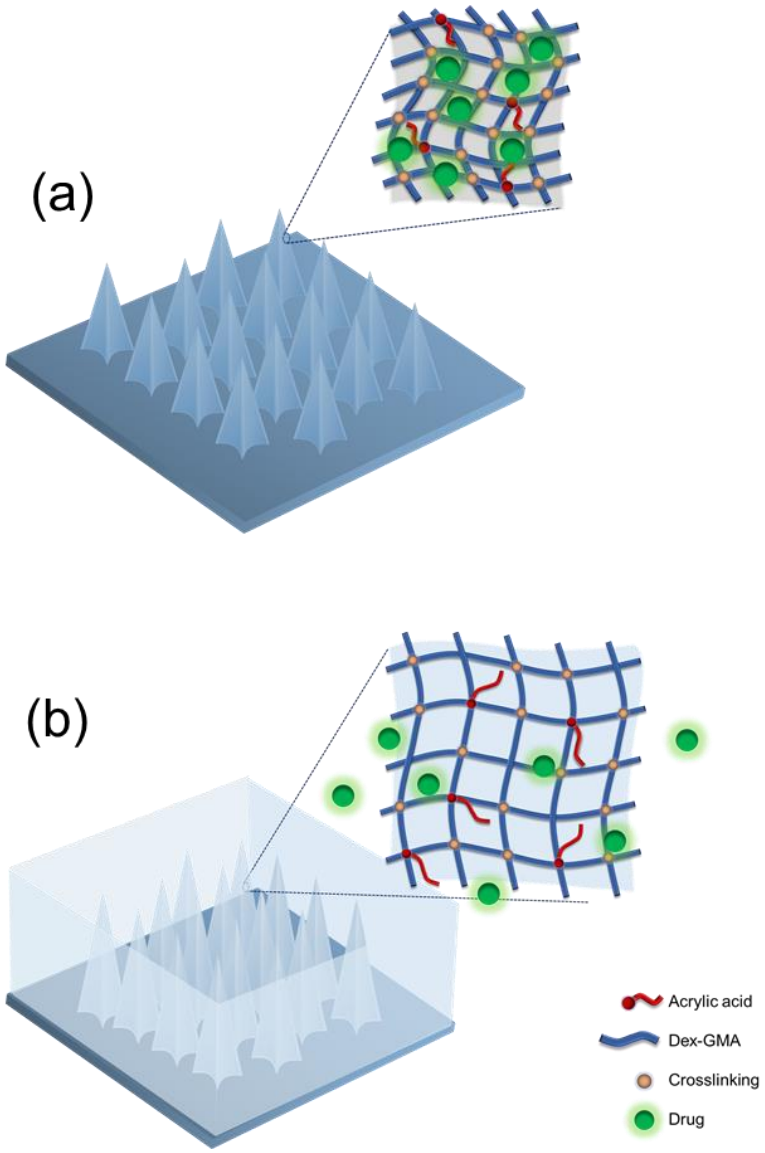

Figure 1.14 The schematic illustration of the concept of hydrogel drug delivery

1.4 Drug delivery

Diabetes

The number of diabetes patients has increased from 108 million in 1980 to about 400 million in 2014[36]. Diabetes prevalence has been rising more rapidly in middle and low-income countries. The disease is a major cause of kidney failure, heart attacks, stroke blindness, and lower limb amputation. World Health Organization (WHO) reported that in 2016, 3.7 million deaths due to diabetes and high blood glucose and 1.5 million deaths were caused by diabetes. People with diabetes must inexhaustibly monitor their blood glucose levels every day and take the correct dose of the hormone insulin to maintain the normal blood glucose level.

The controllable insulin delivery using microneedle pad has introduced a new way of diabetes treatment to overcome painfulness and an imprecise insulin dosage injection. Comparing to oral and nasal drug delivery, the drug delivery across the skin also avoided the hepatic first-pass extraction and delivered to the blood circulation at a pharmacologically relevant rate.

1.5 Hydrogel

1.5.1 Hydrogel in drug delivery

Hydrogel is a three-dimensional polymer network that occurs by the crosslinking of polymer chains via physical interaction, primary covalent crosslinks, hydrogen bonding, polymer crystallites, and Van der Waals interaction. The high-water content of hydrogels has received significant attention because of their related potential in t pharmaceutical industries. The hydrogel has a high (70-99%) absorption of water and biological fluid due to its functional group such as -OH, $CONH_2$, -SO_3H, -CONH, and -COOR. The swollen microneedles are soft and rubbery surface structures and physicochemical properties similar to human tissue, so it will feel pain during inserting into the skin while drug release. The hydrogel microneedle has excellent biocompatibility and the capability to load drug and release into the skin. These characteristic features make hydrogels a potential candidate for microneedle drug delivery.

Hydrogel applications for controlled drug delivery systems (DDS) have become very popular in recent years. In this study, the potentiality of hydrogel for microneedle drug delivery has been explored to reduce drug release rate compared with dissolving microneedle. In previous research, our hydrogel: Dex-GMA/AAc base hydrogel performed the charge interaction with positive charge drug and proteins; consequently, the drug can be entrapped in this microneedle hydrogel.

1.5.2 Dextran

Dextran is a polysaccharide synthesized by fermentation of *Leuconostoc mesenteroids* bacteria when grown on sucrose-containing media, consisting of α-1,6 linked glucopyranoside a small percentage of α-1,3 linked residues (Figure 1.15). Dextran fractions can vary from 1kDa to 2,000kDa molecular weight that contains a large amount of hydroxyl group leading to high hydrophilic properties and capability for chemical modifying. Dextran has been selected for biomedical applications because of its low toxicity[37] and biocompatibility[12][20]. Dextran can degrade and is removed from the human body by various parts such as the colon, spleen, and liver.

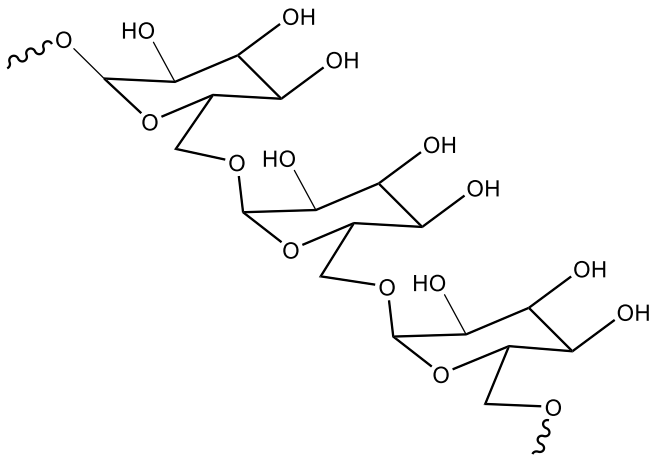

Figure 1.15 Dextran structure

Zwitterionic polymers

The Zwitterionic polymer is a sub-category of a polyampholytes group with unique characteristics[31] consisting of the anionic and cationic groups, commonly on the same repeating unit. The ionic groups are functional over a large pH window. Therefore, the total charge of the zwitterionic polymer in the normal state is equal to zero; polyzwitterions overall charge neutrality exhibit a different, hybrid-like property profile. Furthermore, the zwitterionic polymer reveals a high hydrophilic property [38]. The zwitterionic polymer has similar properties to proteins[39]. The polysulfobetaines (poly-SPB) show the biocompatible properties that resemble phospholipids in recent research[40][41][42]. Sulfobetaine polymers show antifouling properties[43], suppress the nonspecific binding of proteins and do not modify the structure of the hydrogen-bonded network of water molecules at the interface of the polymer and material[41]. In the drug delivery system research, sulfobetaine polymers have been developed due to the polymer exhibited high efficiency inhibits protein aggregation[44][45][46].

In this study, SPB (Figure 1.16) was combined with the Dex-GMA/AAc hydrogel network to prevent protein aggregation during loading proteins into the microneedle patch. The proteins are attached to the SPB side chains in the polymer structure to inhibit protein aggregation or prevent protein denature.

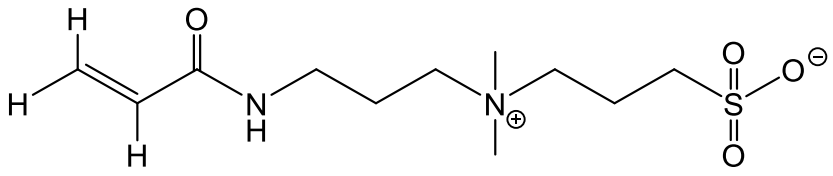

Figure 1.16 Sulfobetaine monomer

1.6 Smart microneedle

This study combined the zwitterionic polymers (SPB) to the main polymer structure (Dex-GMA) to suppress protein aggregation and protein denaturation. In the field of biopharmaceutics, protein instability[25][26][27] is an ongoing challenge for transdermal drug delivery, especially microneedle technology. Protein denaturation and aggregation are some of the primary causes of protein instability[27]. The uniqueness of zwitterion polymers is fascinating in this regard. In our previous report, zwitterionic polymer systems showed significant efficiency against the thermal aggregation of lysozymes and insulin at very low polymer concentration and over 24h incubation periods[27][28][29][30].

In this study, we prepared a photo-crosslinkable hydrogel by introducing glycidyl methacrylate (GMA) through dextran chains to create the double bond modified dextran (Dex-GMA)[21][22][47]. To create a smart microneedle platform, especially for protein drug delivery. Then the Dex-GMA was copolymerized with Sulfobetaine (SPB) and acrylic acid (AAc) to give the Dex-GMA/SPB/AAc hydrogel. PAA has high water uptake capability (super absorbent) due to the very high swelling ratio[48]. PAA hydrogels have been widely used in drug delivery patches by their bioadhesive property due to the hydrogen bonding and covalent bonding ability of such materials. In a recent study, Dex-GMA/PAA microgel particles were applied for a wound dressing as a hemostatic agent[49]. PAA also has anionic properties due to the carboxyl group releasing the drugs by electrode pad.

Herein, we report a novel microneedle fabrication method from biocompatible materials and increased drug delivery performance by combining it with protein inhibition polymer. This mold-free fabrication technique is suitable for the mass production of swelling microneedle at a low price. We developed Dex-GMA/SPB/AAc for the first time for photolithography microneedle fabrication which took less than 1 min for photopolymerization for one microneedle patch. The microneedle substrate is made from acrylated epoxidized

soybean oil (AESO) that does not absorb water while loading the drug, and all mixed solutions will swell into the hydrogel MNs only. Furthermore, the hydrogel microneedle patch was loaded with protein drug and the modified zwitterion polymer side chain for protein pharmaceutical aggregation inhibition. In this report, the fabrication process, morphology, rhodamine B diffusion, and drug release performance are investigated.

1.7 Objective of study

Microneedle technology has attracted increasing interest in medical research. However, the recent microneedle fabrication has some drawbacks; for example, almost all the microneedle is fabricated by mold required the vacuum and centrifugal system, time-consuming, and unsuitable for massive production. The mold-less fabrication techniques require expensive equipment and a special room for fabrication. Even though 3D printing gives the precision microneedle, it has a limitation of material of resin, time-consuming, and the high cost of the printer so, it is not suitable on an industrial scale.

This study aims to develop the microneedle fabrication technique that can produce on a mass scale using the polymeric materials that our group has been developed [50] [44][46]. In this study, the Dex-GMA [50] and inhibitor polymer for protein aggregation[44][46] have been synthesized for photolithography microneedle fabrication. The unique properties of novel microneedles create tremendous opportunities for various potential drug loading and release; the microneedle patch may serve as minimal transdermal drug delivery such as Alzheimer's disease, cancer treatment, diabetes, and cell therapy.

The research objectives proposal are

1. To synthesize the curable biocompatible polymer resin that inhibits protein aggregation and has swelling and releasing properties.

2. To develop the photolithography (mold-less) fabrication technique by using the curable biocompatible polymer resin.

3. To study the capacities of chemical and protein loading and drug loading to microneedle patches.

4. To study drug diffusion properties of microneedle on the artificial skin.

5. To study the protein function after releasing from microneedle patch.

1.8 References

[1] M.R. Prausnitz, R. Langer, Transdermal drug delivery, Nat. Biotechnol. 26 (2008) 1261–1268. https://doi.org/10.1038/nbt.1504.

[2] M.R. Prausnitz, Engineering Microneedle Patches for Vaccination and Drug Delivery to Skin, Annu. Rev. Chem. Biomol. Eng. 8 (2017) 177–200. https://doi.org/10.1146/annurev-chembioeng-060816-101514.

[3] L. Ventrelli, L. Marsilio Strambini, G. Barillaro, Microneedles for Transdermal Biosensing: Current Picture and Future Direction, Adv. Healthc. Mater. 4 (2015) 2606–2640. https://doi.org/10.1002/adhm.201500450.

[4] D.D. N'Da, Prodrug strategies for enhancing the percutaneous absorption of drugs, Molecules. 19 (2014) 20780–20807. https://doi.org/10.3390/molecules191220780.

[5] S. Henry, D. V McAllister, M.G. Allen, M.R. Prausnitz, Microfabricated Microneedles: A Novel Approach to Transdermal Drug Delivery, J. Pharm. Sci. 87 (1998) 922–925. https://doi.org/https://doi.org/10.1021/js980042+.

[6] S.H. Bariya, M.C. Gohel, T.A. Mehta, O.P. Sharma, Microneedles: An emerging transdermal drug delivery system, J. Pharm. Pharmacol. 64 (2012) 11–29. https://doi.org/10.1111/j.2042-7158.2011.01369.x.

[7] L.K. Vora, A.J. Courtenay, I.A. Tekko, E. Larrañeta, R.F. Donnelly, Pullulan-based dissolving microneedle arrays for enhanced transdermal delivery of small and large biomolecules, Int. J. Biol. Macromol. 146 (2020) 290–298. https://doi.org/10.1016/j.ijbiomac.2019.12.184.

[8] J. Kennedy, E. Larrañeta, M.T.C. McCrudden, C.M. McCrudden, A.J. Brady, S.J. Fallows, H.O. McCarthy, A. Kissenpfennig, R.F. Donnelly, In vivo studies investigating biodistribution of nanoparticle-encapsulated rhodamine B delivered via dissolving microneedles, J. Control. Release. 265 (2017) 57–65.

https://doi.org/10.1016/j.jconrel.2017.04.022.

[9] T. Liu, M. Chen, J. Fu, Y. Sun, C. Lu, G. Quan, X. Pan, C. Wu, Recent advances in microneedles-mediated transdermal delivery of protein and peptide drugs, Acta Pharm. Sin. B. (2021). https://doi.org/https://doi.org/10.1016/j.apsb.2021.03.003.

[10] M.T.C. Mccrudden, E. Mcalister, A.J. Courtenay, P. González-Vázquez, T.R. Raj Singh, R.F. Donnelly, Microneedle applications in improving skin appearance, Exp. Dermatol. 24 (2015) 561–566. https://doi.org/10.1111/exd.12723.

[11] J.H. Jung, S.G. Jin, Microneedle for transdermal drug delivery: current trends and fabrication, J. Pharm. Investig. (2021). https://doi.org/10.1007/s40005-021-00512-4.

[12] N. Dabholkar, S. Gorantla, T. Waghule, V.K. Rapalli, A. Kothuru, S. Goel, G. Singhvi, Biodegradable microneedles fabricated with carbohydrates and proteins: Revolutionary approach for transdermal drug delivery, Int. J. Biol. Macromol. 170 (2021) 602–621. https://doi.org/10.1016/j.ijbiomac.2020.12.177.

[13] S. Zhang, P. Xin, Q. Ou, G. Hollett, Z. Gu, J. Wu, Poly(ester amide)-based hybrid hydrogels for efficient transdermal insulin delivery, J. Mater. Chem. B. 6 (2018) 6723–6730. https://doi.org/10.1039/C8TB01466C.

[14] R. Ye, J. Yang, Y. Li, Y. Zheng, J. Yang, Y. Li, B. Liu, L. Jiang, Fabrication of Tip-Hollow and Tip-Dissolvable Microneedle Arrays for Transdermal Drug Delivery, (2020). https://doi.org/10.1021/acsbiomaterials.0c00120.

[15] D. Han, R.S. Morde, S. Mariani, A.A. La Mattina, E. Vignali, C. Yang, G. Barillaro, H. Lee, 4D Printing of a Bioinspired Microneedle Array with Backward-Facing Barbs for Enhanced Tissue Adhesion, Adv. Funct. Mater. 30 (2020). https://doi.org/10.1002/adfm.201909197.

[16] P.P. Samant, M.R. Prausnitz, Mechanisms of sampling interstitial fluid from skin using a microneedle patch, Proc. Natl. Acad. Sci. U. S. A. 115 (2018) 4583–4588.

https://doi.org/10.1073/pnas.1716772115.

[17] X. Zhang, Y. Wang, J. Chi, Y. Zhao, Smart Microneedles for Therapy and Diagnosis, Research. 2020 (2020) 1–26. https://doi.org/10.34133/2020/7462915.

[18] H.S. Gill, M.R. Prausnitz, Coated microneedles for transdermal delivery, J. Control. Release. 117 (2007) 227–237. https://doi.org/10.1016/j.jconrel.2006.10.017.

[19] J. Gupta, H.S. Gill, S.N. Andrews, M.R. Prausnitz, Kinetics of skin resealing after insertion of microneedles in human subjects, J. Control. Release. 154 (2011) 148–155. https://doi.org/10.1016/j.jconrel.2011.05.021.

[20] F. Chabri, K. Bouris, T. Jones, D. Barrow, A. Hann, C. Allender, K. Brain, J. Birchall, Microfabricated silicon microneedles for nonviral cutaneous gene delivery, Br. J. Dermatol. 150 (2004) 869–877. https://doi.org/10.1111/j.1365-2133.2004.05921.x.

[21] S. Paik, S. Byun, J. Lim, Y. Park, A. Lee, S. Chung, J. Chang, K. Chun, D. Dan, In-plane single-crystal-silicon microneedles for minimally invasive microfluid systems, 114 (2004) 276–284. https://doi.org/10.1016/j.sna.2003.12.029.

[22] S. Bhatnagar, N.G. Bankar, M.V. Kulkarni, V.V.K. Venuganti, Dissolvable microneedle patch containing doxorubicin and docetaxel is effective in 4T1 xenografted breast cancer mouse model, Int. J. Pharm. 556 (2019) 263–275. https://doi.org/10.1016/j.ijpharm.2018.12.022.

[23] S. Huang, H. Liu, S. Huang, T. Fu, W. Xue, R. Guo, Dextran methacrylate hydrogel microneedles loaded with doxorubicin and trametinib for continuous transdermal administration of melanoma, Carbohydr. Polym. 246 (2020) 116650. https://doi.org/10.1016/j.carbpol.2020.116650.

[24] M.A. Lopez-Ramirez, F. Soto, C. Wang, R. Rueda, S. Shukla, C. Silva-Lopez, D. Kupor, D.A. McBride, J.K. Pokorski, A. Nourhani, N.F. Steinmetz, N.J. Shah, J. Wang, Built-In Active Microneedle Patch with Enhanced Autonomous Drug Delivery, Adv. Mater.

32 (2020) 1–10. https://doi.org/10.1002/adma.201905740.

[25] M. Wang, L. Hu, C. Xu, Recent advances in the design of polymeric microneedles for transdermal drug delivery and biosensing, Lab Chip. 17 (2017) 1373–1387. https://doi.org/10.1039/C7LC00016B.

[26] Y. Zhang, G. Jiang, W. Yu, D. Liu, B. Xu, Microneedles fabricated from alginate and maltose for transdermal delivery of insulin on diabetic rats, Mater. Sci. Eng. C. 85 (2018) 18–26. https://doi.org/10.1016/j.msec.2017.12.006.

[27] R. Jamaledin, C. Di Natale, V. Onesto, Z. Taraghdari, E. Zare, P. Makvandi, R. Vecchione, P. Netti, Progress in Microneedle-Mediated Protein Delivery, J. Clin. Med. 9 (2020) 542. https://doi.org/10.3390/jcm9020542.

[28] A.R. Johnson, C.L. Caudill, J.R. Tumbleston, C.J. Bloomquist, K.A. Moga, A. Ermoshkin, D. Shirvanyants, S.J. Mecham, J.C. Luft, J.M. De Simone, Single-step fabrication of computationally designed microneedles by continuous liquid interface production, PLoS One. 11 (2016) 1–17. https://doi.org/10.1371/journal.pone.0162518.

[29] A.R. Johnson, A.T. Procopio, Low cost additive manufacturing of microneedle masters, 3D Print. Med. 5 (2019). https://doi.org/10.1186/s41205-019-0039-x.

[30] K. Lee, H. Jung, Drawing lithography for microneedles: A review of fundamentals and biomedical applications, Biomaterials. 33 (2012) 7309–7326. https://doi.org/10.1016/j.biomaterials.2012.06.065.

[31] J.D. Kim, M. Kim, H. Yang, K. Lee, H. Jung, Droplet-born air blowing: Novel dissolving microneedle fabrication, J. Control. Release. 170 (2013) 430–436. https://doi.org/10.1016/j.jconrel.2013.05.026.

[32] H. Takahashi, T. Kan, G. Lee, N. Dönmez, J. Kim, J. Park, D. Kim, Y.J. Heo, Self-focusing 3D lithography with varying refractive index polyethylene glycol diacrylate, Appl. Phys. Express. 13 (2020). https://doi.org/10.35848/1882-0786/ab9ba3.

[33] H. Takahashi, Y.J. Heo, N. Arakawa, T. Kan, K. Matsumoto, R. Kawano, I. Shimoyama, Scalable fabrication of microneedle arrays via spatially controlled UV exposure, Microsystems Nanoeng. 2 (2016) 1–5. https://doi.org/10.1038/micronano.2016.49.

[34] J.S. Kochhar, P. Anbalagan, S.B. Shelar, J.K. Neo, C. Iliescu, L. Kang, Direct microneedle array fabrication off a photomask to deliver collagen through skin, Pharm. Res. 31 (2014) 1724–1734. https://doi.org/10.1007/s11095-013-1275-1.

[35] W.G. Bae, H. Ko, J.Y. So, H. Yi, C.H. Lee, D.H. Lee, Y. Ahn, S.H. Lee, K. Lee, J. Jun, H.H. Kim, N.L. Jeon, W. Jung, C.S. Song, T. Kim, Y.C. Kim, H.E. Jeong, Snake fang-inspired stamping patch for transdermal delivery of liquid formulations, Sci. Transl. Med. (2019). https://doi.org/10.1126/scitranslmed.aaw3329.

[36] C.D. Mathers, D. Loncar, Projections of global mortality and burden of disease from 2002 to 2030, PLoS Med. 3 (2006) 2011–2030. https://doi.org/10.1371/journal.pmed.0030442.

[37] S.H. Hyon, N. Nakajima, H. Sugai, K. Matsumura, Low cytotoxic tissue adhesive based on oxidized dextran and epsilon-poly- l -lysine, J. Biomed. Mater. Res. - Part A. 102 (2014) 2511–2520. https://doi.org/10.1002/jbm.a.34923.

[38] R.G. Laughlin, Fundamentals of the Zwitterionic Hydrophilic Group, Langmuir. 7 (1991) 842–847. https://doi.org/10.1021/la00053a006.

[39] C.J. Huang, Y. Li, S. Jiang, Zwitterionic polymer-based platform with two-layer architecture for ultra low fouling and high protein loading, Anal. Chem. 84 (2012) 3440–3445. https://doi.org/10.1021/ac3003769.

[40] N. Sharma, R. Rajan, S. Makhaik, K. Matsumura, Comparative Study of Protein Aggregation Arrest by Zwitterionic Polysulfobetaines : Using Contrasting Raft Agents, ACS Omega. 4 (2019) 12186–12193. https://doi.org/10.1021/acsomega.9b01409.

[41] T. Matsuda, J. Nagase, A. Ghoda, Y. Hirano, S. Kidoaki, Y. Nakayama,

Phosphorylcholine-endcapped oligomer and block co-oligomer and surface biological reactivity, Biomaterials. 24 (2003) 4517–4527. https://doi.org/10.1016/S0142-9612(03)00344-2.

[42] Y. Chang Chung, Y. Hong Chiu, Y. Wei Wu, Y. Tai Tao, Self-assembled biomimetic monolayers using phospholipid-containing disulfides, Biomaterials. 26 (2005) 2313–2324. https://doi.org/10.1016/j.biomaterials.2004.06.043.

[43] R. Lalani, L. Liu, Electrospun zwitterionic poly(sulfobetaine methacrylate) for nonadherent, superabsorbent, and antimicrobial wound dressing applications, Biomacromolecules. 13 (2012) 1853–1863. https://doi.org/10.1021/bm300345e.

[44] R. Rajan, Y. Suzuki, K. Matsumura, Zwitterionic Polymer Design that Inhibits Aggregation and Facilitates Insulin Refolding: Mechanistic Insights and Importance of Hydrophobicity, Macromol. Biosci. 18 (2018) 1–6. https://doi.org/10.1002/mabi.201800016.

[45] R. Rajan, S. Ahmed, N. Sharma, N. Kumar, A. Debas, K. Matsumura, Review of the current state of protein aggregation inhibition from a materials chemistry perspective: special focus on polymeric materials, Mater. Adv. (2021).

[46] R. Rajan, K. Matsumura, A zwitterionic polymer as a novel inhibitor of protein aggregation, J. Mater. Chem. B. 3 (2015) 5683–5689. https://doi.org/10.1039/c5tb01021g.

[47] P. Nonsuwan, A. Matsugami, F. Hayashi, S.H. Hyon, K. Matsumura, Controlling the degradation of an oxidized dextran-based hydrogel independent of the mechanical properties, Carbohydr. Polym. 204 (2019) 131–141. https://doi.org/10.1016/j.carbpol.2018.09.081.

[48] H. Cruz, B. Laycock, E. Strounina, T. Seviour, A. Oehmen, I. Pikaar, Modified Poly(acrylic acid)-Based Hydrogels for Enhanced Mainstream Removal of Ammonium

from Domestic Wastewater, Environ. Sci. Technol. 54 (2020) 9573–9583. https://doi.org/10.1021/acs.est.9b07032.

[49] C. Yan, T. Yang, S. Zhu, H. Wu, Synthesis and properties of poly(DEX-GMA/AAc) microgel particle as a hemostatic agent, J. Mater. Chem. B. 5 (2017) 3697–3705. https://doi.org/10.1039/C7TB00768J.

[50] P. Nonsuwan, A. Matsugami, F. Hayashi, S.H. Hyon, K. Matsumura, Controlling the degradation of an oxidized dextran-based hydrogel independent of the mechanical properties, Carbohydr. Polym. 204 (2019) 131–141. https://doi.org/10.1016/j.carbpol.2018.09.081

Chapter 2: Polymer synthesis and mold-less microneedle fabrication

2.1 Introduction

Over the past decades, microneedle drug delivery systems have attracted increasing attention in biomedical research. It offers the advantages of new active pharmaceutical ingredients (API) for the following reasons; (1) the large molecules can be administered, (2) enhanced drug efficiency in the reduction dosage, (3) targeted to the skin area to delivery, (4) faster healing after administration. The drug delivery microneedles (Figure 2.1) are classified into 5 types according to their functions: hollow, solid, coated solid, dissolving, and hydrogel microneedles[1].

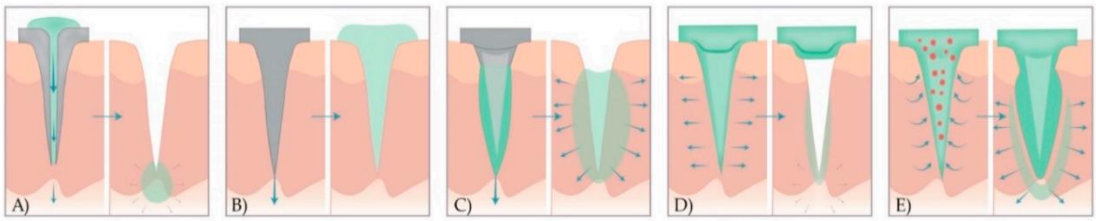

Figure 2.1 A schematic of different microneedle drug release methods (a) hollow, (b) solid, (c) coated solid, (d) dissolving, and (e) hydrogel microneedles [1].

2.1.1 Microneedle Classifications

Hollow microneedle can be used for infusion liquid formulation flows (typically, 10-100 μL/min) from the reservoir into the skin through the hollow microneedles. Hollow microneedle can deliver a higher API than other microneedle delivery methods. The biggest drawback found in this method is a clogging problem in the needle tip in the tissue and requires a microfluidic chip or micropump connected to the microneedle array. Figure 2.2a shows an in-plane single-crystal-silicon microneedle array that releases rhodamine B into the agarose gel with about 20 μm diameter microchannel (Figure 2.b).[2]

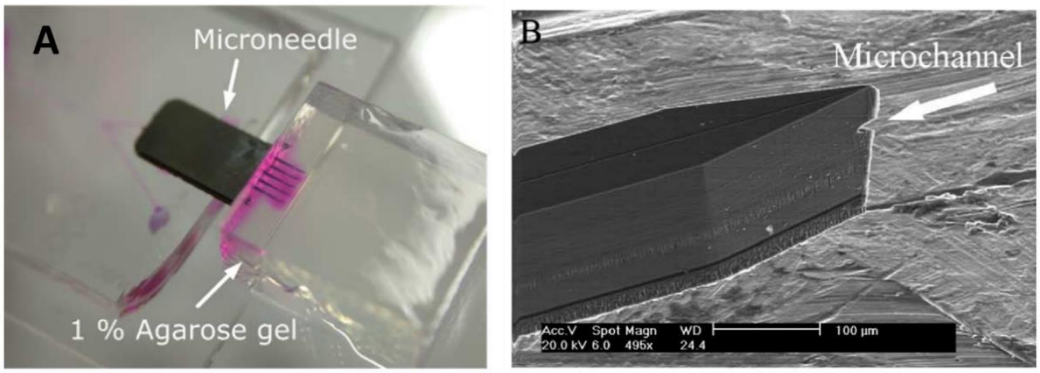

Figure 2.2 (a) Injection of Rhodamine B solution into the agarose gel (b) microchannel entrance at the tip[2]

Solid microneedles are commonly used for skin pre-treatment in the field of cosmetic medicine[3]. The microneedles pierce the skin to create the microchannels in the stratum corneum layer, the conventional drug in the form of dream, solution, or gel is applied in this region. Solid microneedle can make from metal, ceramic and polymer (Figure 2.3).[4] The solid microneedles can fabricate by the etching process for silicon or metal and micro-molding for polymer.

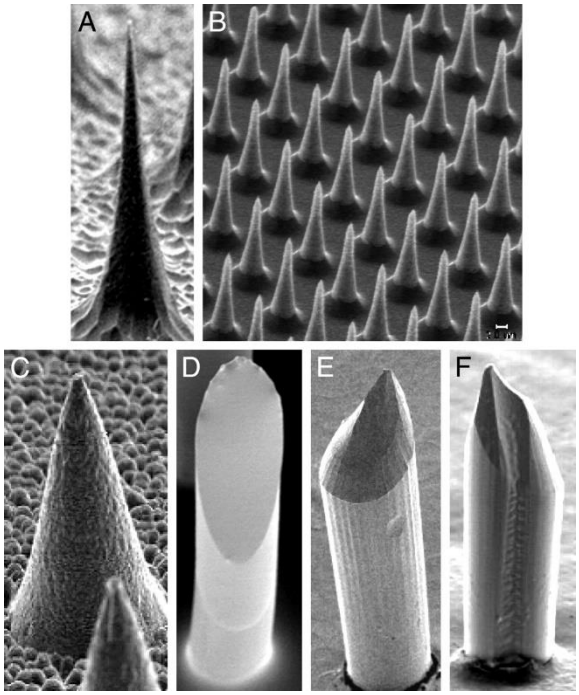

Figure 2.3 Solid microneedles fabricated out of (a-b) silicon, (c) metal, and (d-f) polymer, imaged by scanning electron microscopy[4].

Coated solid microneedles (coat and poke approach) are the solid microneedle coated with a water-soluble drug formulation. After inserting microneedle, the coated drug dissolves and then continuously releases into the skin. Although the solid microneedle allows rapid

therapeutic pharmaceutical ingredients (APIs) delivery, less than 0.7 μg/needle of materials can be coated.[5]

Dissolving microneedles (poke and release) consist of biodegradable polymers or sugars-based matrices that can be completely dissolved or degraded in the skin. This method is easy to fabricate by micro-molding and has increased attention recently. The delivery rate is controlled by adjusting the polymeric composition of the microneedle array in the fabrication process. The microneedle may be used device for applying to the skin. The interstitial fluid under the skin dissolves the microneedle material-based rapidly, and the drug has released into the skin and diffuses to the blood vessel over time.

Recently, dissolvable water and degradable material have been used for microneedle fabrication, such as sugars, galactose, dextran, pullulan[5], gelatin[6], sodium hyaluronate (HA)[7], poly(vinylpyrrolidone), carboxymethyl cellulose (CMC), hydroxy-propyl-methyl-cellulose (HPMC)[8], chitosan[7], chitin, silk[9], and poly(vinylpyrrolidone)[10]. Figure 2.4 illustrates the concept of dissolving microneedle; the drug was dissolved in the water-soluble or degradable material(s). The mixed solution was poured into the micro-molding followed by centrifugal or vacuum to force the liquid to fill all gaps in the mold. The microneedle was taken off 6-24 h after drying in the mold.

The advantages of this method are the low cost of polymeric materials and processes at the ambient temperature that is possible for industrial mass production. The disadvantages are that the process requires a vacuum system or centrifugal methods to fill the liquid into the micro-mold, which is time-consuming.

The dissolving microneedle is also used for ocular drug delivery for eye diseases and injuries[6]. Aung Than et al. [6] enhanced therapeutic efficacy by the double-layered micro-reservoirs by using corneal neovascularization as the disease model. One eye microneedle patch can produce about 90% reduction of the neovascular area by delivering an anti-

angiogenic monoclonal antibody (DC101). They proposed that the eye patch microneedle for intraocular drug delivery method possibly to self-treatment at home for many eye diseases. Figure 2.5 shows the diffusion of two fluorescence drugs diffusion, IgG(680) (red) dissolving in HeMA, IgG(488)(green) dissolving in HA, in agarose gel. The outer layer (IgG 488) was rapidly diffused to the agarose gel first, then after 30 min, the inner drug (IgG 680) was diffused throughout the gel later.

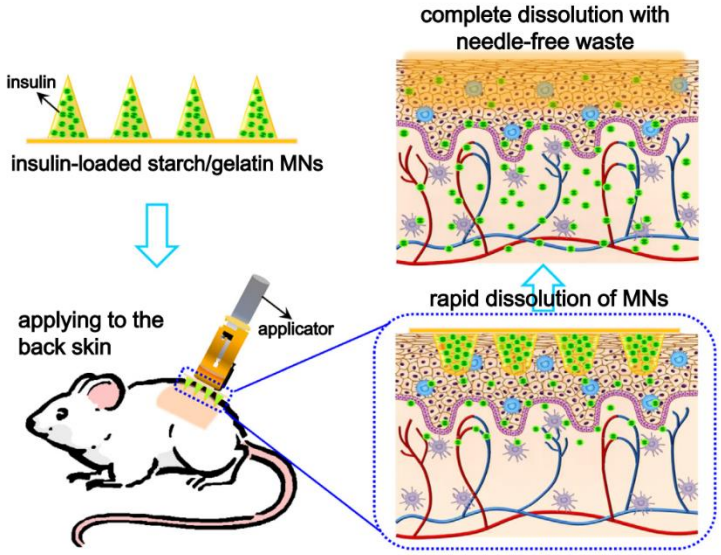

Figure 2.4 Schematic illustration of the concept of dissolving microneedle, the encapsulated insulin was combined with starch/gelatin microneedles and dissolved rapidly in the skin to release encapsulated insulin[7].

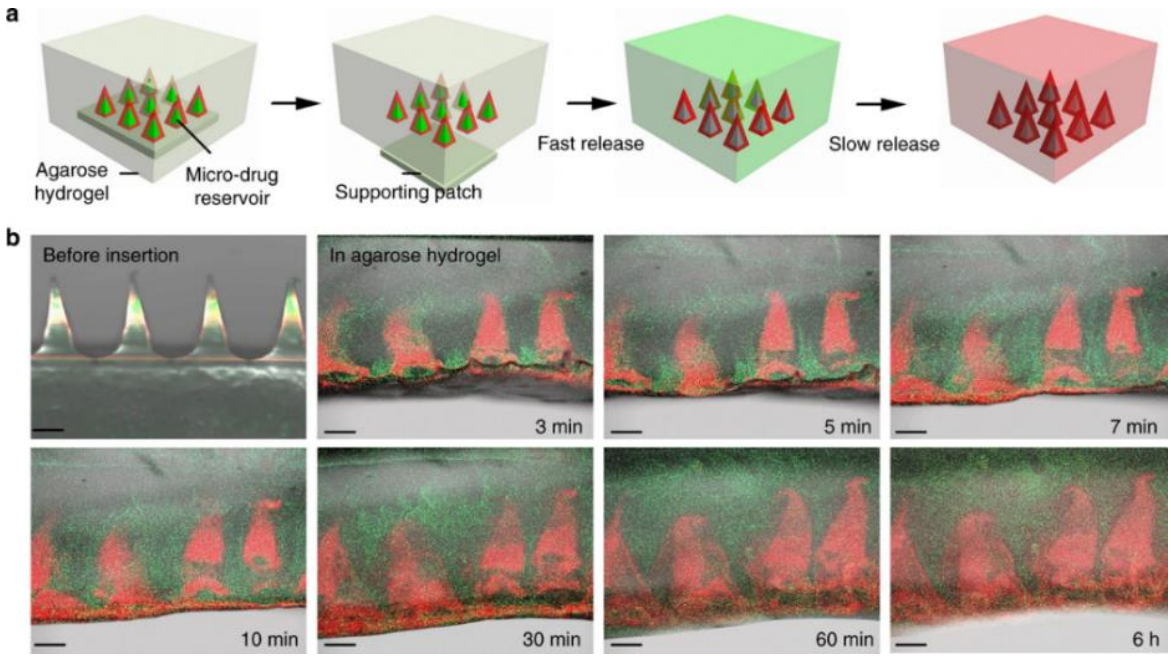

Figure 2.5 Schematic illustration of the double-layer drug coating microneedles. (a) the release profile of double-layer microneedle in agarose gel, (b) The merge of the optical and fluorescence image of double-layer drug release in real-time [6].

Hydrogel (swellable) microneedles consist of an insoluble polymeric network. The dry polymeric microneedle is inserted into the skin. The microneedles are uptaken the interstitial fluid around the tissue and become a hydrogel. The polymer network has swelled the liquid and extended the size of the pore so that it allowed the drug to diffuse from a higher concentration (hydrogel) to a lower concentration (tissue). Figure 2.6 illustrates the mechanism of drug release via hydrogel microneedle

The hydrogel microneedles have two functions to overcome the limitation of dissolving microneedle: (1) absence of microneedle material in the skin after removing the microneedle patch; (2) the treatment able to terminate if adverse drug reactions or overdose occur. The crosslinking density of the polymer controls the swelling and releasing properties, but it has to maintain the microneedle strength to penetrate the stratum corneum and epidermic layer. Before removing the microneedle, the swelled hydrogel should retain the mechanical toughness to remove all materials from the skin[8]. Figure 2.7 shows that the microneedle retains the swollen microneedle structure after being removed from mouse back skin[9].

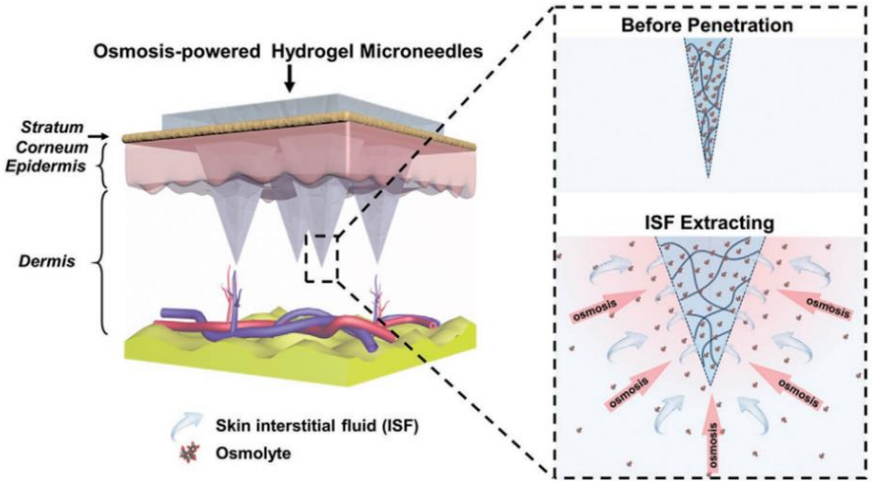

Figure 2.6 A Schematic illustration of the hydrogel-microneedle drug delivery mechanism[10]

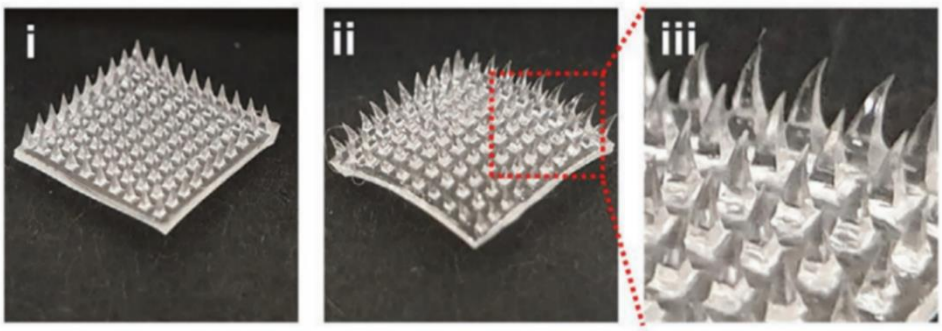

Figure 2.7 The digital images of maltose 200 mg/ml–MeHA microneedle patch before (i) and after removal (ii) (iii) zoom-in image of the microneedle tips after removing from mouse back[9].

The microneedle drug delivery methods have provided a versatile platform to increase transdermal drug delivery efficiency. Currently, the microneedle technology applications have been developed to deliver from a common drug; vitamins, minerals, ibuprofen, and advanced drug treatment such as donepezil hydrochloride (DPH) used for the treatment of Alzheimer's disease[11], anticancer drugs; doxorubicin (DOX)[12][13], and trametinib (Tra)[13], antibody, antigen[14], insulin[7], lysozyme[15], vaccine[16][17][18], and cells for cell therapy[19].

Generally, the researchers have combined the drug with microneedle materials solution before the microneedle fabrication process. So, there are some drawbacks to those methods: (1) the drug denaturation before use, (2) fixed drug dosages per microneedle patch, (3) impossible to deliver on-demand purpose. In this study, a new type of microneedle patch was designed to overcome those limitations; the dry microneedle can load several types of drugs all on-demand, for example, cancer drug treatment, insulin, the vaccine that can adjust dose before loading to microneedle patch.

2.2 Materials and Methods

2.2.1 Materials

Dextran (molecular weight (MW) = 70 kDa) was obtained from Meito Sangyo (Nagoya, Japan). Glycidyl methacrylate (GMA) and 4-dimethyl aminopyridine (DMAP), Acrylic acid (AAc), ethylene glycol dimethacrylate (EGDMA), 2,2-Dimethoxy-2-phenylacetophenone (DMPA), acrylated epoxidized Soybean oil (AESO) (Figure 2.8), and rhodamine B were obtained from Sigma-Aldrich(St. Louis, MO, USA). 2,2'-Azobis(2-methylpropionamidine) dihydrochloride was obtained from Wako Pure Chemical Industries (Osaka, Japan). EGDMA and AAc were used with purification.

2.2.2 Synthesis of AESO resin

The AESO resin was synthesized for making a substrate of the microneedle array. First, the photoinitiator, DMPA, 2g, was dissolved in 20 ml of EGDMA. The mixed solution was added to the 180 ml AESO in the round brown bottle and stirred for 24 h in a dark room at room temperature. The AESO resin was covered with aluminum foil and stored at room temperature. FTIR analysis was conducted using FT-IR spectrometer spectrum 100 PerkinElmer in 4000-380 cm^{-1} to investigate the functional groups of synthesized products.

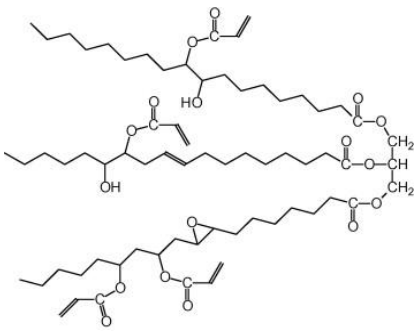

Figure 2.8 The chemical structure of AESO

2.2.3 Synthesis of Dex-GMA

Dextran-glycidyl methacrylate (Dex-GMA) synthesis was synthesized using our previously reported method.[20] In brief, 20 g of dextran was slowly added to 80 mL of dimethyl sulfoxide (DMSO), and the solution was stirred until complete dissolution. The transparent solution was then stirred for another 30 min under nitrogen gas. Then, 3.2 g of DMAP and 8.8 g of GMA were added to the solution and purged nitrogen gas for 30 min. The mixture was stirred at 50 °C overnight before neutralization by 6.5 mmol hydrochloric acids (HCl). The mixture was dialyzed against distilled water for 7 days using a dialysis membrane (MWCO = 3.5 kDa). The resulting product was dried in the oven for 48 h at 47 °C, followed by vacuum drying for 48 h at 25 °C to obtain Dex-GMA derivative as a pale yellow-brown flake product.

The synthesized material was characterized by ^{1}H nuclear magnetic resonance (NMR) (400 MHz equipped with a cryogenic probe, Bruker). The results of the ^{1}H-NMR spectroscopy were used to investigate the degree of substitution (%DS).

2.2.4 Synthesis of Dex-GMA/AAc

The hydrogel resin was prepared by 2g of Dex-GMA was dissolved in 3.5ml distilled water at 50 °C in a brown glass tube and stirred until they were completely dissolved. The photoinitiator of 2,2'-Azobis(2-methylpropionamidine) dihydrochloride, 125 mg, was added to the mixed solution. Then, 4 ml of acrylic acid and DMPA, the photoinitiator, 150 mg, were added to the mixed solution and stirred for 2 h at room temperature. The resin was covered with aluminum foil and stored in the fridge (4-5 °C) for long-term use.

2.2.5 Mold-less Microneedle Fabrication

2.2.5.1 Photomask

The photolithography method was used for the microneedle fabrication arrays. A photomask was used for blocking UV light, preventing photopolymerization outside of microneedle fabrication areas. Briefly, a glass slide was coated by a single-side aluminum 40 nm thick by a sputtering technique (Figure 2.9a). Next, the low-energy laser was used for evaporating the thin aluminum layer to create the four-points star micro-windows mask array (Figure 2.9b) with a based-diameter 400 μm (Figure 2.9c). The micro-size patterns were aligned in a 6 mm x 6 mm square area. The UV light passing photomask was generated the free radical in the polymer resin in the fabrication process, causing a photopolymerization and creating 3D microneedle structure patterns.

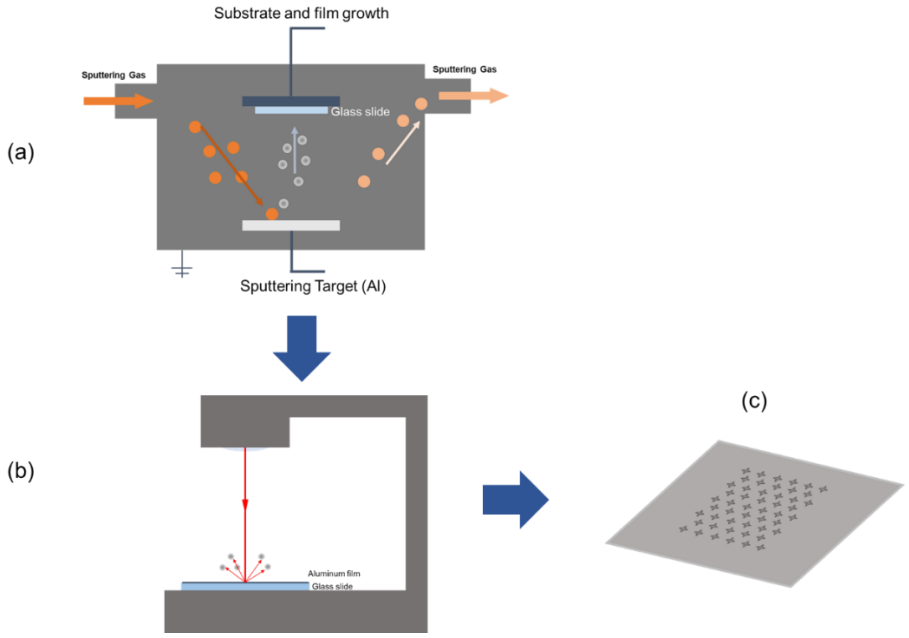

Figure 2.9 The photomask fabrication process (a) sputtering methods (b) photomask drawing (c) photomask

2.2.5.2 Photolithography microneedle fabrication set up

The microneedle fabrication was set up following Figure 2.10; a lens has guided the UV beam into the photomask was located 2 cm above the LED. The photomask was installed vertically above the lens about 1 cm, and the resin frame was placed on the top.

The LED UV (380-400 nm), the light source, was connected to the portable power supply (3.3 V,700mV). Figures 2.10 and 2.11 illustrate the compact size of the microneedle fabrication setup around 10 cm x.10 cm and does not require a special room and extra equipment for the fabrication process. In addition, the total price is about 4,000 yen (40 dollars), which is suitable for applying in academic research.

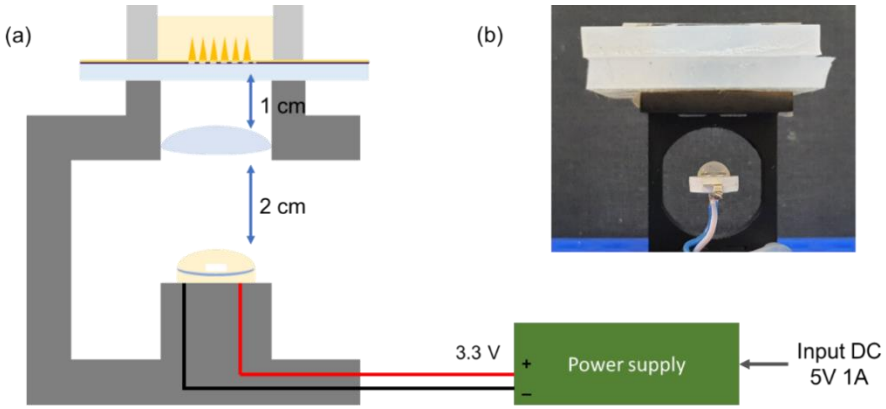

Figure 2.10 microneedle fabrication set up

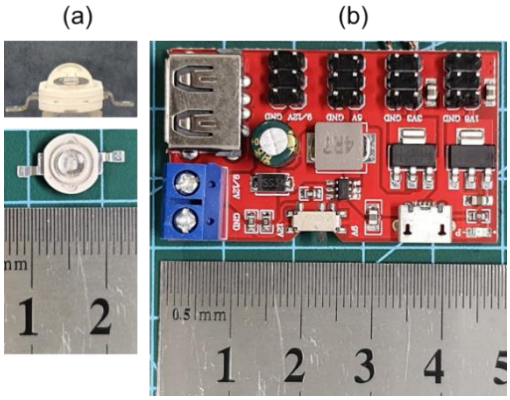

Figure 2.11 The photographs show the UV LED and power supply dimensions.

2.2.5.3 Mold-less microneedle fabrication process

First, preparing substrate of microneedle array, the 100 µl AESO resin was dropped on a photomask glass slide, then covered with a clear plastic sheet, while a 0.2 mm thickness spacer was placed in between (Figure 2.12a) then the resin was cured by UV irradiation for the 30s (Figure 2.12b). After completely cured, the clear plastic was removed and continued 10s UV irradiation to harden the AESO sheet. The PDMS frame was placed on the AESO sheet, then filled with Dex-GM/AAc resin about 3 mm height (Figure 2.12c) and UV irradiation was conducted for 10, 30, 60 and 120s. The 3D microneedle structures were created after UV irradiation(Figure 2.12d). The uncured resin was carefully removed by pipette from the PDMS frame. The PDMS frame was taken off, and the microneedle patch was removed carefully by knife. The microneedle was washed with distilled water to remove the non-polymerization polymer and was pros-cured immediately for 10 s. The microneedle patch was dried at room temperature and stored in the desiccator.

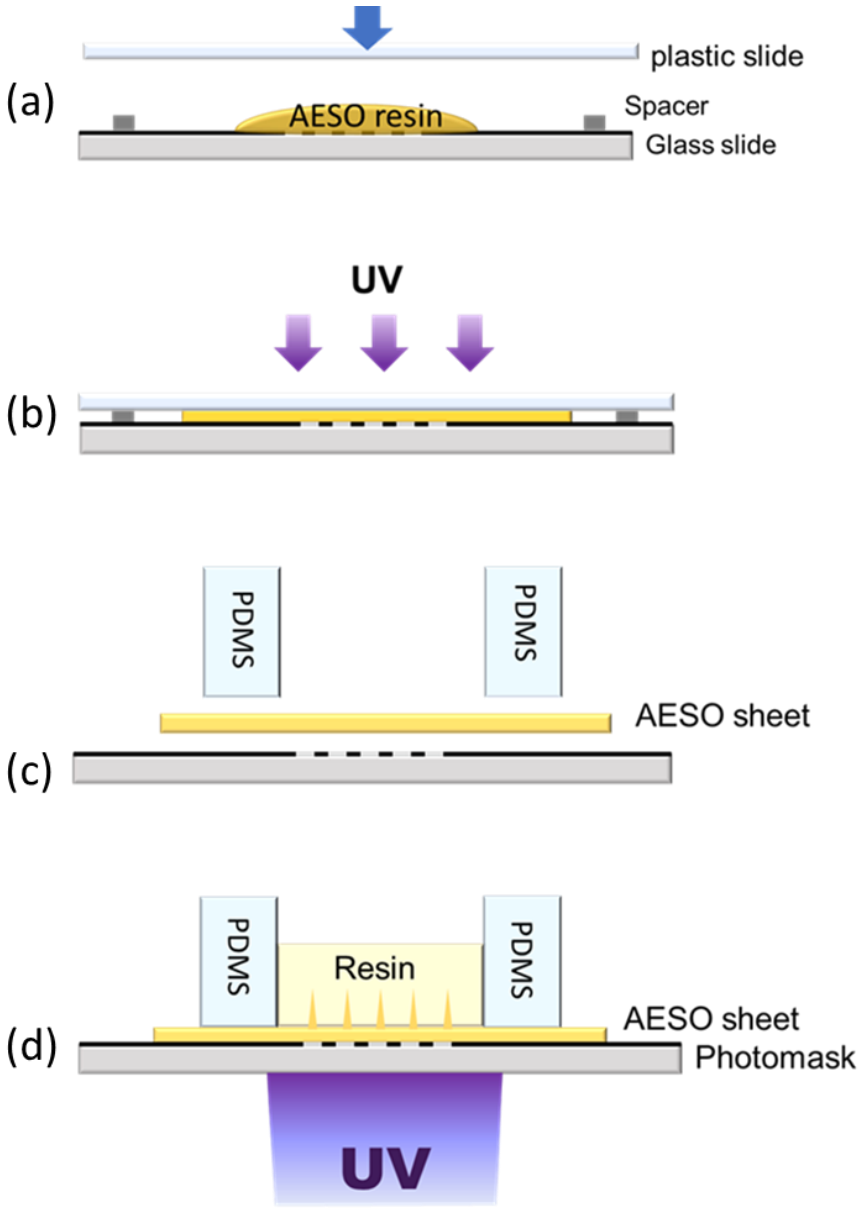

Figure 2.12 Schematic (a-d) illustration of the fabrication of microneedle arrays via inverted light UV lithography

2.2.5.4 Drug loading studies

In this study, rhodamine B (Figure 2.13) was used as a model drug to calculate the capacity of chemical loading into the microneedle. The 200 μg/ml rhodamine B was prepared in PBS solution, 50 μl was dropped on the microneedle patch (Figure 2.14). After 15, 30, 60 and 90 min, the rhodamine B solution was absorbed into the microneedle in different amounts of concentration. The microneedle was changed from white to red, and the rhodamine B solution changed from dark red to light pink. The unloaded solutions were correct by rinsing 1ml PBS to calculate loading capacity(Figure 2.14). The 96-well plate micro-reader, TECAN Infinite® 200 PRO M nano+, was used to determine rhodamine B concentrations at 555nm.

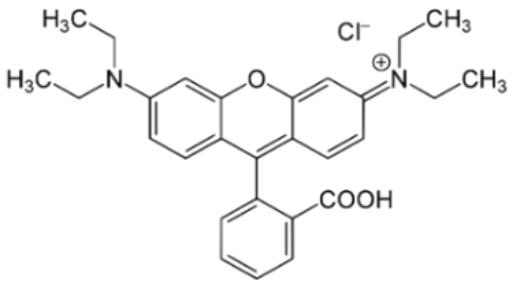

Figure 2.13 The chemical structure of rhodamine B

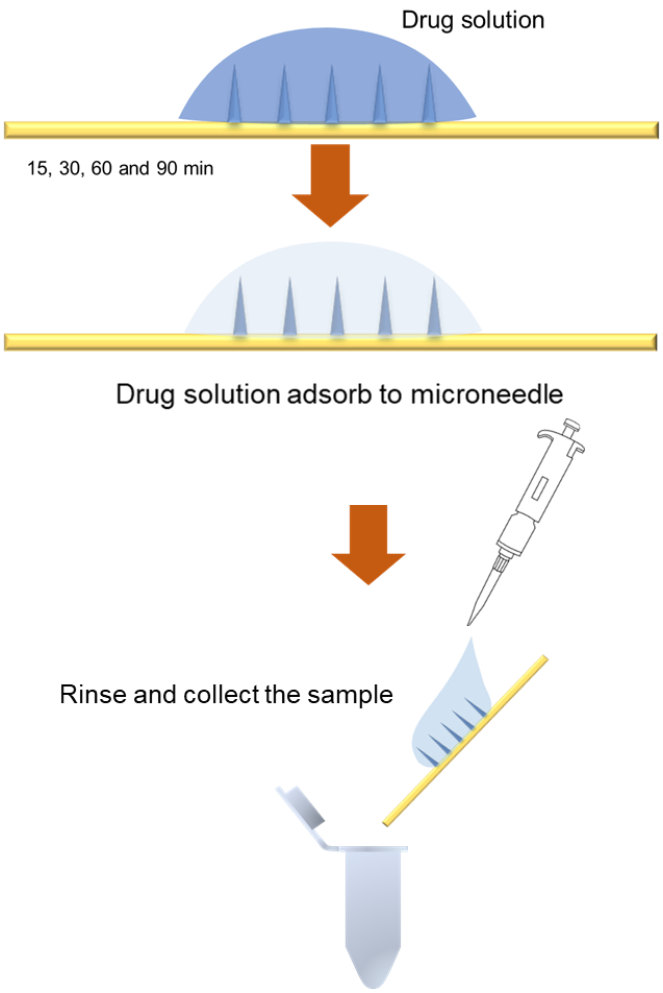

Figure 2.14 Schematic illustration of the drug loading and rinsing method

2.3 Results and discussion

2.3.1 AESO Substrate and Surface Characterization

The substrate should be clear and UV transparent to achieve the fabrication of microneedles via photolithography. The AESO thin sheets were fabricated with UV irradiation for 10 s (Figure 2.15) and peeled off the sheet from the glass slide using a knife. Figure 2.16 shows the flexibility and transparency of the AESO sheet, which curved against the skin surface when the microneedle patch was placed on the skin. Moreover, to control the microneedle array quality during the fabrication process, the AESO sheet should be clear, with a thickness of 200 µm and no air bubbles.

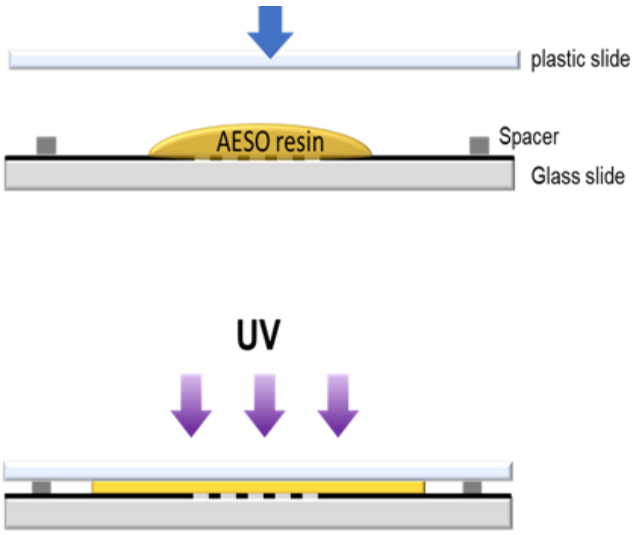

Figure 2.15 Schematic illustration depicting the AESO sheet substrate fabrication.

Figure 2.16 the flexible and transparent AESO sheets.

The FTIR spectra were depicted in Figure 2.17, the AESO film; the most significant bands are hydroxyl (-OH) groups at 3500 cm^{-1}, methyl groups (-CH_3-) at 2920 cm^{-1} and methylene groups (-CH_2-) at 2853 cm^{-1}, stretching vibration (C=O) in esters groups is located at 1730 cm^{-1}, double bonds (C=C) from the acrylic pendant groups are found at 1633 cm^{-1}. Lastly, at about 750-730 cm^{-1} is represented the fatty acid chains (-$CH_2CH_2CH_2CH_2$)[21].

The FTIR characterization was confirmed that the methacrylate groups have occurred on the surface. In the fabrication process, the hydrogel microneedles were adhered to the AESO sheet surface by covalent bonds after the photopolymerization reaction occurred because methacrylate groups were present on the AESO sheet (Figure 2.18).

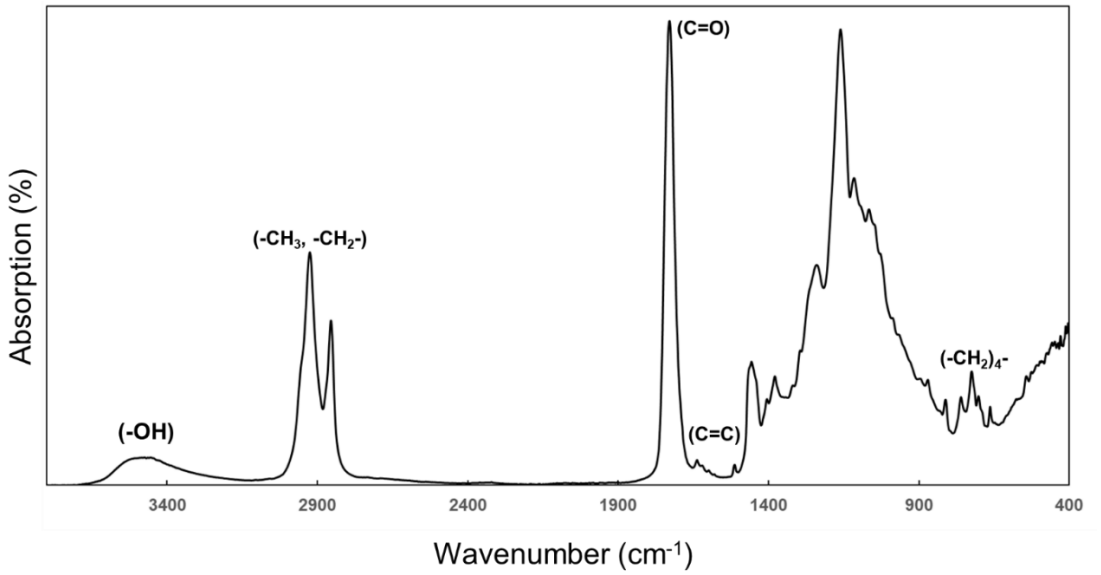

Figure 2.17 FTIR spectra of AESO sheet

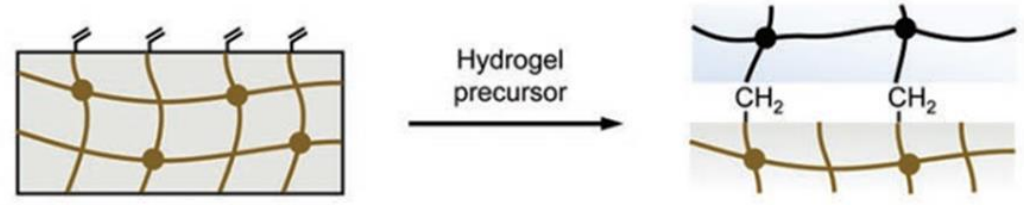

Figure 2.18 (a) the methacrylate group on the substrate surface (b) the hydrogel binding with the surface substrate by covalent bonds[22]

2.3.1 Characterization of the Dextran-GMA

To design a photopolymerization resin, we combined a base-catalyzed ring-opening of the epoxide of glycidyl methacrylate (GMA) with the hydroxyl groups of dextran to generate Dex-GMA. The degree of substitution (DS) of GMA into dextran, estimated using ^{1}H-NMR spectroscopy, was 21.2% (Figure 2.19). DS was calculated by comparing the area under the proton peaks at 2.0 ppm (methyl protons in GMA; $A\delta_{1.8–2.0}$) and that at 3.4–4.2 ppm (dextran sugar unit protons, H2-H6; $A\delta_{3.4–4.2}$), as shown in

(Equation 1). Here, the DS of GMA was important for the photopolymerization reaction as high DS causes low swelling properties. Consequently, the Dex-GMA with DS in the 19–22% range was used in all experiments to ensure uniformity during the microneedle fabrication.

$$DS \text{ for } GMA\ (\%) = \frac{\left(\frac{A_{\delta 1.8-2.0}}{3}\right)}{\left(\frac{A_{\delta 3.4-4.2}}{6}\right)} \qquad (1)$$

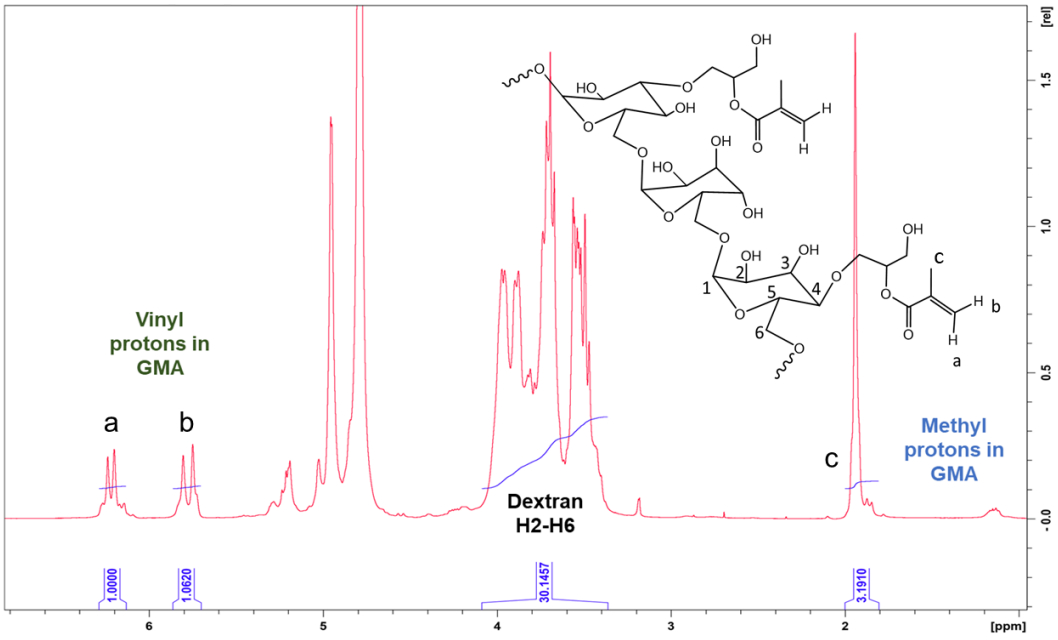

Figure 2.19 ^{1}H-NMR spectra of the Dex-GMA for calculating the degree of substitution of GMA in D_2O.

2.3.3 Photomask

Photolithography was used to fabricate the microneedle arrays. A photomask was used to block UV light, which prevented photopolymerization outside the microneedle fabrication areas. Subsequently, a glass slide was coated with aluminum (thickness = 40 nm) on one side using a sputtering technique. Next, a low-energy laser was used to evaporate the thin aluminum layer, and a four-point star-shaped micro-window mask array with a base diameter of 400 μm was created (Figure 2.20). The micro-size patterns were aligned in a 6 mm × 6 mm square area.

The UV light passing through the photomask generated free radicals in the polymer resin during the fabrication process, resulting in photopolymerization and creating 3D microneedle structure patterns.

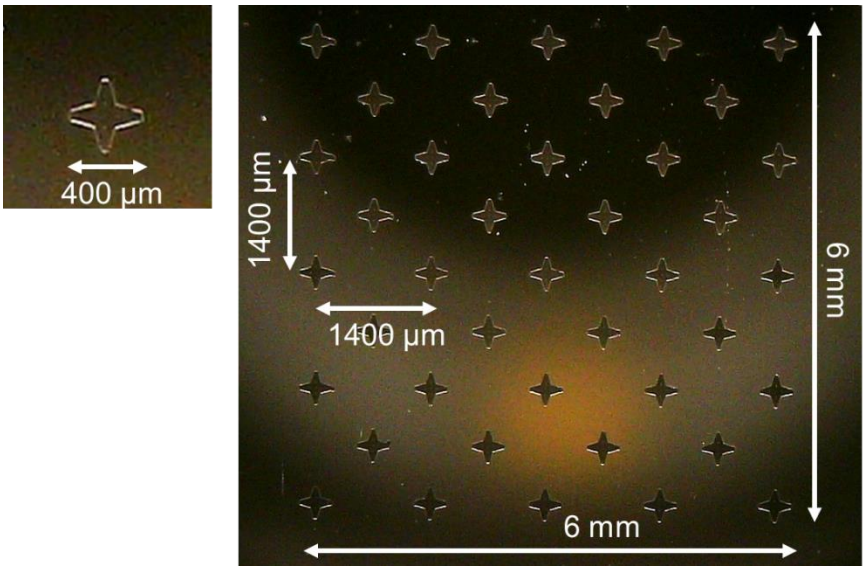

Figure 2.20 Photograph of the photomask pattern.

2.3.4 Microneedle fabrication

The microneedle array was fabricated on a clear, flexible AESO sheet. The AESO resin was dropped at the center of the photomask glass slide about 100 µl then placed a clear polyurethane (PU) plastic sheet that the 200 µm spacer in between. After 30 s UV irradiation, the PU plastic sheet was removed, whereas the AESO sheet was still attached to the photomask glass slide. The thickness of the microneedle substrate sheets was fixed at about 200±20 µm for controlling the UV light intensity pass through the micro-size windows, affecting the length of the microneedle height and shape. Next step, the PDMS frame was placed on the AESO sheet and placed tightly to ensure the resin would not leak during the fabrication process. The

Dex-GMA/AAc resin has filled to the PDMS frame about 3 mm height and ensures no bubble in the resin. . To fabricate the microneedle, we chose four different time UV exposures of 10 s, 30 s, 60 s, and 120 s. In table 1, the sizes of microneedle were measured and analyzed by ImageJ version 1.53e.

The exposure at 60 s shows the highest aspect ratio of microneedle and gives a good symmetry shape (Figure 2.21). The 600 µm height microneedle is long enough to penetrate the stratum corneum layer and locate in the epidermis layer [23]. Figure 2.21 illustrates the dry microneedle patch size compared with the hypodermic needle(for intramuscular injection) that the microneedle width is narrower than 4-times the hypodermic needle. The four-points-star shape microneedle has been designed to reduce a wound's size after microneedle insertion compared with a square and a circular base shape; therefore, a wound will recover faster.

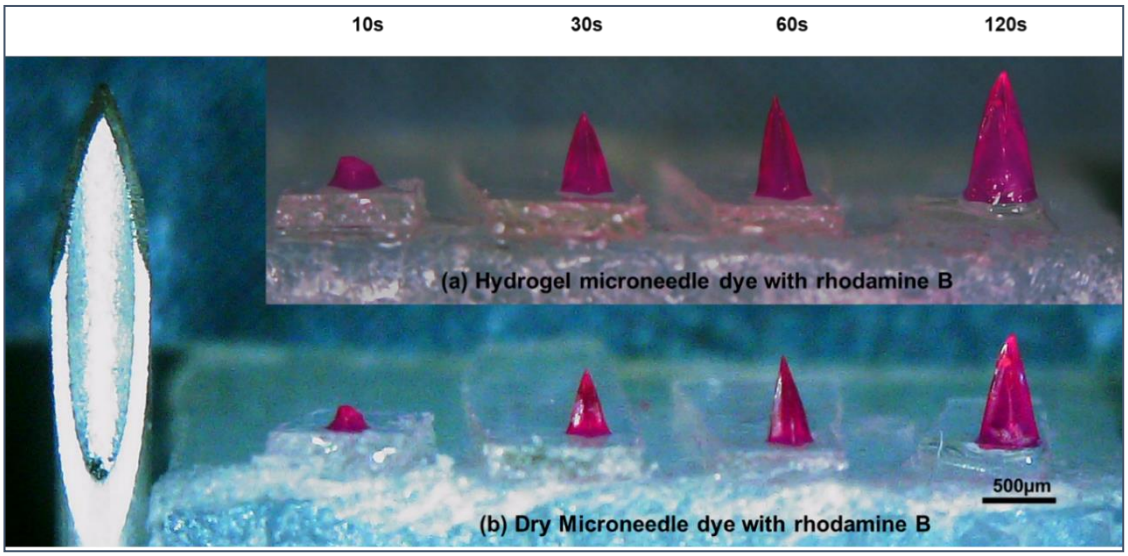

Figure 2.21 Light microscope images comparing the hypodermic needle with the microneedle different UV irradiation time fabrication (a) the hydrogel microneedle dye with rhodamine B (b) the dry microneedle dye with rhodamine B.

Table 1 the dry microneedle average sizes on different time UV exposure

Microneedle type	Exposure time (second)	Base width (µm)	Height (µm)	Aspect ratio
MN-10	10	200	250	1:1.3
MN-30	30	280	460	1:7.0
MN-60	60	300	600	1:2.0
MN-120	120	440	800	1:1.8

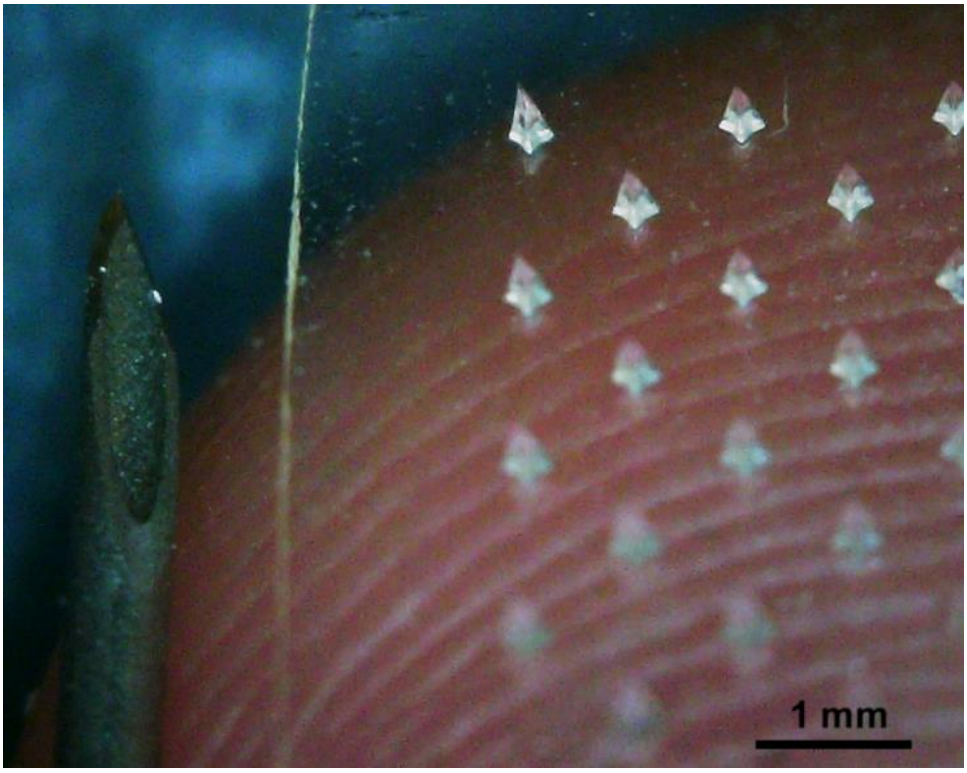

Figure 2.22 the microneedle on the fingertip comparing the size with a hypodermic needle

Figure 2.23 depicts the concept of UV light projection to create the 3D microneedle structure. When UV light is irradiated into Dex-GMA/AAc resin via the four-points star micro-windows on the photomask, the resin near the AESO sheet becomes polymerized, forming a lens-like shape (t= 10s), as shown in Figure 2.23. The cured resin presents a larger refractive

index than the uncured area. UV irradiation time from 20 s to 60 s, the UV light refracts at the cured surface microneedle and projects to the micro-lens at a tip needle. The convergence of UV irradiation causes photopolymerization along the light pathway and creates the pyramid-like shape 3D microneedle structure.

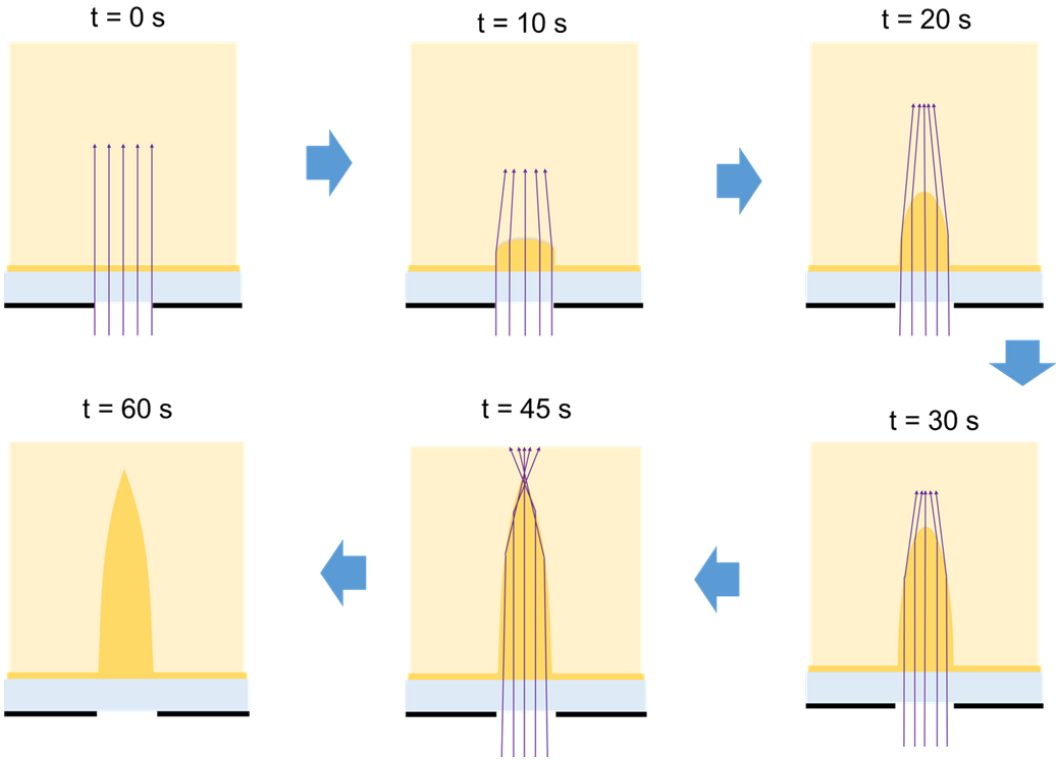

Figure 2.23 The schematic illustrates the UV light pathway in the microneedle fabrication and causing photopolymerization

2.3.5 Drug loading capacity

This study used rhodamine B as the chemical loading drug model representing the low molecular weight. The 200 µg/ml rhodamine B 50 µl was dropped on the microneedle (Figure 2.23 at t=0 min). The rhodamine B solution was absorbed/diffused into the microneedle at different times; 15, 30, 60 and 90 min. The microneedle was changed from white to red, and the rhodamine B solution changed from dark red to light pink (Figure 2.24 at t=30 min). We studied rhodamine B loading capacity by rinsing an unabsorbed solution using 1 ml of PBS.

The 200 µl was taken for determination concentrations by the micro-plate reader at 555 nm. In this study, we knew that the rhodamine B 10 µg (in 50µl) loading to each microneedle patch. The concentration in the rinsing solution has conversed to the weight of rhodamine B loading to the microneedle patch that shows in Figure 2.25.

Figure 2.25 illustrates that the rhodamine B loading was increased over time and reached 80 % (8 µg) at 90 min loading. From this result, some therapeutic drugs have the potential to apply to this method, such as doxorubicin hydrochloride (DOX, MW 580) [25] and fentanyl(pain killer drug)[3] because they can dissolve in water and the molecular weight is quite similar to rhodamine B.

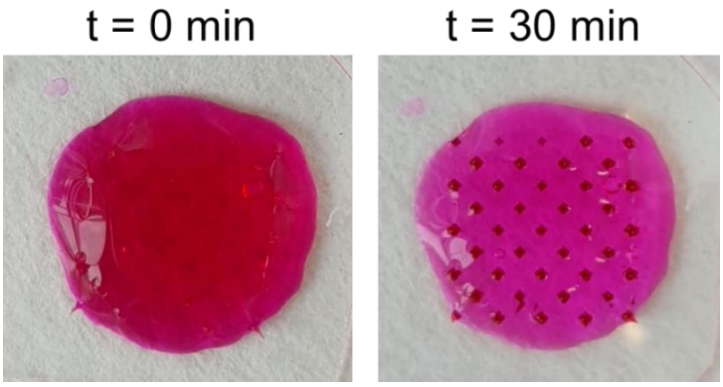

Figure 2.24 photograph of the changing color of rhodamine B solution after 30 min loading in Dex-GMA/AAc microneedle patch.

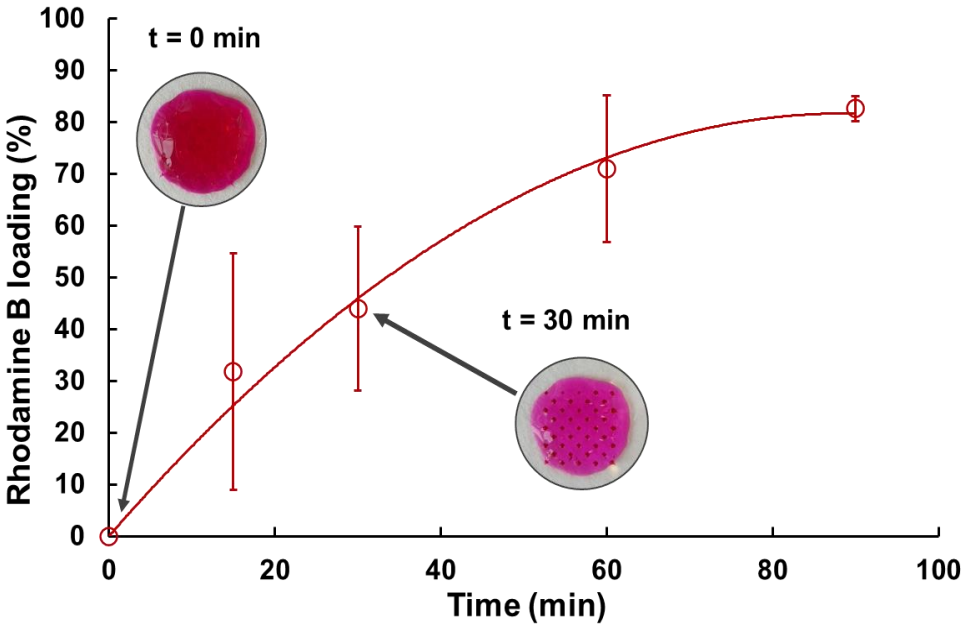

Figure 2.25 The rhodamine B loading capacity; at t=0 min shows the dark pink color of the solution, and t=30 min shows the light pink color of the solution.

2.4 Conclusion

As described, the microneedle technology gets high attention in transdermal drug delivery systems (TDDS) research due to play an excellent feature in oral and parenteral drug delivery systems. However, recently, the microneedle fabrication methods mentioned in the introduction section have drawbacks that are difficult to produce for industrial scale. In this study, the photolithography method, our microneedle fabrication method, overcomes the limitation of other fabrication methods. It takes less than 5 minutes for each fabrication process. In addition, it was able to control the microneedle's length and shape by very time UV irradiation and the pattern micro-windows on the photomask.

The water-based microneedle resin (Dex-GMA/AAc) fabricated on the AESO sheet(oil-base) creates the novel microneedle patch. While drug loading, the water-based drug will diffuse/absorb into the needle, whereas the substrate is unabsorbable water. Therefore, it can use less drug in the drug loading preparation process compared with mold-base fabrication. The hydrogel microneedle was attached AESO sheet by covalent binding that FTIR results show plenty of methacrylate groups on the surface. When the microneedle patch is applied to the artificial skin, the microneedle substrate does not expand; unlike hydrogel microneedles[24], the needles and substrate are the same material. The rhodamine B drug loading model shows that the microneedle can load drug up to 8μg on one microneedle patch, with only 41 needles. Furthermore, the microneedle patch is environment-friendly, so it does not require a special disposal container like the hypodermic needle.

2.5 References

[1] A. Tucak, M. Sirbubalo, L. Hindija, O. Rahić, J. Hadžiabdić, K. Muhamedagić, A. Čekić, E. Vranić, Microneedles: Characteristics, materials, production methods and commercial development, Micromachines. 11 (2020) 1–30. https://doi.org/10.3390/mi11110961.

[2] S. Paik, S. Byun, J. Lim, Y. Park, A. Lee, S. Chung, J. Chang, K. Chun, D. Dan, In-plane single-crystal-silicon microneedles for minimally invasive microfluid systems, 114 (2004) 276–284. https://doi.org/10.1016/j.sna.2003.12.029.

[3] T. Waghule, G. Singhvi, S.K. Dubey, M.M. Pandey, G. Gupta, M. Singh, K. Dua, Microneedles: A smart approach and increasing potential for transdermal drug delivery system, Biomed. Pharmacother. 109 (2019) 1249–1258. https://doi.org/10.1016/j.biopha.2018.10.078.

[4] D. V. McAllister, P.M. Wang, S.P. Davis, J.H. Park, P.J. Canatella, M.G. Allen, M.R. Prausnitz, Microfabricated needles for transdermal delivery of macromolecules and nanoparticles: Fabrication methods and transport studies, Proc. Natl. Acad. Sci. U. S. A. 100 (2003) 13755–13760. https://doi.org/10.1073/pnas.2331316100.

[5] L. Liang, Z.Q. Zhao, Y. Chen, G.Y. Ren, J.Y. Li, X.D. Guo, Some attempts to increase the amount of drug coated onto the microneedles, J. Drug Deliv. Sci. Technol. 67 (2022) 102986. https://doi.org/10.1016/j.jddst.2021.102986.

[6] A. Than, C. Liu, H. Chang, P.K. Duong, C.M.G. Cheung, C. Xu, X. Wang, P. Chen, Self-implantable double-layered micro-drug-reservoirs for efficient and controlled ocular drug delivery, Nat. Commun. 9 (2018) 1–12. https://doi.org/10.1038/s41467-018-06981-w.

[7] M.H. Ling, M.C. Chen, Dissolving polymer microneedle patches for rapid and efficient transdermal delivery of insulin to diabetic rats, Acta Biomater. 9 (2013) 8952–8961.

https://doi.org/10.1016/j.actbio.2013.06.029.

[8] M. Wang, L. Hu, C. Xu, Recent advances in the design of polymeric microneedles for transdermal drug delivery and biosensing, Lab Chip. 17 (2017) 1373–1387. https://doi.org/10.1039/C7LC00016B.

[9] M. Zheng, Z. Wang, H. Chang, L. Wang, S.W.T. Chew, D.C.S. Lio, M. Cui, L. Liu, B.C.K. Tee, C. Xu, Osmosis-Powered Hydrogel Microneedles for Microliters of Skin Interstitial Fluid Extraction within Minutes, Adv. Healthc. Mater. 9 (2020) 1–11. https://doi.org/10.1002/adhm.201901683.

[10] M. Zheng, Z. Wang, H. Chang, L. Wang, S.W.T. Chew, D.C.S. Lio, M. Cui, L. Liu, B.C.K. Tee, C. Xu, Osmosis-Powered Hydrogel Microneedles for Microliters of Skin Interstitial Fluid Extraction within Minutes, Adv. Healthc. Mater. 9 (2020). https://doi.org/10.1002/adhm.201901683.

[11] J.Y. Kim, M.R. Han, Y.H. Kim, S.W. Shin, S.Y. Nam, J.H. Park, Tip-loaded dissolving microneedles for transdermal delivery of donepezil hydrochloride for treatment of Alzheimer's disease, Eur. J. Pharm. Biopharm. 105 (2016) 148–155. https://doi.org/10.1016/j.ejpb.2016.06.006.

[12] S. Bhatnagar, N.G. Bankar, M.V. Kulkarni, V.V.K. Venuganti, Dissolvable microneedle patch containing doxorubicin and docetaxel is effective in 4T1 xenografted breast cancer mouse model, Int. J. Pharm. 556 (2019) 263–275. https://doi.org/10.1016/j.ijpharm.2018.12.022.

[13] S.S. Huang, H. Liu, S.S. Huang, T. Fu, W. Xue, R. Guo, Dextran methacrylate hydrogel microneedles loaded with doxorubicin and trametinib for continuous transdermal administration of melanoma, Carbohydr. Polym. 246 (2020) 116650. https://doi.org/10.1016/j.carbpol.2020.116650.

[14] M. Leone, M.I. Priester, S. Romeijn, M.R. Nejadnik, J. Mönkäre, C. O'Mahony, W.

Jiskoot, G. Kersten, J.A. Bouwstra, Hyaluronan-based dissolving microneedles with high antigen content for intradermal vaccination: Formulation, physicochemical characterization and immunogenicity assessment, Eur. J. Pharm. Biopharm. 134 (2019) 49–59. https://doi.org/10.1016/j.ejpb.2018.11.013.

[15] S. Fakhraei Lahiji, Y. Jang, Y. Ma, M. Dangol, H. Yang, M. Jang, H. Jung, Effects of dissolving microneedle fabrication parameters on the activity of encapsulated lysozyme, Eur. J. Pharm. Sci. 117 (2018) 290–296. https://doi.org/10.1016/j.ejps.2018.03.003.

[16] P.C. Demuth, Y. Min, D.J. Irvine, P.T. Hammond, Implantable silk composite microneedles for programmable vaccine release kinetics and enhanced immunogenicity in transcutaneous immunization, Adv. Healthc. Mater. 3 (2014) 47–58. https://doi.org/10.1002/adhm.201300139.

[17] Y.C. Kim, J.H. Park, M.R. Prausnitz, Microneedles for drug and vaccine delivery, Adv. Drug Deliv. Rev. 64 (2012) 1547–1568. https://doi.org/10.1016/j.addr.2012.04.005.

[18] A. Vrdoljak, E.A. Allen, F. Ferrara, N.J. Temperton, A.M. Crean, A.C. Moore, Induction of broad immunity by thermostabilised vaccines incorporated in dissolvable microneedles using novel fabrication methods, J. Control. Release. 225 (2016) 192–204. https://doi.org/10.1016/j.jconrel.2016.01.019.

[19] H. Chang, S.W.T. Chew, M. Zheng, D. Chin, S. Lio, C. Wiraja, Y. Mei, X. Ning, M. Cui, A. Than, P. Shi, D. Wang, K. Pu, P. Chen, H. Liu, C. Xu, Cryomicroneedles for transdermal cell delivery, Nat. Biomed. Eng. (n.d.). https://doi.org/10.1038/s41551-021-00720-1.

[20] P. Nonsuwan, K. Matsumura, Amino-Carrageenan@Polydopamine Microcomposites as Initiators for the Degradation of Hydrogel by near-Infrared Irradiation for Controlled Drug Release, ACS Appl. Polym. Mater. 1 (2019) 286–297. https://doi.org/10.1021/acsapm.8b00209.

[21] S. Hernandez, E. Vigueras, Acrylated-Epoxidized Soybean Oil-Based Polymers and Their Use in the Generation of Electrically Conductive Polymer Composites, Soybean - Bio-Active Compd. (2013). https://doi.org/10.5772/52992.

[22] J. Yang, R. Bai, B. Chen, Z. Suo, Hydrogel Adhesion: A Supramolecular Synergy of Chemistry, Topology, and Mechanics, Adv. Funct. Mater. 30 (2020) 1–27. https://doi.org/10.1002/adfm.201901693.

[23] S.H. Bariya, M.C. Gohel, T.A. Mehta, O.P. Sharma, Microneedles: An emerging transdermal drug delivery system, J. Pharm. Pharmacol. 64 (2012) 11–29. https://doi.org/10.1111/j.2042-7158.2011.01369.x.

[24] R.F. Donnelly, M.T.C. McCrudden, A.Z. Alkilani, E. Larrañeta, E. McAlister, A.J. Courtenay, M.C. Kearney, T.R. Raj Singh, H.O. McCarthy, V.L. Kett, E. Caffarel-Salvador, S. Al-Zahrani, A.D. Woolfson, Hydrogel-forming microneedles prepared from "super swelling" polymers combined with lyophilised wafers for transdermal drug delivery, PLoS One. 9 (2014). https://doi.org/10.1371/journal.pone.0111547.

Chapter 3 Protein aggregation inhibition microneedle for transdermal drug delivery

3.1 Introduction

Microneedles are a viable alternative to conventional drug administration. They have various advantages, including the possibility of self-administration, painless delivery without bleeding or skin trauma, and high bioavailability.[1] Furthermore, drugs during oral and parenteral administration are prone to degradation in the gastrointestinal tract or due to first-pass hepatic metabolism.[2–4]

3.1.1 Protein aggregation for transdermal drug delivery

In a transdermal drug delivery system (TDDS), the hydrogel microneedle for drug delivery system can regulate the drug release rate (controlled release).[5][6][7][8] Additionally, owing to their high efficiency and biocompatibility. Therefore, protein delivery via microneedles is an attractive alternative in protein biopharmaceuticals.[4] However, protein aggregation is a serious problem. Under various environmental conditions such as temperature, pH, ionic strength, salt type and concentration, co-solutes, ligands, and processes in protein handling, proteins are susceptible to denaturation and aggregation.[9] During the delivery process, aggregation may reduce the effective dosage or result in increased toxicity.[10][11]

3.1.2 Zwitterionic polymers

Considering the protein aggregation aspects, the zwitterionic polymers, such as a poly-sulfobetaine (poly-SPB) in Figure 3.1, can efficiently suppress protein aggregation.[9,12–14] The Zwitterionic polymer is a sub-category of a polyampholytes group with unique

characteristics consisting of the anionic and cationic groups, commonly on the same repeating unit. The ionic groups are functional over a large pH window. Therefore, the total charge of the zwitterionic polymer in the normal state is equal to zero; poly-zwitterions overall charge neutrality exhibits a different, hybrid-like property profile. Furthermore, the zwitterionic polymer reveals a high hydrophilic property.[15] The zwitterionic polymer has similar properties to proteins.[16] In recent research, polysulfobetaines (poly-SPB) show biocompatible properties that resemble phospholipids.[17][18][19] This property likely results from the antifouling properties of poly-SPB[15], which suppress nonspecific protein binding while retaining the hydrogen-bonded network structure of water molecules at the interface of the polymer and material.[18] Hence, microneedles with poly-SPB as the core material may improve protein delivery by transporting the desired proteins in the native state, which can aid in the treatment of numerous conditions.

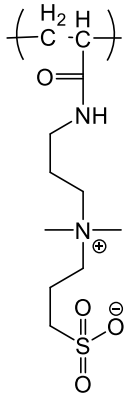

Figure 3.1 Poly-Sulfobetaine (poly-SPB)

To facilitate the fabrication of microneedles, a photolithography technique was utilized to overcome the time-consuming process and complexity of filling a female mold with a high viscosity polymer solution. Although three-dimensional (3D)-printed microneedles have high resolution and are available for different purposes, their production is time-consuming and requires expensive instrumentation and a sterilized room for processing.[20][21] These

methods are primarily of academic significance due to their small-scale preparation applications. Polymeric microneedles can be fabricated in a single step by using photomasks.[21] With the help of UV light, a photoinitiator forms cross-linked polymeric 3D microneedle structures.

Additionally, I successfully developed a biocompatible polymer using a dextran-glycidyl methacrylate/acrylic acid (Dex-GMA/AAc) hydrogel as the microneedle polymer-based material for cross-linking via photolithographic fabrication as present in chapter 2.[22][23] The sulfobetaine (SPB) monomer was combined with the Dex-GMA/AAc hydrogel network during the fabrication process to suppress protein aggregation.[9][13] Subsequently, the microneedles retained and released drugs in a controlled manner were analyzed (with a reduction in the volume of the needle degradation into the skin).

Reportedly, the efficacy of drug pre-loading of zwitterionic polymer-based microneedles in delivering therapeutic drugs (chemicals and proteins) has not been previously evaluated. In the case of protein delivery, this study was evaluated whether different proteins can be transported in a viable manner even when subjected to external stress. Furthermore, a microneedle patch was designed for drug pre-loading (50 μl) with a simple loading process (Figure 3.2). The ability to safely deliver proteins in this manner would allow a lower volume of drugs and remove refrigeration requirements. The superior characteristics of microneedles can alter the way drugs are administered and enable the development and delivery of advanced protein-based drugs for the treatment of various disorders.

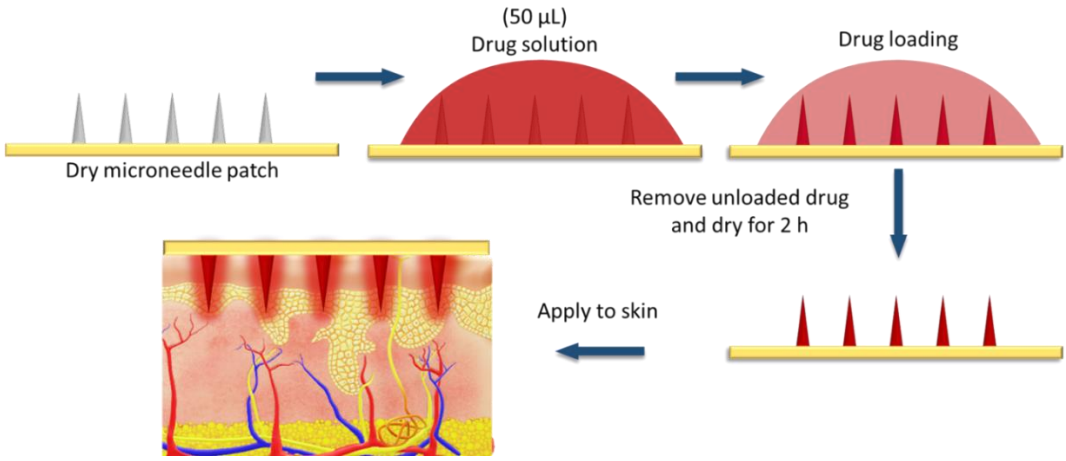

Figure 3.2 Schematic illustration of the drug loading process in the microneedle patch.

3.2 Materials and methods

3.2.1 Materials

Dextran (MW = 70 kDa) was obtained from Meito Sangyo (Nagoya, Japan). Glycidyl methacrylate (GMA) and poly (ethylene glycol) diacrylate (PEG-DA) (MW = 500 Da, number of repeating units ~ 9) were purchased from Tokyo chemical industry (Tokyo, Japan). 4-dimethylamino pyridine (DMAP), acrylic acid (AAc), ethylene glycol dimethacrylate (EGDMA), 2,2-dimethoxy-2-phenylacetophenone (DMPA), acrylated epoxidized soybean oil (AESO), insulin (bovine pancreas), human insulin, lysozyme (chicken egg white), rhodamine B, fluorescein isothiocyanate-dextran (FITC-dextran), sodium pyruvate, and β-nicotinamide adenine dinucleotide were obtained from Sigma-Aldrich (St. Louis, MO, USA). AAc was purified prior to use by passing it through an inhibitor remover column (prepacked column, Sigma-Aldrich Corp., St. Louis, MO, USA). L-Lactate dehydrogenase (LDH) from rabbit muscle was purchased from Roche Diagnostic GmbH (Germany). 2,2'-azobis (2-methylpropionamidine) dihydrochloride was obtained from Wako Pure Chemical Industries (Osaka, Japan). Sulfobetaine was donated from Osaka Organic Chemical (Osaka, Japan) and used without further purification.

3.2.2 Synthesis of Dex-GMA

Dex-GMA was synthesized using our previously reported method.[24,25] In brief, dextran (20 g) was slowly dissolved in dimethyl sulfoxide (80 mL), and the solution was stirred until complete dissolution. The transparent solution was stirred for 30 min under nitrogen gas. Then, DMAP (3.2 g) and GMA (8.8 g) were added, and the solution was purged with nitrogen gas for 30 min. The mixture was stirred at 50 °C overnight before neutralization with

hydrochloric acid. Dialysis was performed with distilled water for 7 days using a dialysis membrane (molecular weight cut-off = 3.5 kDa). The solution was dried in an oven for 48 h at 47 °C, and vacuum dried for 48 h at 25 °C to obtain the Dex-GMA derivative (a pale yellow-brown flake product). The synthesized material was characterized by ^{1}H nuclear magnetic resonance (NMR) spectroscopy (400 MHz equipped with a cryogenic probe, Bruker). The result of ^{1}H-NMR spectroscopy was used to investigate DS.

3.2.3 Synthesis of Dex-GMA/SPB/AAc resin

The hydrogel resin was prepared in a brown tube by dissolving Dex-GMA (2 g) and SPB (1 g) in distilled water (4 mL) at 50 °C and stirred for 1 h. Then, acrylic acid (3 mL) and the DMPA (100 mg) were incorporated, and the solution was stirred for 2 h at room temperature. For long-term use, the resin was covered with aluminum foil and refrigerated (4-5 °C). FTIR analysis was conducted using an FTIR spectrometer (100 PerkinElmer, 380–4000 cm^{-1}) to investigate the functional groups in the synthesized products. Characterization of the microneedles was performed using a scanning electron microscope (TM3030Plus, Hitachi, Japan) equipped with an EDX system.

3.2.4 Synthesis of Dex-GMA/AAc resin and PEG-DA resin

The Dex-GMA/AAc resin was prepared and characterized using the same method as Dex-GMA/SPB/AAc resin, without adding SPB monomer during the synthesis process but adding 1 mL of acrylic acid instead. I used PEG-DA hydrogel to compare the swelling and penetration properties with Dex-GMA/AAc based polymer. Briefly, the DMPA (10 mg) and 600 µl of PEG-DA monomer were mixed in 400 µl distilled water.

3.2.5 Synthesis of AESO resin

The AESO resin was synthesized to make the substrate for the microneedle patch. First, DMPA (2 g) was dissolved in EGDMA (20 mL), which was then combined with AESO (180 mL) in a round brown bottle and stirred for 24 h in a dark room at room temperature. The AESO resin was covered with aluminum foil and stored at room temperature. FTIR analysis was conducted using an FT-IR spectrometer (Spectrum 100, PerkinElmer, USA), and the functional groups in the synthesized products were investigated.

3.2.6 Preparation of microneedle patches

First, the substrate of the microneedle array was prepared by placing the AESO resin (70 μL) on a photomask glass slide. Then, the AESO resin drop was covered with a clear plastic slide, and a spacer of 0.2 mm thickness was placed between them. Next, the resin was cured by UV irradiation for 10 s (Figure 3.3). After curing was completed, the clear plastic was removed, and 10 s of UV irradiation was applied to harden the AESO sheet. The PDMS frame was placed on the AESO sheet and then filled with PEG-DA, Dex-GMA/AAc or Dex-GMA/SPB/AAc resin to a height of approximately 3 mm, and 20 s of UV irradiation was applied from beneath (Figure 3.3). 3D microneedle structures were generated after the UV irradiation, and the uncured resin was carefully removed from the PDMS frame using a pipette. Subsequently, the PDMS frame was removed, and the microneedle patch was collected using a knife. The microneedle patch was washed with distilled water to remove the non-polymerized monomer and immediately cured by UV for 10 s. The microneedle patches were washed again by immersing them in distilled water (200 mL) for 30 min to remove the non-polymerized

monomer. The microneedle patch was dried at room temperature and stored in a desiccator.

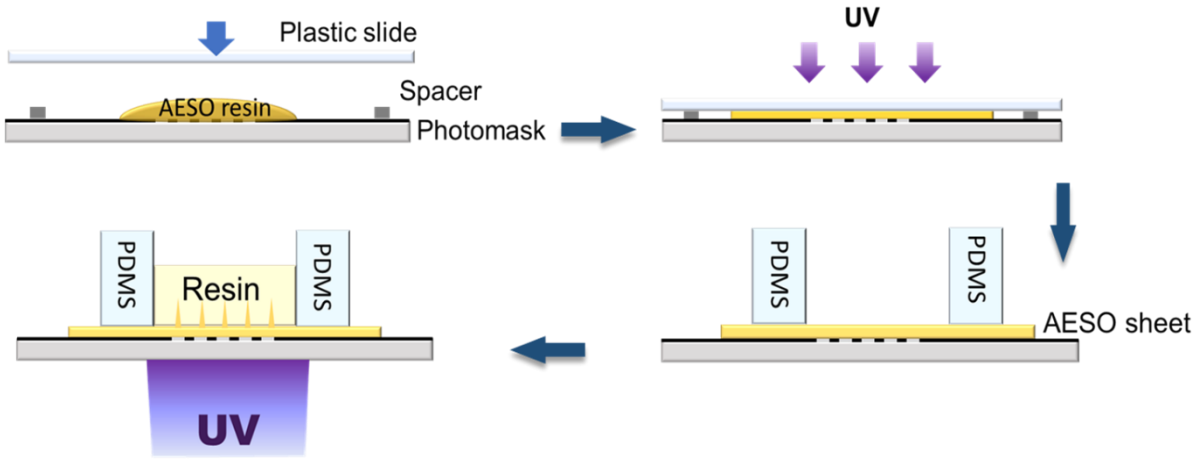

Figure 3.3 Schematic illustration depicting fabrication of microneedle arrays via inverted light UV lithography.

3.2.7 Swelling study

The water uptake of the microneedle was determined in comparison to the dried weight of the material. In this study, a hydrogel tablet was used as a model in the swelling study. The PEG-DA, Dex-GMA/AAc and Dex-GMA/SPB/AAc resin (50 μL) was poured into a cylindrical silicone mold (5 mm in diameter and 5 mm deep), and UV irradiation was performed for 10 s. The tablets were removed, rinsed with distilled water, and dried overnight in the oven at 50 °C. The dried samples were weighed (W_{dry}) and immersed in PBS at 24–25 °C for different periods. The wet samples were carefully blotted with filter paper to absorb water and then weighed again (W_{wet}). The water uptake is defined by Equation 1.

$$\text{Water uptake (\%)} = [(W_{wet}-W_{dry})/W_{dry}]x100 \qquad (1)$$

3.2.8 Microneedle mechanical property test

The maximum compressive mechanical loads for the PEG-DA, Dex-GMA/AAc and Dex-GMA/AAc/SPB microneedle patches were measured using a ZTA-1 Digital Force Gauge (IMADA, Incorp., USA). Each microneedle patch containing 41 needles on a 6 cm x 6 cm area was attached to the lower substrate. The force sensor was attached to the stepping motor with a moving speed of 30 μm/s downward to the microneedle array (Figure 3.4). During compression, the force sensor was programmed to move a further 50 μm after detecting the first microneedle failure, after which the recording was stopped.

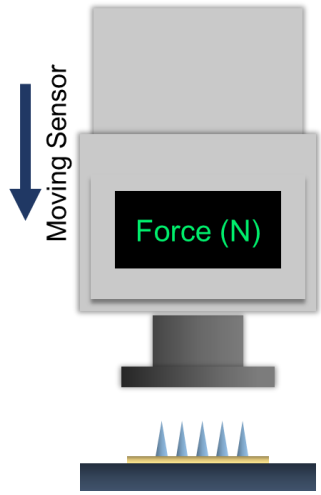

Figure 3.4 Schematic illustration of the digital force gauge measuring setup.

3.2.9 Drug loading studies

Rhodamine B was used as a model drug to calculate the chemical loading capacity of the microneedle. Rhodamine B (200 μg/mL) was prepared in PBS solution, and 50 μL was placed on the microneedle patch (Figure 3.5). For 15, 30, 60, and 90 min, the rhodamine B solution was absorbed into the microneedle at different concentrations that can be observed by the change in color of the microneedle from white to red, and the rhodamine B solution from dark red to light pink. The unloaded rhodamine B in each absorption time was rinsed with PBS (1 mL), and the collected solution was analyzed to calculate the loading capacity (Figure 3.5).

A 96-well plate micro-reader (TECAN Infinite® 200 PRO M nano+) was used to determine the rhodamine B concentration at 555 nm.

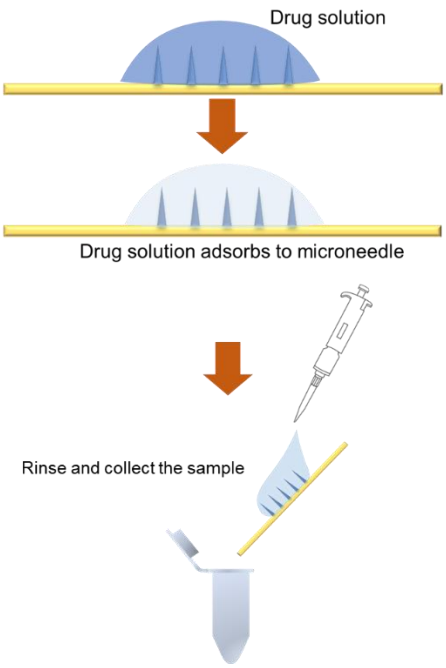

Figure 3.5 Schematic illustration of the drug loading and sample collection process.

3.2.10 Drug diffusion and release studies

The drug diffusion study used rhodamine B and FITC-dextran as a chemical drug model; rhodamine B represented low molecular weight drugs, and FITC-dextran represented large molecular weight drugs. An artificial skin model was prepared using 1% agarose. Agarose (1 g) was dissolved in PBS (100 mL), heated in a microwave for 30 s, and stirred for 1 min. The agarose solution was poured into a plastic cuvette and refrigerated overnight before use. The chemical model drug was prepared using rhodamine B (0.04% w/v) in distilled water. Then, rhodamine B solution (50 µL) was placed on the dry microneedle patch, and the microneedle was allowed to absorb the solution for 15 min. The unabsorbed solution was rinsed

with methanol (500 μL) and dried at room temperature overnight. Rhodamine B was diffused in the agarose gel, and images were acquired every 30 s for 1 h at room temperature. However, the rhodamine B release study was performed using PBS solution (1 mL), and the microneedle-loaded rhodamine B was prepared as before (diffusion study). A microplate reader was used to determine the rhodamine B concentration release at 555 nm using a UV–VIS spectrophotometer (TECAN Infinite® 200 PRO M nano+). FITC-dextran (10 kDa; 1% w/v), was prepared by dissolving FITC-dextran (10 mg) in PBS solution (1 mL). The FITC-dextran (50 μL) solution was placed on the microneedle patch for 15 min and rinsed with distilled water (1 mL). A fluorescence microscope (Keyence, Japan) was used to study the diffusion pattern of FITC-dextran into the gel.

3.2.11 Protein loading

In this study, lysozyme and insulin (bovine pancreas) were prepared at the same concentration (1 mg mL^{-1}) in PBS with a pH of 7.4 and 2, respectively, before being loaded onto the microneedle patch. Both solutions were prepared 1 h before use. The protein solutions (50 μL; 50 μg) were placed on the dry microneedle patches and were absorbed into the hydrogel microneedle for 30 min and 60 min in a closed container. The unabsorbed protein solution was rinsed with the respective PBS solutions (1 mL) for lysozyme and insulin, and the solutions were collected for further measurements. I used the collected solutions (20 μL), PBS (80 μL), and Bradford dye agents (100 μL) to determine the protein concentration at 595 nm in a 96-well plate reader. The loaded microneedle patches were stored in an incubation oven at 37 °C for 24 h before the drug release study.

3.2.12 Protein Release Study

A protein release study was performed in a buffer solution in a plastic tube (1.5 mL). The protein-loaded microneedle patches were immersed in PBS (pH 7.4; 1 mL) for lysozyme and insulin (pH 2; 1 mL) (Figure 3.6). The released proteins were collected (20 µL) at 1, 2, and 6 h. The samples were assayed using PBS (80 µL) and Bradford dye agent. The concentrations were determined at 595 nm in a 96-well plate reader. The Bradford protein assay calculated the released protein concentrations.

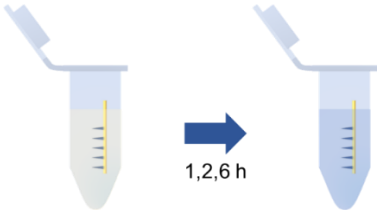

Figure 3.6 Schematic illustration depicting the drug release and sample collection process.

3.2.13 Bradford protein assay

The Bradford protein assay rapidly measures protein concentration within a low concentration range (1–1000 µg mL^{-1}).[26] The 96-well plates were used to measure a small volume (200 µL). After the protein was bound with Coomassie dye, the absorbance shifted from 465 nm to 595 nm. A microplate reader (TECAN Infinite® 200 PRO M nano+) was used to determine the protein concentration at 595 nm.[27]

3.2.14 Determination of protein protection within the microneedle materials:

LDH from a rabbit muscle was used in this experiment because it easily aggregates and loses activity after heat treatment at 40 °C for 1 h.[28] For the analysis, LDH (1.78 nM) solution

in PBS was loaded onto Dex-GMA/SPB/AAc and Dex-GMA/AAc polymers and then heated at 45 °C for 1 h (for denaturation). The protein released from hydrogels with and without poly-SPB was analyzed to evaluate the protective nature of SPB-containing hydrogels. This assay is of clinical importance, as several dehydrogenases are present in the human serum. LDH is cytoplasmic, and all tissues contain one or two of the five possible isoenzymes.[29] In this enzymatic assay, the conversion of pyruvate to lactate (Equation 2) was used to determine the kinetic enzyme activity; the reaction was monitored by recording the decrease in absorbance at 340 nm.[30] LDH was loaded onto Dex-GMA/AAc, and Dex-GMA/SBP/AAc dried polymers for 1 h; then, the samples were rinsed with PBS to remove the unloaded enzyme. The protein-loaded polymer was then incubated at 45 °C for 1 h. The incubated polymers were immersed in PBS (1 mL) for 60 min, which released the enzymes into the buffer. Consequently, a sample (50 µL) from the buffer was mixed with sodium pyruvate and NADH solution (150 µL), and absorbance was measured at 340 nm for 10 min using a microplate reader.

$$\text{Pyruvate} + \text{NADH} + \text{H}^+ \xrightarrow{\text{Lactate dehydrogenase}} \text{L} - \text{Lactate} + \text{NAD}^+ \qquad (2)$$

3.2.15 Fibril Formation of Human Insulin

The human insulin 10 mg mL^{-1} in PBS (pH 7.4) was loaded onto the dry Dex-GMA/AAc, and Dex-GMA/AAc/SPB polymerized sheets in the ratio of 1 µl of solution per 1 mg of materials. After one hour, the loaded insulin hydrogel sheets were rinsed with PBS to remove unloaded insulin, then dried and heated at 45 °C for 72 h. Next, the dried-polymer sheet was immersed in 500 µL of PBS to extract the insulin from each material. A ThT assay was used to determine the fibril formation in human insulin. The binding of ThT to β-amyloid fibrils leads to an increase in fluorescence intensity.[12] The concentration of insulin in the released solutions was initially calculated using the Bradford assay and adjusted to the same

concentration for the ThT assay. Briefly, the stock solution was prepared by adding 8 mg ThT to a 10 mL PBS solution (pH 7.4) and filtered with a 0.22 μm filter. The working solution was prepared by adding 1 mL of stock solution to 49 mL of PBS. Subsequently, 150 μL of the test solution was mixed with 2 mL of the ThT solution, and the fluorescence was measured using a JASCO FP-8600 spectrometer with an excitation wavelength of 450 nm and emission wavelength of 485 nm.

3.2.16 Parafilm penetration profile

The microneedle penetration pattern was observed using Parafilm M (Bemis Company Inc., Neenah, WI) as a skin model; the 16 layers of Parafilm M were stacked and pressed together. The microneedle patches were attached to the flat surface and pressed on the stacking parafilm by thumb until all microneedles penetrated the parafilm.

3.2.17 Porcine skin insertion

The rhodamine B loaded onto the Dex-GMA/AAc/SPB microneedle patch from the drug diffusion and release studies section was utilized to determine microneedle insertion depth and drug diffusion. The microneedle patch was applied *in vitro* to porcine skin. For porcine skin preparation, briefly, the fresh porcine skin was cut to 3 cm x 3 cm with 5 mm thickness and frozen at -20 °C. Before use, the frozen porcine skin was thawed in a Ziploc bag at room temperature for 30 min. The microneedles patch was attached to the Tegaderm^{TM} tape and pressed on the porcine skin by thumb for 30 s (Figure 3.7). After 30 min, the microneedle patch was removed, and the cross-section was cut along the microneedle array. The images were captured from the top and side views under white and UV light.

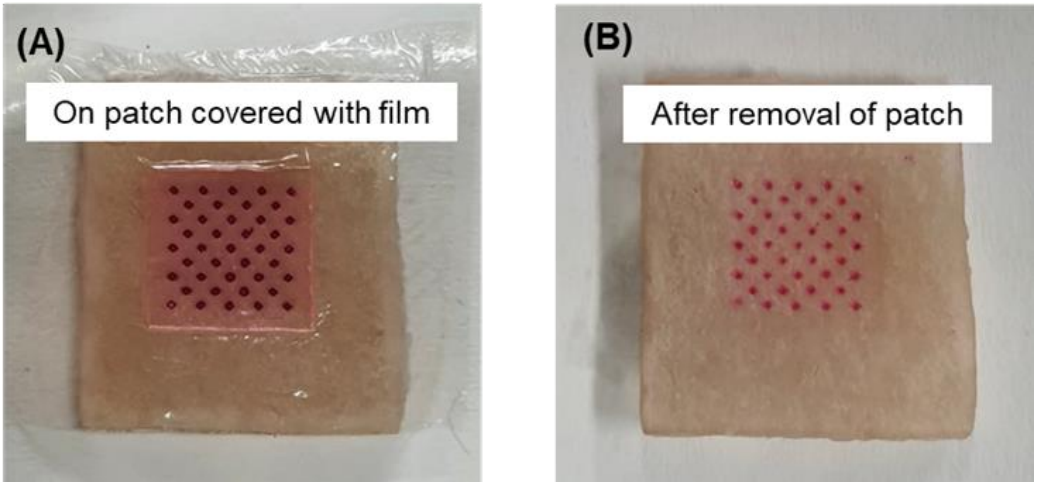

Figure 3.7 A) The rhodamine B loaded microneedles patch insertion onto porcine skin and covered with Tegaderm TM tap, B) the porcine skin after removing microneedles patch (After 30 min insertion).

3.2.18 Cytotoxic assay

L929 (American Type Culture Collection, Manassas, VA, USA) cells were cultured in Dulbecco's modified Eagle's medium (Sigma-Aldrich, St. Louis, MO), supplemented with 10% heat-inactivated fetal bovine serum in a humidified atmosphere of 5% CO_2 at 37 °C. Before *in vitro* cytotoxicity testing, 20 mg of dry polymerized materials were immersed in 1 mL cell culture medium. Extraction was performed in the cell culture incubator at 37 °C for 24 h. The original extracted solutions (100%) were then diluted in a culture medium to obtain a series of dilutions with 50, 25, 12.5, and 6.25% concentrations. The cytotoxicity assay was performed according to the MTT method in a 96-well plate. Briefly, 1×10^3 cells in 0.1 mL of culture media were seeded in a 96-well plate. After incubation for 72 h, 0.1 mL of the culture medium, which contained different concentrations of the extracted polymers, were added to the 96-well plates. After re-incubation for 24 h, 0.1 mL of the MTT solution (300 μg/mL) was added to each well, and the cells were incubated for an additional 3 h. After discarding the media, 0.1 mL of DMSO was added to dissolve the purple formazan crystals that had formed.

The number of viable cells was determined at 540 nm. In addition, the cytotoxicity of Dex-GMA and PEG-DA monomer were also investigated; 0.1 mL of monomers of different concentrations were added to the cells and cytotoxicity was evaluated using a similar procedure as mentioned above.

3.3 Results and discussion

3.3.1 Synthesis and Characterization of Dex-GMA/AAc and Dex-GMA/SPB/AAc

The polymerization of Dex-GMA with AAc or AAc/SPB was initiated with UV (0.3 $mWcm^{-2}$) to obtain a hydrogel 3D structure. Figure 3.8 shows the Fourier-transform infrared (FTIR) spectra of Dex-GMA/AAc, Dex-GMA/SPB/AAc, and Dex-GMA/SPB polymers. Compared with Dex-GMA/AAc, the characteristic peak of the sulfobetaine polymer was present only in the Dex-GMA/SPB/AAc and Dex-GMA/SPB polymers. The most significant peak was 1150 cm^{-1} (S=O stretching).[31] The observed spectra in Figure 3.9 represent the result of Energy Dispersive X-ray (EDX) analyses. Results clearly show the presence of sulfur in Dex-GMA/SPB/AAc, which further confirms the cross-linking of SPB with Dex-GMA structure.

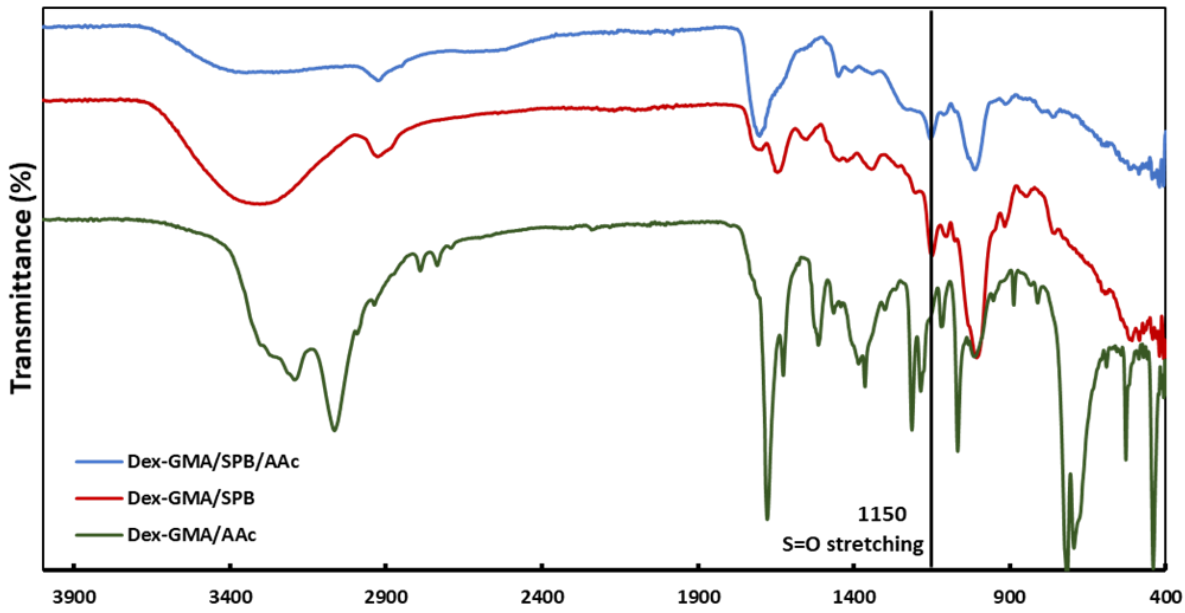

Figure 3.8 FTIR spectra of cured Dex-GMA/SPB/AAc, Dex-GMA/SPB, and Dex-GMA/AAc.

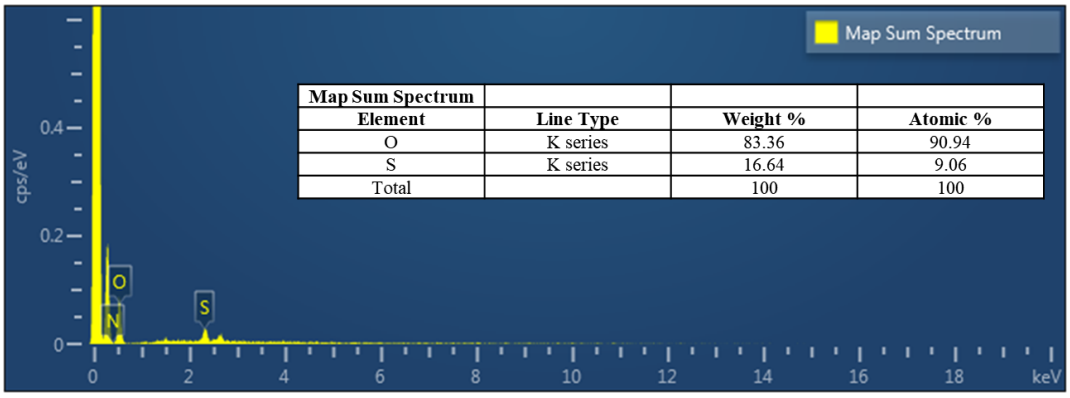

Map Sum Spectrum			
Element	Line Type	Weight %	Atomic %
O	K series	83.36	90.94
S	K series	16.64	9.06
Total		100	100

Figure 3.9 EDX spectra of Dex-GMA/SPB/AAc microneedle.

3.3.2 Microneedle Fabrication Process

To avoid loading the drug into the microneedle substrate (backing), a non-water-absorbing AESO resin was used for the microneedle backing layer. In comparison, the needle material is a highly absorbent material (Dex-GMA/AAc). Therefore, the drug solution will solely absorb into the needle parts during the loading process. First, the microneedle array was fabricated on a clear and flexible AESO sheet. The AESO resin

(approximately 70 μL) was placed at the center of the photomask glass slide (four-point star-shaped micro-sized windows in an area of 6 mm x 6 mm (Chapter 2, Figure 2.19), and then a clear polyurethane (PU) plastic sheet with a spacer (200 μm) was positioned on the photomask. After 10 s of UV irradiation from the top, the PU plastic sheet was removed, whereas the AESO sheet remained attached to the photomask glass slide. The thickness of the microneedle substrate sheets was fixed at ~200±20 μm to control the UV light intensity passing through the micro-sized windows and ensure that the microneedle length, height, and shape were maintained. Next, the PDMS frame was placed tightly on the AESO sheet to avoid resin leakage during fabrication. The PEG-DA, Dex-GMA/AAc or Dex-GMA/SPB/AAc resin was poured into the PDMS frame (~3 mm in height), and it was ensured that no bubbles were formed in the resin matrix (Figure 3.3).

The microneedle height and base were controlled by applying UV irradiation for 15 s for PEG-DA and 20 s for the Dex-GMA/AAc and Dex-GMA/SPB/AAc resin. This created microneedles with an average height and base of 600 μm and 300 μm (Figure 3.10 A-D, which is sufficiently long enough to penetrate the stratum corneum layer in the epidermis.[32,33] Figure 3.10C illustrates the dry microneedle patch size compared to a hypodermic needle (for intramuscular injection). Here, the microneedle width is four times narrower than the hypodermic needle.

The four-point star-shaped microneedle (Figure 3.10 D) was designed to reduce the wound size at the insertion site compared to those with a cone or pyramid-shaped base. The star-shaped microneedle has a higher surface area than those with a square or circular base of the same dimension. The removal of the microneedle from the parafilm confirmed the small shape and size of the imprint left by the needle (Figure 3.10 E-F).

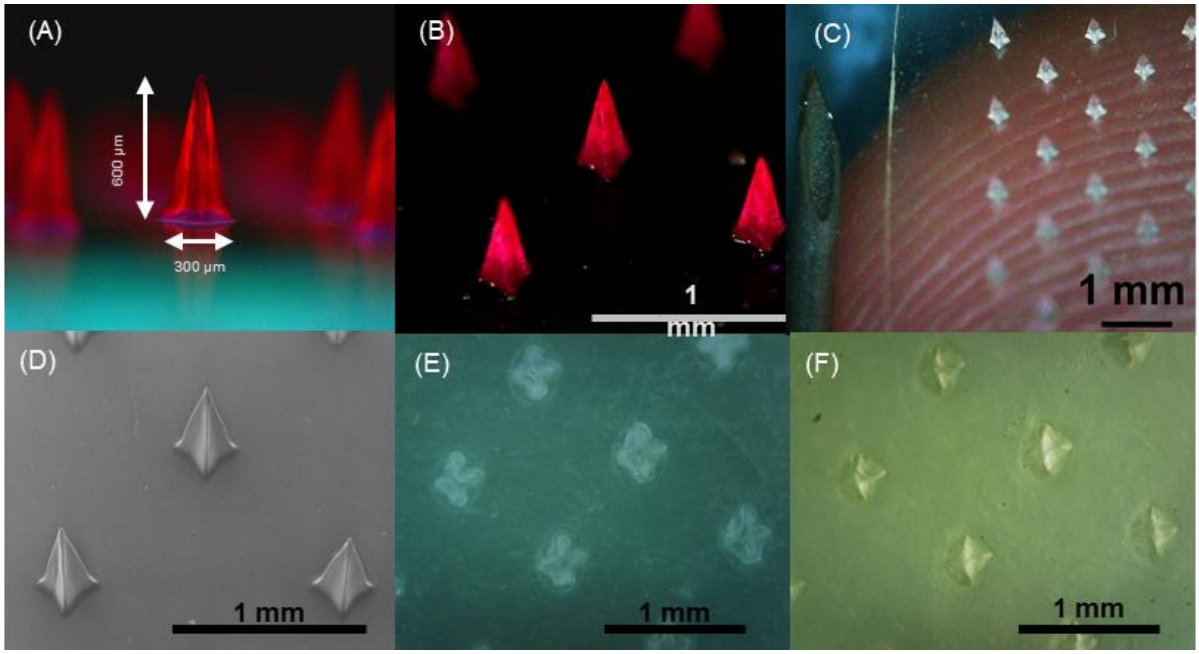

Figure 3.10 A) The side-view image of rhodamine B loaded microneedle. B) The bird's-eye view image of rhodamine B loaded microneedle. C) Microneedle and hypodermic needle with a fingertip for size comparison. D) SEM image. Photographs of parafilm after insertion of the four-point-star-shaped microneedle, E) the photograph captured during the light source project direct to the parafilm, and F) the light source project direct from behind the parafilm.

3.3.3 Swelling Study

In this study, poly(ethylene glycol) diacrylate (PEG-DA) was utilized as a standard polymer for comparing the swelling properties of the Dex-GMA/AAc based polymers for the water uptake study.[34–36] The water uptake was calculated using Equation (1) and was depicted in Figure 3.11. The water uptake was approximately 30% for PEG-DA, 65% for Dex-GMA/AAc, and 120% for Dex-GMA/SPB/AAc after 10 min, which increased to 160% after 6 h for both Dex-GMA/AAc and Dex-GMA/SPB/AAc, whereas PEG-DA merely had 60% water uptake after 6 h. PEG-DA exhibited swelling three times lower than the Dex-GMA-based polymers even though they had the same water content ratio in the resin solution. Therefore, the PEG-DA

would not function in the pre-loading and releasing drug studies because the material would have difficulty adsorbing the drugs.[35] The swelling rate of the Dex-GMA/SPB/AAc microneedle, which reached its maximum expansion in 1 min, was higher than that of the tablet because of its thinner shape. The maximum size expansion was ~160% from the dry samples to the hydrogel microneedles.

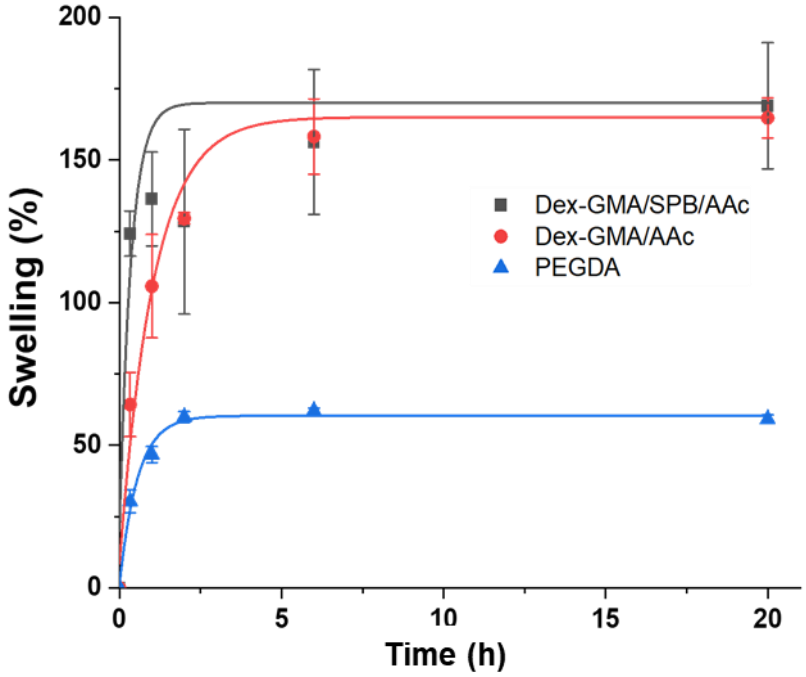

Figure 3.11 Swelling ratio of the hydrogel. Mechanical properties testing.

3.3.4 Microneedle Mechanical Properties

The dry polymer for the microneedle patches was attached to the lower stage. Force was applied to the microneedles up to and past their mechanical failure point. Figure 3.12 shows the force-displacement curve. It shows that after failure has occurred and when the applied force does not increase, the displacement of the force sensor is nevertheless moving downward to the microneedle patch. This investigation shows that

the PEG-DA and Dex-GMA/AAc microneedles were bent rather than broken or shattered. The failure occurred at 275 μm at a low compression force of 0.225 N and 0.325 N, respectively. In contrast, the Dex-GMA/SPB/AAc microneedle failed at 1.35 N at 350 μm, and its failure resulted in broken and shattered needles (Figure 3.13).

Although high mechanical strength is a requirement of microneedles to break through the skin barrier, in this study, the Dex-GMA/SPB/AAc microneedles with four-point star shapes require less mechanical strength for skin penetration than others due to their sharp tip and thin wings (Figure 3.10D).[37–40] The microneedle was performed insertion testing on a porcine skin model. The test was conducted only with Dex-GMA/AAc/SPB microneedles. The loaded rhodamine B microneedle patch was attached to thin paper to hold the patch above the porcine skin. The four-point star-shaped microneedles easily penetrated the skin with less compression distance when applying a compressive force. The microneedle will minimize outer skin damage according to its thin four-blade wings and sharp tips (Figure 3.10 E–F).

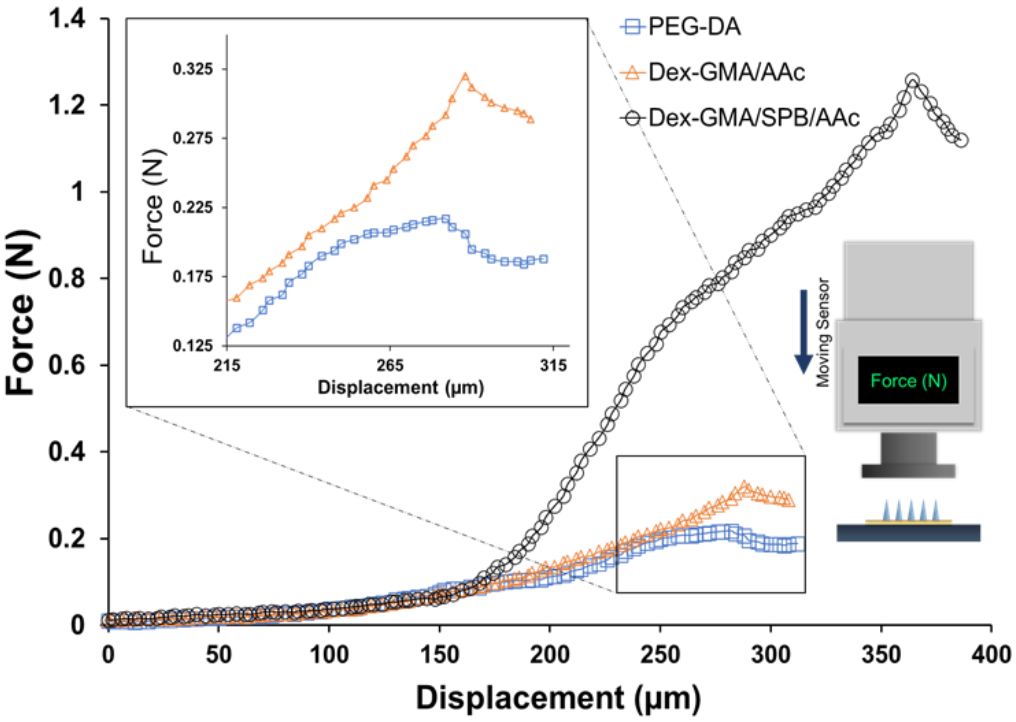

Figure 3.12 Force-displacement curve obtained from the compression testing of microneedles patches; the right-hand side shows the compression set-up.

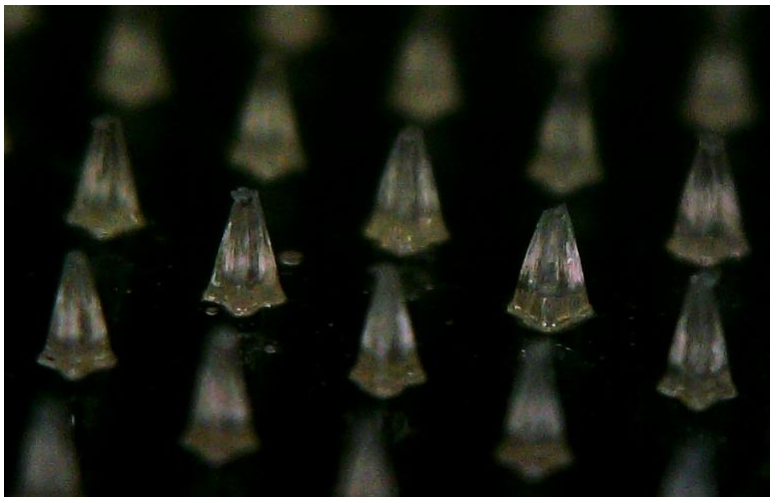

Figure 3.13 Photograph of failure Dex-GMA/SPB/AAc microneedles presented the broken and shattered needles after compression.

3.3.5 Drug Loading Capacity

Herein, a versatile microneedle was developed for a water-soluble drug, which controls drug delivery by varying the initial drug loading concentration or releasing time. In this study, rhodamine B was used as a low molecular weight model drug to demonstrate the efficacy of the microneedles in loading and releasing drugs in a controlled manner.[35,41] The polyacrylic-acid constituent in the Dex-GMA/AAc/SPB microneedles has a high water uptake capability (super absorbent) suitable for drug loading and releasing in this study.[42] Rhodamine B solution (200 μg mL^{-1}, 50 μL) was placed on the Dex-GMA/AAc/SPB microneedle patch (Figure 3.14C, t = 0 min). The solution was allowed to be absorbed into the microneedles for 15, 30, 60, and 90 min. The color of the microneedle changed from white to red, and the rhodamine B solution turned from dark red to light pink (Figure 3.14C, t = 30 min). The microneedle loading capacity was measured by rinsing off the unabsorbed rhodamine B using PBS (1 mL). Using the extinction coefficient calculated with the help of the rhodamine B calibration curve and a microplate reader at 555 nm, the rinsed PBS (200 μL) was analyzed to determine the remaining drug concentration (unloaded drug). The initial loading amount of rhodamine B was 10 μg (in 50 μL) for each microneedle patch; this was used to calculate the drug loading along with the amount of unloaded drug.

Figure 3.14C illustrates that the rhodamine B loading increased over time and reached 80% (8 μg) at 90 min exposure with 41 needles (≈ 2 mg). Based on this observation, This technique can be used to load therapeutic drugs, such as doxorubicin hydrochloride[37] and fentanyl (pain killer drug)[43], as they are water-soluble and their molecular weights are quite similar to that of rhodamine B.

3.3.6 Drug Release

In this study, the maximum rhodamine B loading was 2 μg patch^{-1} because of the limitations of real-time measurement and maximum concentration. The loaded rhodamine B microneedles were first oven-dried at 50 °C for 2 h and immersed in PBS (1 mL) for different times up to 6 h. The microneedle patches were removed from PBS, and the rhodamine B content in PBS was determined using a microplate reader at 555 nm. The cumulative rhodamine B release increased over time and reached a maximum in the first hour (Figure 3.14D). In the first hour, the release rate was constant at 1.5 μg h-1 and reached a plateau at 80%, caused by the equilibrium of rhodamine B concentration in the PBS and the microneedle array. These results unambiguously show that microneedles can efficiently load and release water-soluble drugs in a controlled manner without the need for additional drug carriers; therefore, Dex-GMA/SPB/AAc has a higher release rate than PEG-DA and Dex-GMA polymer-based materials. Several research groups have shown a higher drug release for these materials, but it took them more than 48 h to reach 80% release.[34][37] In terms of administering a higher dosage of the drug in a short period, the number of microneedles per patch could be increased up to 100 needles where the loading capacity would be approximately 20 μg, and the release rate would be up to 16 μg h^{-1}.

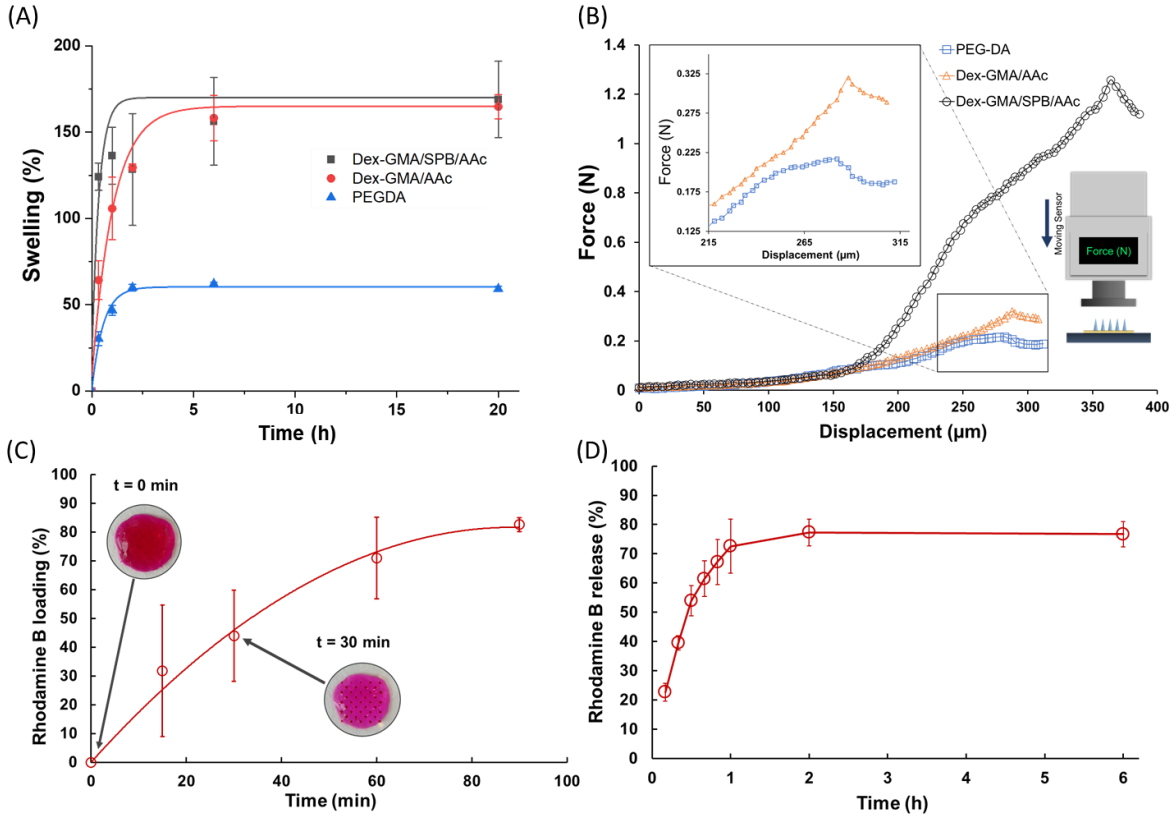

Figure 3.14 A) Swelling ratio of the hydrogel. Mechanical properties testing B) Force-displacement curve obtained from the compression testing of microneedles patches; the right-hand side shows the compression set-up. C) The rhodamine B loading capacity; at t=0 min shows the dark pink color of the solution, and t=30 min shows the light pink color of the solution. D) Cumulative rhodamine B release over time.

3.3.7 Drug Diffusion Study

The ability of the developed microneedles to release the desired drug upon skin application was evaluated. This study used rhodamine B (40 μg mL-1) as a drug model to represent low molecular weight drugs. It was diffused in 1% agarose gel in PBS in preparation for the diffusion study and refrigerated overnight before use.[44][32] The rhodamine B-stained microneedle array was divided into four needles per row and was

gently placed on the agarose gel. The pictures of the rhodamine B diffusion were captured every 30 s for 1 h at room temperature, as shown in Figure 3.15. As the rhodamine B concentration was higher in the microneedle, it diffused within the gel in all directions where the concentration was lower. The diffusion was observed up to a distance of ~0.5 mm in 10 min, and ~1 mm in 20 min (The diffusion rate was approximately 3 mm h^{-1}).[45] Moreover, the needle shape changed from triangle to lotus-like (Figure 3.16) when the microneedle base was fixed in the substrate and could not expand. After 20 min, the microneedle tips and wings became clear gel instead of dark pink when rhodamine B completely diffused into the agarose gel.

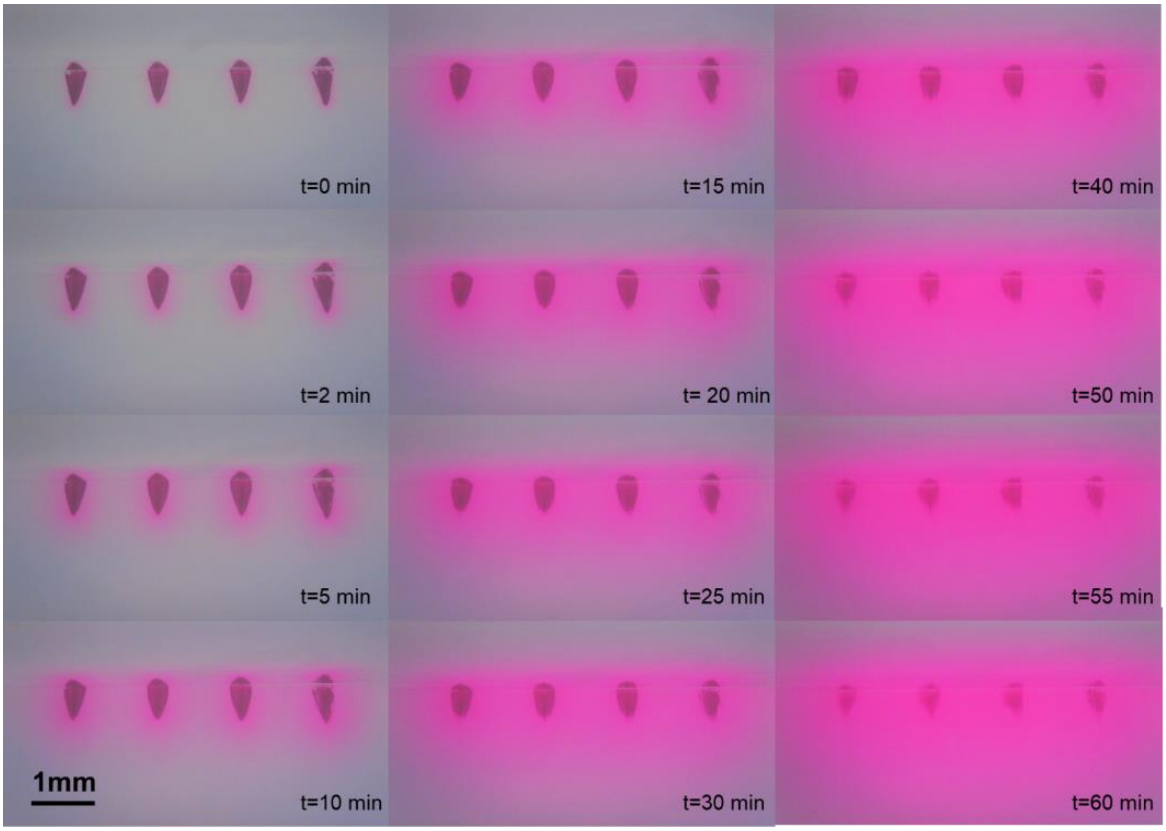

Figure 3.15 The time lap of rhodamine B diffusion in 1% agarose.

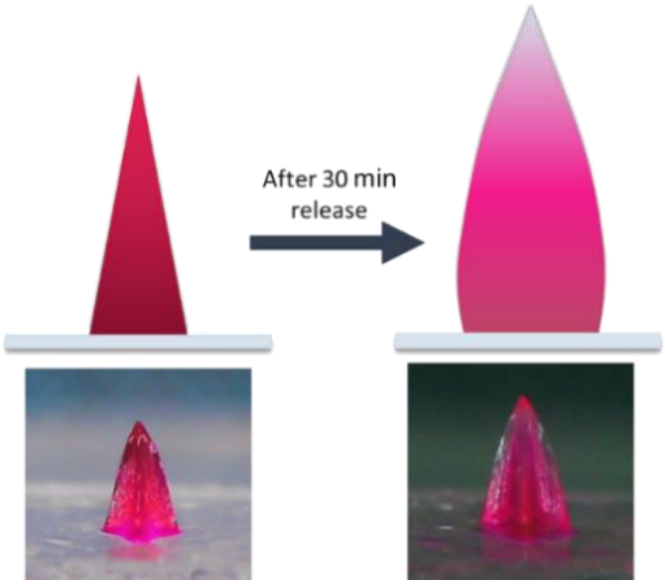

Figure 3.16 Microneedle shape after rhodamine B solution uptake. The microneedle shape changed from pyramidal to lotus-like.

Fluorescein isothiocyanate (FITC)-dextran (1% w/v) was loaded onto the dry microneedle using the same method as that for rhodamine B. A single microneedle was inserted into the agarose gel (1%) in PBS to release the fluorescent dye. FITC-dextran was employed to represent drugs with a molecular weight higher than 10 kDa. Figure 3.17 shows the dry microneedle before gel insertion. Here, the fluorescence indicated that FITC-dextran was present inside the microneedle at a high concentration around the tip area. Figure 3.17 also depicts the microneedle within the gel and the time-lapse images in which FITC-dextran gel diffusion was observed. At 10 min, FITC-dextran diffused out of the hydrogel microneedle but was located around the needle. However, after 15 min, FITC-dextran diffused in all directions within the gel. Thus, the model drug analysis suggested that this system can be used to deliver therapeutic proteins like insulin (6 kDa) and low molecular weight antibodies.[46]

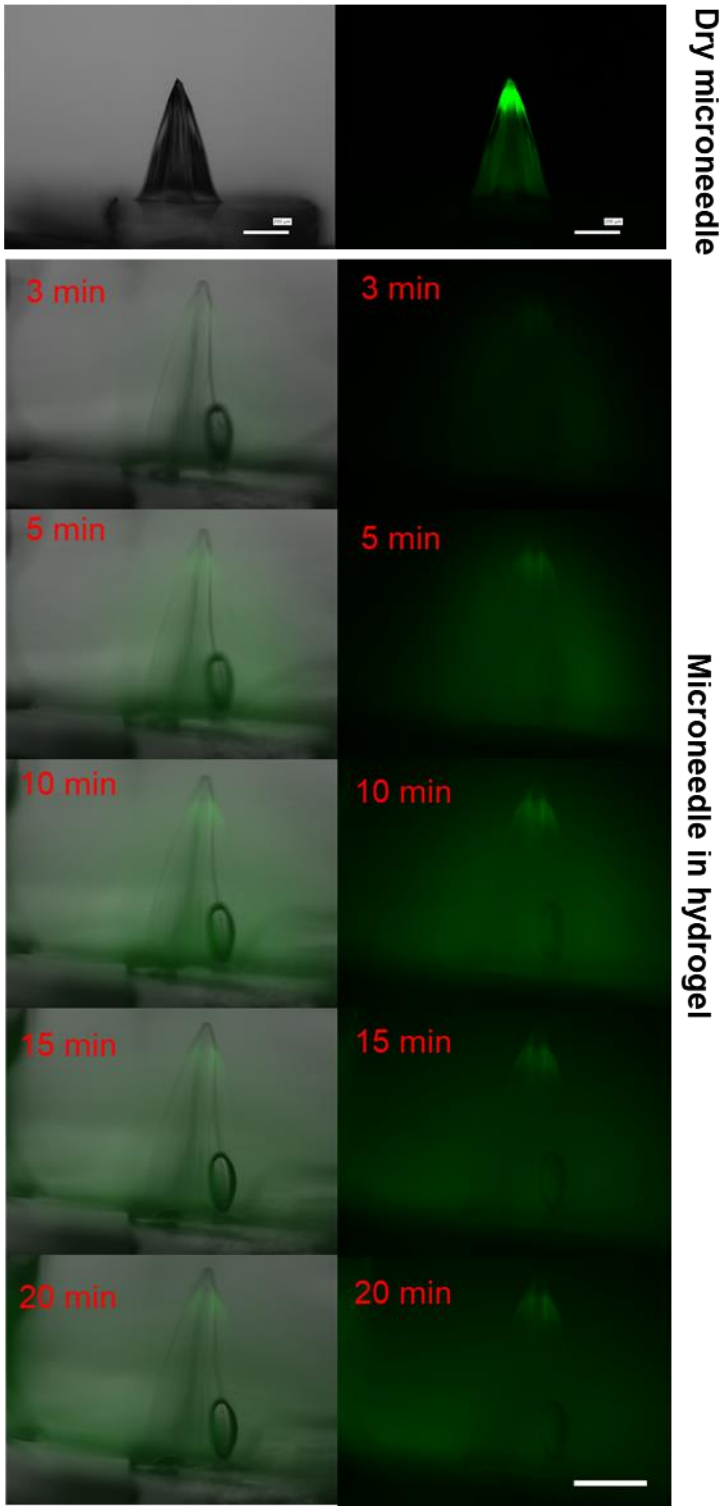

Figure 3.17 Time lap of the dextran-FITC diffusing from microneedle insertion into 1% agarose; the left-hand side shows the combination of fluorescent and bight field pictures, and the right-hand side shows only fluorescent pictures.

3.3.8 Skin Penetration of Microneedle Patches

The skin penetration performance of the microneedle patch was tested on porcine skin. The rhodamine B-stained microneedle patch prepared as mentioned in section 3.2.17 was applied onto porcine skin and covered by Tegaderm^{TM} tape for 20 min. After removing the microneedle patch, the cross-section image and top-view (Figure 3.18C–F) showed the wounds on the porcine skin.[47] Figure 3.18C and 5D were captured under white light, and Figure 3.18E and 5F were captured under UV light to observe the rhodamine B diffusion pathway. The yellow-dotted lines in Figure 3.18F indicated where microneedles pierced the skin. The rhodamine B had diffused approximately 500 μm from the needle into the fatty layer. This clearly shows that the concept of pre-drug loading can be easily applied in animal testing.

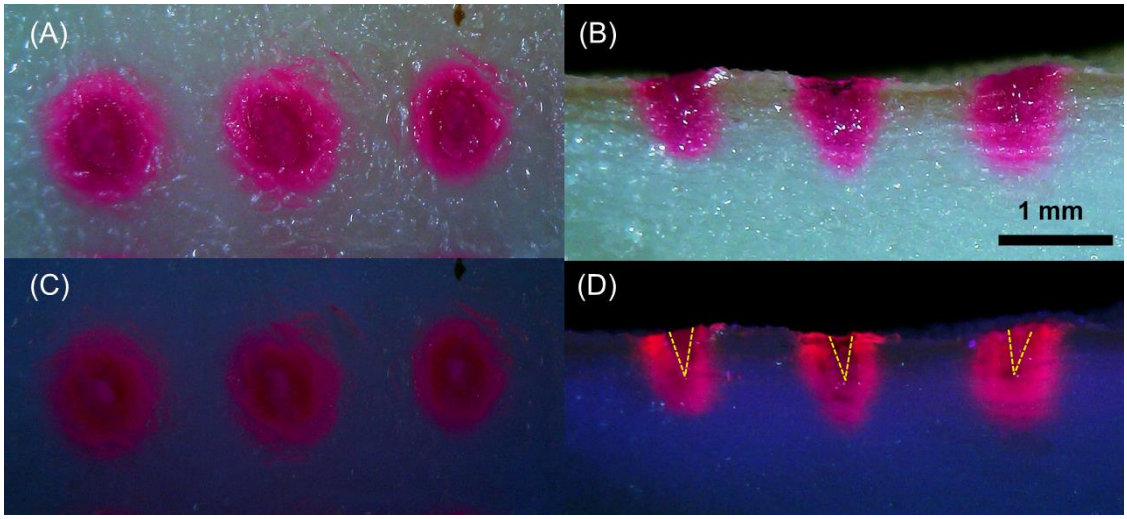

Figure 3.18 The penetration and diffusion testing of microneedle rhodamine B loaded on porcine skin. A) the picture shows the top-view, and B) the picture shows the side-view of cross-section; A) and B) were taken under white light; C) and D) were taken under UV light. The yellow dot lines indicate where the needles pierced the porcine skin, and the pink color represents the rhodamine B diffusion in 20 min of the microneedle insertion before removal.

3.3.9 Protein Loading

To evaluate the protein loading capacity of the microneedles, bovine insulin and lysozyme were considered. The bar graphs in Figure 3.19 show the amount of protein loaded from the original 50 μg dropped onto the microneedle patch. Both lysozyme and insulin could be loaded at almost the same capacity into 1.8±0.2 mg of the dry microneedle section. For loading times of 30 min and 60 min, the loading weights were calculated 26 μg (~52%) and 35 μg (~70%) respectively in microneedles in the case of the lysozyme (Figure 3.19A). The loading capacity for bovine insulin was 26 μg (~52%) and 33 μg (~66%) at 30 min, respectively. This was slightly lower than the lysozyme loading capacity at 60 min and is probably caused by an instability of polyacrylic-acid side chains at a solution pH of 2 (Figure 3.19B). Reportedly, protein loading capacity onto hydrogel microneedles after fabrication has not been previously evaluated. In other studies, the insulin solution was sprayed onto the frozen hydrogel microneedles; the insulin coated 80 μg per patch (100 needles).[46] Traditional protein-coated stainless-steel microneedles were found to have a protein loading capacity of 10–20 ng per needle, which is lower than in this study.[48]

3.3.10 Protein Release

Bovine insulin and lysozyme were utilized to estimate whether the microneedles can release proteins. The line graphs in Figure 3.19 show the proteins released related to the initial feeding % in different pH conditions.[49] After lysozyme loading (60 min), at 6 h, a release weight of 16 μg was observed, which was ~32% of the original load. However, with 30 min loading time, after 6 h, 14 μg was released, which was ~28% of the original load (Figure 3.19A). The 60 min loading time for lysozyme showed a higher

release rate than the 30 min loading time, especially in the first two hours of protein release (Figure 3.19A).

In contrast, the bovine insulin with loading times of 30 min and 60 min (Figure 3.19B) showed the same release rate in the first two hours, even though at 60 min it showed a higher loading capacity. After 6 h, the accumulated insulin released slightly increased to 20% of the original load solution. Here, bovine insulin was prepared in a 1 M phosphate buffer solution (pH 2). Therefore, while the microneedles were absorbing and releasing bovine insulin, the polymer network expanded less because the polyacrylic-acid side chains were neutral (pH 2) rather than anionic (at original powder), which blocks the absorption and release of bovine insulin. For transdermal applications, the outermost skin-surface (stratum corneum) pH is in the range of 4.1–5.8 [50,51], with the pH increase in the epidermis and dermis layer. From the swelling results, the Dex-GMA/SPB/AAc microneedle can rapidly absorb liquid from the interstitial fluids under the skin (pH of 6.6–7.6[52]), which can cause the acrylic-acid side chains to become anionic and increase the release rate. In this study, the microneedles could be used for protein delivery, which suggests the possibility that one can load and deliver therapeutic proteins to treat disorders that cannot otherwise be treated with conventional drugs.

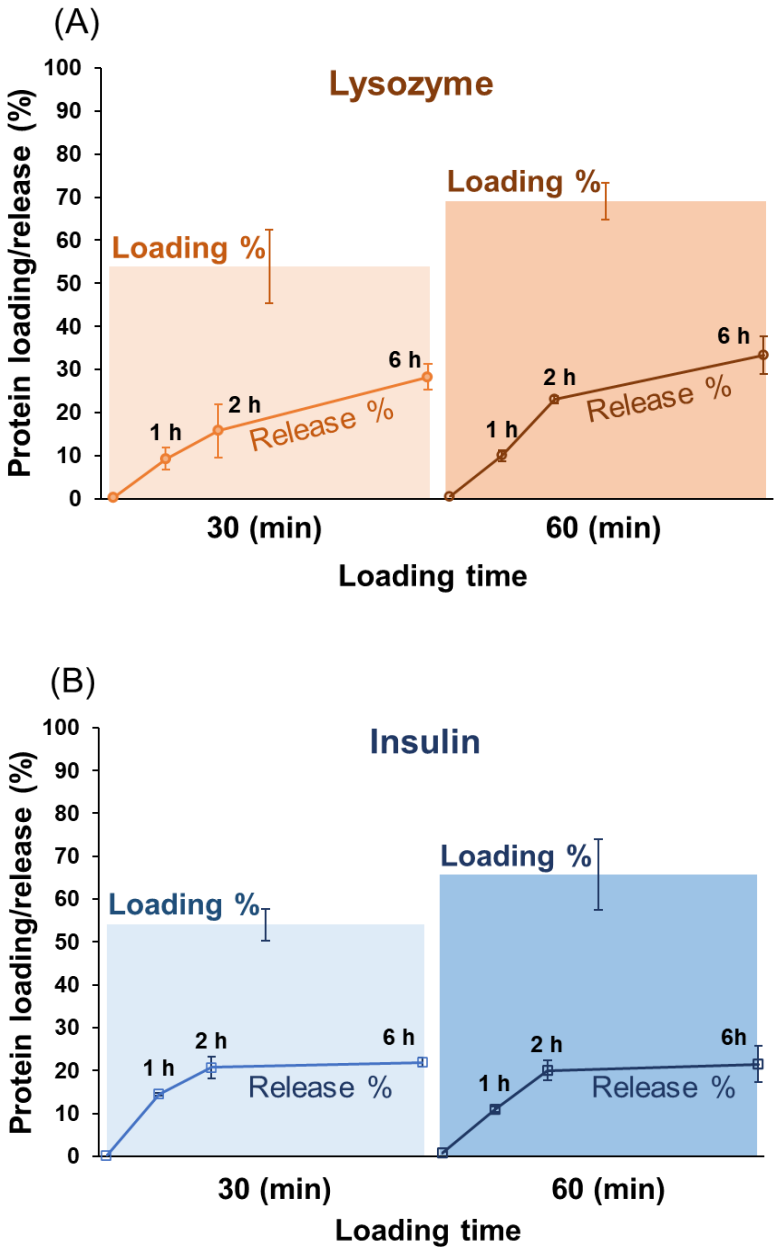

Figure 3.19 The protein loading and release at different pH values, A) extent of lysozyme loading percent at pH 7.4 to microneedles (bar graph) and the release to PBS (line graph), B) Insulin loading percent at pH 2 to microneedles (bar graph) and the release percent (line graph).

3.3.11 Dex-GMA/SPB/AAc Microneedles Avoid Protein Denaturation

Additionally, it could be confirmed that SPB side chains efficiently preserve the loaded proteins in their native state within the microneedle. For the preliminary investigation of protein denaturation by heating at 45 °C for 1 h during the delivery process, lactate dehydrogenase (LDH) was used as a model protein because LDH residual activity can be monitored even at extremely low concentrations.[28] When β-NADH is oxidized to β-NAD by pyruvate in the presence of LDH, the absorbance decreases. Consequently, the rate of decrease in absorbance was used to calculate the residual LDH activity, in which a rapid decrease indicated higher residual activity of LDH. The change in absorbance per min at 340 nm after 20 min suggested that LDH in loading Dex-GMA/SPB/AAc had higher activity than that of Dex-GMA/AAc (Figure 3.21) in both cases of heated and non-heated materials. The protein-loaded polymer network model (Figure 3.21) depicts how poly-SPB prevents protein denaturation. It shows the poly-SPB side chains interacting with the proteins stored in the dry microneedles (poly-Dex-GMA) by charge interaction. This result aligns well with our previous reports, which suggest that the presence of poly-SPB protects proteins from denaturation under different conditions.[9,12,13,17,53,54] Thus, the Dex-GMA/SPB/AAc hydrogels can maintain enzyme activity more efficiently than the Dex-GMA/AAc hydrogel, probably due to the presence of poly-SPB.

Furthermore, the amyloid fibril formation of human insulin was measured by ThT assay. Thioflavin T selectively binds to the amyloid fibrils formed during the protein denaturation process.[55] Formation of fibrils on heating results in an increase in the fluorescence intensity of ThT. The releases of human insulin from Dex-

GMA/AAc and Dex-GMA/SPB/AAc polymers after incubation at 45 °C for 3 days in the dry condition show a decrease in ThT fluorescence intensity compared with the dry that of human insulin incubated solely in PBS. As shown in Figure 3.22, the amount of aggregation (% aggregation) was calculated using the difference in fluorescence intensity of denatured protein with that of the native human insulin. These results indicate that the human insulin-loaded Dex-GMA/AAc and Dex-GMA/SPB/AAc could effectively suppress the formation of fibrils in human insulin by suppressing aggregation, even under the dry condition and high-temperature condition that presented only 25% and 20% aggregation, respectively. In the heated condition, the SPB side chain in the polymer imparts higher efficiency than Dex-GMA/AAc polymer, which also corresponds well with the results obtained with the LDH residual activity study.

In addition, owing to lower protein aggregation, drug delivery via the Dex-GMA/SPB/AAc microneedle can achieve the same efficiency with a lower amount of drug than other types of microneedles. In turn, microneedle-based drug delivery will increase the efficiency of TDDSs.

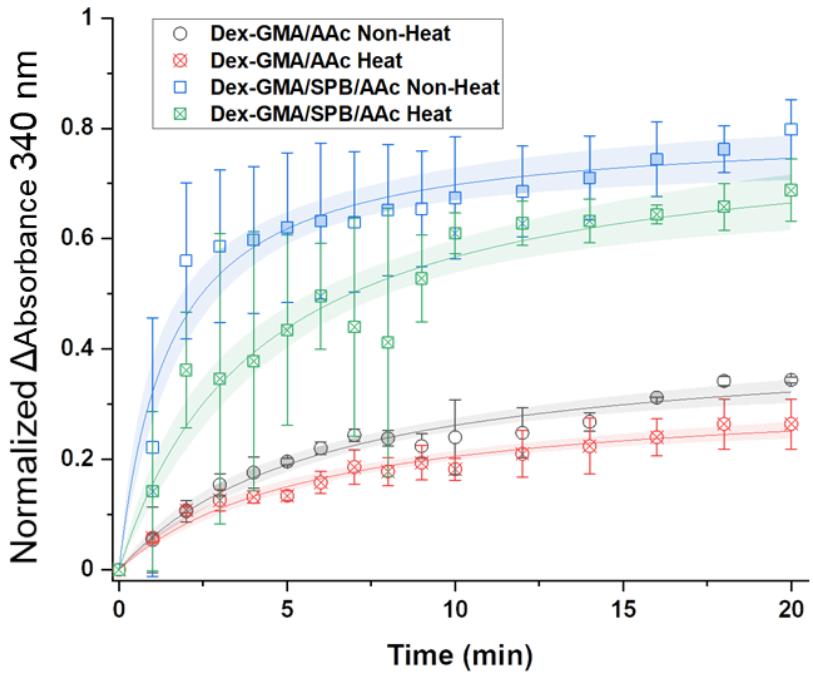

Figure 3.20 Change in absorbance at 340 nm due to reduction of NADH to NAD^+ after being released from the polymers (shaded colors represent 95% confidence band)

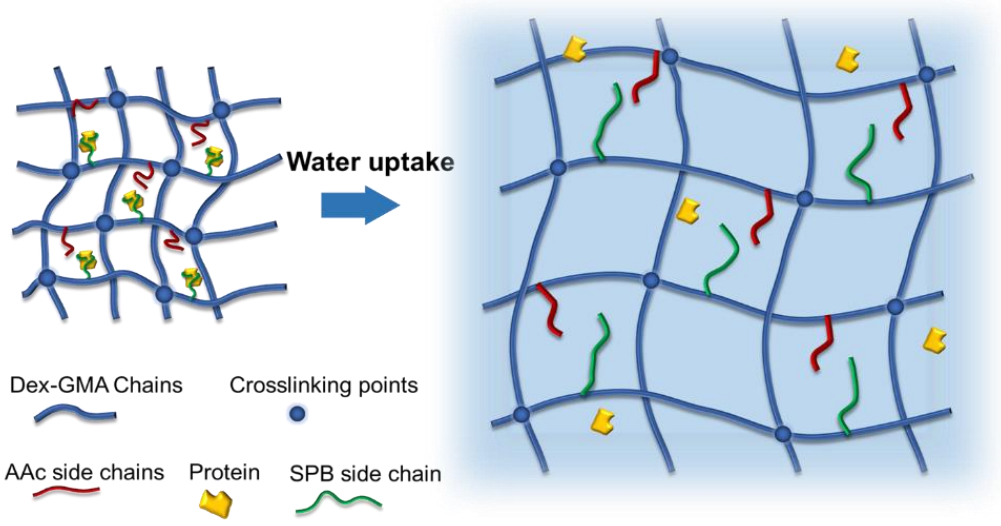

Figure 3.21 The model of polymer structure loaded proteins (pH 7) of dry microneedle and hydrogel microneedle

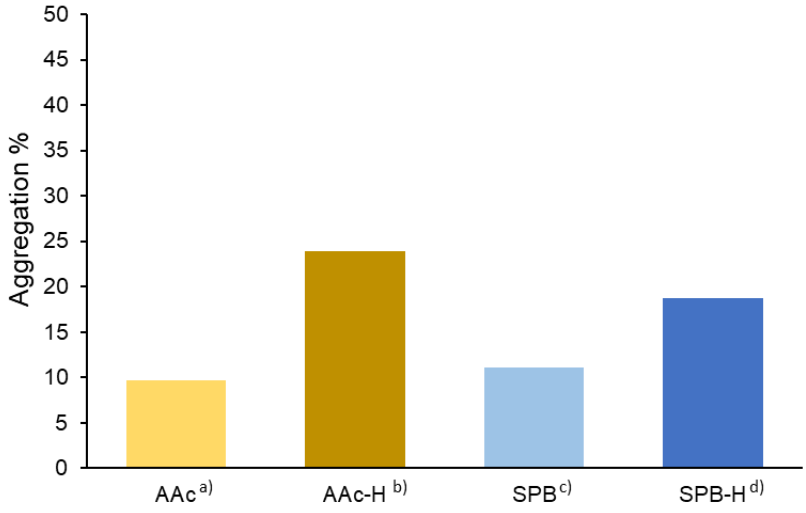

a) Dex-GMA/AAc non-heated; b) Dex-GMA/AAc heated; c) Dex-GMA/SPB/AAc non-heated; d) Dex-GMA/SPB/AAc heated

Figure 3.22 Analysis of fibril formation of human insulin after release from polymers under heat at 45 °C for 3 days and without heat for 3 days determined by the ThT fluorescence assay.

3.3.12 Cytotoxicity Study

Figure 3.23 shows the cytotoxicity of the microneedle polymers, and the results clearly demonstrate that all extraction solutions of cured polymers have very low toxicity, even at the original extraction concentration (100%) of cured polymers. IC_{50} (the concentration at which 50% of the cells are killed) was not observed for any concentration in the extracted medium concentrations, with Dex-GMA/AAc/SPB showing the lowest toxicity. Therefore, the Dex-GMA/AAc/SPB polymer can be considered extremely biocompatible and safely used in living organisms for transdermal application. Moreover, the cytotoxicity of the residual monomer after UV irradiation was also examined. Figure 3.24 shows that the Dex-GMA monomer had very low toxicity, whereas the PEG-DA monomer presented high toxicity even at a very low concentration. Therefore, the residual of Dex-GMA microneedles left in the skin will not become toxic in the *in vitro* scale.

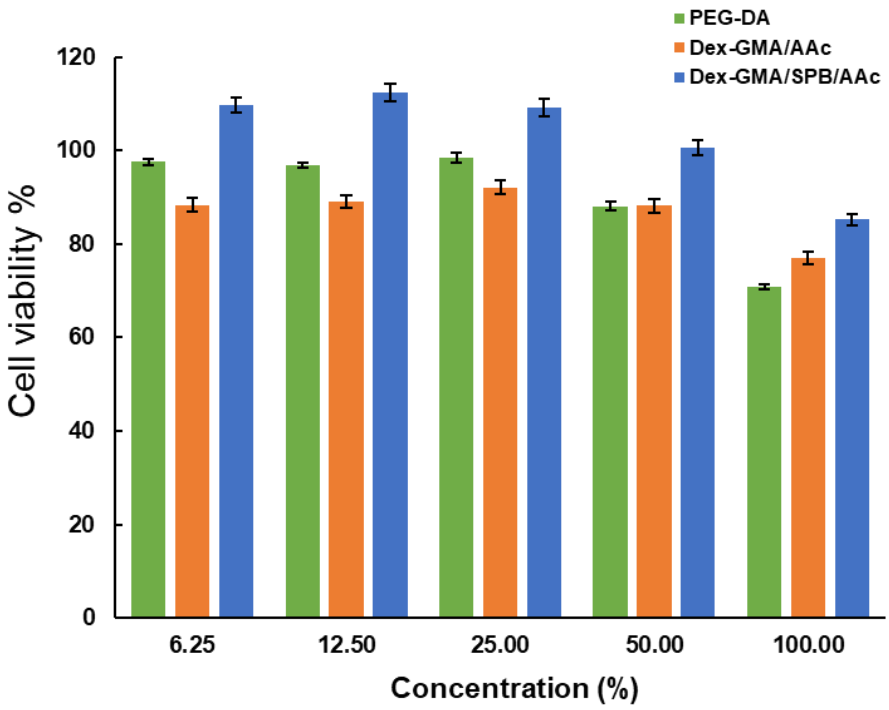

Figure 3.23 Cytotoxicity of the extraction solution from different polymers. L929 cells were treated with a series of dilutions from the original concentration with 100, 50, 25, 12.5, and 6.25%.

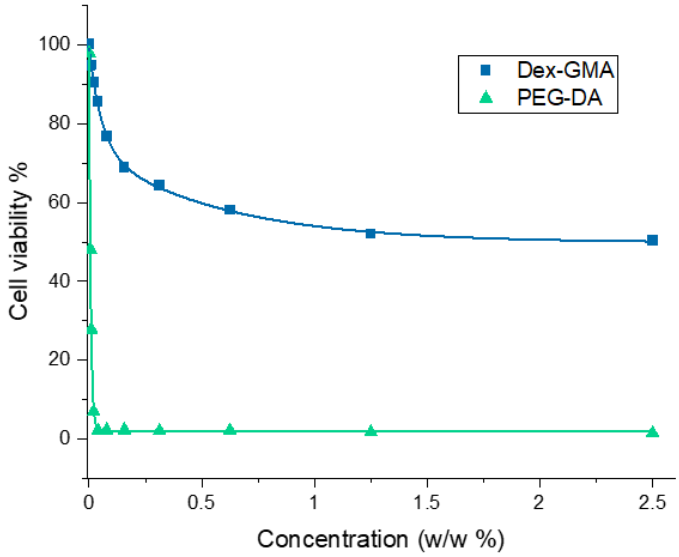

Figure 3.24 Cytotoxicity of Dex-GMA and PEG-DA monomer from different polymers concentrations. L929 cells were treated with a series of concentrations.

3.4 Conclusion

In summary, the microneedles were fabricated using a dextran-glycidyl methacrylate-based biomaterial through photolithography. The hydrogel microneedle array was created on a clear and flexible AESO sheet substrate that enables the microneedle patch to curve along the skin surface upon application, suggesting that it can be applied to any part of the body. Additionally, the drug cannot be absorbed by the substrate material. Reportedly, the photolithography method has not been used previously for zwitterionic polymer-based microneedle fabrication, which overcomes the limitations of other methods in terms of less equipment and fewer tools, a low-cost set-up, and only a 5 min fabrication process. The Dex-GMA/SPB/AAc microneedles presented a higher mechanical strength than PEG-DA, and the skin penetration performance was outstanding because of the sharpness of the tips and the thin wings formed by the four-point star-shaped microneedles.

The hydrogel microneedles with sulfobetaine side chains are suitable for biopharmaceutical transdermal drug delivery, particularly protein-based drugs with improved bioavailability. The microneedles exhibited high drug loading capacity, efficient drug release, and protein preservation by suppressing aggregation.

Moreover, the developed microneedles are capable of loading and preserving different water-soluble drugs and proteins simultaneously, even under physical and chemical stress. Additional experiments can be performed to incorporate different monomers in the hydrogel such that the rate of drug release can be better regulated. Thus, our system can be used to safely deliver therapeutic proteins in their native state instead of using hypodermic needles that are painful and inconvenient. Furthermore, unlike hypodermic needles that require a trained professional to administer drugs, these microneedles can be used by an untrained person. The

technique can also be adapted to efficiently deliver sensitive therapeutic drugs or vaccines.

3.5 References

[1] N. Dabholkar, S. Gorantla, T. Waghule, V.K. Rapalli, A. Kothuru, S. Goel, G. Singhvi, Biodegradable microneedles fabricated with carbohydrates and proteins: Revolutionary approach for transdermal drug delivery, Int. J. Biol. Macromol. 170 (2021) 602–621. https://doi.org/10.1016/j.ijbiomac.2020.12.177.

[2] S. Zhang, P. Xin, Q. Ou, G. Hollett, Z. Gu, J. Wu, Poly(ester amide)-based hybrid hydrogels for efficient transdermal insulin delivery, J. Mater. Chem. B. 6 (2018) 6723–6730. https://doi.org/10.1039/C8TB01466C.

[3] R. Ye, J. Yang, Y. Li, Y. Zheng, J. Yang, Y. Li, B. Liu, L. Jiang, Fabrication of Tip-Hollow and Tip-Dissolvable Microneedle Arrays for Transdermal Drug Delivery, ACS Biomater. Sci. Eng. 6 (2020) 2487–2494. https://doi.org/10.1021/acsbiomaterials.0c00120.

[4] M.R. Prausnitz, Engineering Microneedle Patches for Vaccination and Drug Delivery to Skin, Annu. Rev. Chem. Biomol. Eng. 8 (2017) 177–200. https://doi.org/10.1146/annurev-chembioeng-060816-101514.

[5] J. Yu, J. Wang, Y. Zhang, G. Chen, W. Mao, Y. Ye, A.R. Kahkoska, J.B. Buse, R. Langer, Z. Gu, Glucose-responsive insulin patch for the regulation of blood glucose in mice and minipigs, Nat. Biomed. Eng. 4 (2020) 499–506. https://doi.org/10.1038/s41551-019-0508-y.

[6] M. Zheng, Z. Wang, H. Chang, L. Wang, S.W.T. Chew, D.C.S. Lio, M. Cui, L. Liu, B.C.K. Tee, C. Xu, Osmosis-Powered Hydrogel Microneedles for Microliters of Skin Interstitial Fluid Extraction within Minutes, Adv. Healthc. Mater. 9 (2020). https://doi.org/10.1002/adhm.201901683.

[7] S. Yang, F. Wu, J. Liu, G. Fan, W. Welsh, H. Zhu, T. Jin, Phase-Transition Microneedle

Patches for Efficient and Accurate Transdermal Delivery of Insulin, Adv. Funct. Mater. 25 (2015) 4633–4641. https://doi.org/10.1002/adfm.201500554.

[8] Z. Chen, H. Li, Y. Bian, Z. Wang, G. Chen, X. Zhang, Y. Miao, D. Wen, J. Wang, G. Wan, Y. Zeng, P. Abdou, J. Fang, S. Li, C.-J. Sun, Z. Gu, Bioorthogonal catalytic patch, Nat. Nanotechnol. (2021). https://doi.org/10.1038/s41565-021-00910-7.

[9] R. Rajan, S. Ahmed, N. Sharma, N. Kumar, A. Debas, K. Matsumura, Review of the current state of protein aggregation inhibition from a materials chemistry perspective: special focus on polymeric materials, Mater. Adv. (2021).

[10] J.R. Brennan, S.S.P. Gebhart, W.G. Blackard, Pump-induced Insulin Aggregation: A Problem with the Biostator, Diabetes. 34 (1985) 353–359. https://doi.org/10.2337/diab.34.4.353.

[11] A.B. Caballero, P. Gamez, Nanochaperone-Based Strategies to Control Protein Aggregation Linked to Conformational Diseases, Angew. Chemie - Int. Ed. 60 (2021) 41–52. https://doi.org/10.1002/anie.202007924.

[12] R. Rajan, Y. Suzuki, K. Matsumura, Zwitterionic Polymer Design that Inhibits Aggregation and Facilitates Insulin Refolding: Mechanistic Insights and Importance of Hydrophobicity, Macromol. Biosci. 18 (2018) 1–6. https://doi.org/10.1002/mabi.201800016.

[13] R. Rajan, K. Matsumura, A zwitterionic polymer as a novel inhibitor of protein aggregation, J. Mater. Chem. B. 3 (2015) 5683–5689. https://doi.org/10.1039/c5tb01021g.

[14] P. Zhang, F. Sun, C. Tsao, S. Liu, P. Jain, A. Sinclair, H.C. Hung, T. Bai, K. Wu, S. Jiang, Zwitterionic gel encapsulation promotes protein stability, enhances pharmacokinetics, and reduces immunogenicity, Proc. Natl. Acad. Sci. U. S. A. 112 (2015) 12046–12051. https://doi.org/10.1073/pnas.1512465112.

[15] R.G. Laughlin, Fundamentals of the Zwitterionic Hydrophilic Group, Langmuir. 7 (1991) 842–847. https://doi.org/10.1021/la00053a006.

[16] C.J. Huang, Y. Li, S. Jiang, Zwitterionic polymer-based platform with two-layer architecture for ultra low fouling and high protein loading, Anal. Chem. 84 (2012) 3440–3445. https://doi.org/10.1021/ac3003769.

[17] N. Sharma, R. Rajan, S. Makhaik, K. Matsumura, Comparative Study of Protein Aggregation Arrest by Zwitterionic Polysulfobetaines : Using Contrasting Raft Agents, ACS Omega. 4 (2019) 12186–12193. https://doi.org/10.1021/acsomega.9b01409.

[18] T. Matsuda, J. Nagase, A. Ghoda, Y. Hirano, S. Kidoaki, Y. Nakayama, Phosphorylcholine-endcapped oligomer and block co-oligomer and surface biological reactivity, Biomaterials. 24 (2003) 4517–4527. https://doi.org/10.1016/S0142-9612(03)00344-2.

[19] Y. Chang Chung, Y. Hong Chiu, Y. Wei Wu, Y. Tai Tao, Self-assembled biomimetic monolayers using phospholipid-containing disulfides, Biomaterials. 26 (2005) 2313–2324. https://doi.org/10.1016/j.biomaterials.2004.06.043.

[20] A.R. Johnson, A.T. Procopio, Low cost additive manufacturing of microneedle masters, 3D Print. Med. 5 (2019) 2. https://doi.org/10.1186/s41205-019-0039-x.

[21] L. Barnum, J. Quint, H. Derakhshandeh, M. Samandari, F. Aghabaglou, A. Farzin, L. Abbasi, S. Bencherif, A. Memic, P. Mostafalu, A. Tamayol, 3D-Printed Hydrogel-Filled Microneedle Arrays, Adv. Healthc. Mater. 10 (2021) 1–12. https://doi.org/10.1002/adhm.202001922.

[22] J. Lim, D. Tahk, J. Yu, D.H. Min, N.L. Jeon, Design rules for a tunable merged-tip microneedle, Microsystems Nanoeng. 4 (2018). https://doi.org/10.1038/s41378-018-0028-z.

[23] C.W. Lo, H. Jiang, Photopatterning and degradation study of dextran-glycidyl

methacrylate hydrogels, Polym. Eng. Sci. 50 (2010) 232–239. https://doi.org/10.1002/pen.21531.

[24] P. Nonsuwan, K. Matsumura, Amino-Carrageenan@Polydopamine Microcomposites as Initiators for the Degradation of Hydrogel by near-Infrared Irradiation for Controlled Drug Release, ACS Appl. Polym. Mater. 1 (2019) 286–297. https://doi.org/10.1021/acsapm.8b00209.

[25] P. Nonsuwan, A. Matsugami, F. Hayashi, S.H. Hyon, K. Matsumura, Controlling the degradation of an oxidized dextran-based hydrogel independent of the mechanical properties, Carbohydr. Polym. 204 (2019) 131–141. https://doi.org/10.1016/j.carbpol.2018.09.081.

[26] M.M. Bradford, A rapid and sensitive method for the quantitation of microgram quantities of protein utilizing the principle of protein-dye binding, Anal. Biochem. 72 (1976) 248–254. https://doi.org/10.1016/0003-2697(76)90527-3.

[27] B. Sarmento, A. Ribeiro, F. Veiga, D. Ferreira, Development and characterization of new insulin containing polysaccharide nanoparticles, Colloids Surfaces B Biointerfaces. 53 (2006) 193–202. https://doi.org/10.1016/j.colsurfb.2006.09.012.

[28] M. Torkzadeh-Mahani, M. Zaboli, M. Barani, M. Torkzadeh-Mahani, A combined theoretical and experimental study to improve the thermal stability of recombinant D-lactate dehydrogenase immobilized on a novel superparamagnetic Fe3O4NPs@metal–organic framework, Appl. Organomet. Chem. 34 (2020) 1–17. https://doi.org/10.1002/aoc.5581.

[29] R.E. Vanderlinde, Measurement of Total Lactate Dehydrogenase Activity, Ann. Clin. Lab. Sci. 15 (1985) 13–31.

[30] J.J.Holbrook et al, Lactate Dehydrogenase, Enzym. 11 (1975) 191.

[31] J.S. Koo, J.R. Cha, S.H. Oh, M.S. Gong, Preparation of sulfobetaine chitosan, silk

blended films, and their properties, Polym. 38 (2014) 54–61. https://doi.org/10.7317/pk.2014.38.1.54.

[32] S.H. Bariya, M.C. Gohel, T.A. Mehta, O.P. Sharma, Microneedles: An emerging transdermal drug delivery system, J. Pharm. Pharmacol. 64 (2012) 11–29. https://doi.org/10.1111/j.2042-7158.2011.01369.x.

[33] M. Khiao In, K.C. Richardson, A. Loewa, S. Hedtrich, S. Kaessmeyer, J. Plendl, Histological and functional comparisons of four anatomical regions of porcine skin with human abdominal skin, J. Vet. Med. Ser. C Anat. Histol. Embryol. 48 (2019) 207–217. https://doi.org/10.1111/ahe.12425.

[34] Y. Gao, M. Hou, R. Yang, L. Zhang, Z. Xu, Y. Kang, P. Xue, PEGDA/PVP Microneedles with Tailorable Matrix Constitutions for Controllable Transdermal Drug Delivery, Macromol. Mater. Eng. 303 (2018) 1–12. https://doi.org/10.1002/mame.201800233.

[35] Y. Gao, M. Hou, R. Yang, L. Zhang, Z. Xu, Y. Kang, P. Xue, Highly Porous Silk Fibroin Scaffold Packed in PEGDA/Sucrose Microneedles for Controllable Transdermal Drug Delivery, Biomacromolecules. 20 (2019) 1334–1345. https://doi.org/10.1021/acs.biomac.8b01715.

[36] R.F. Donnelly, M.T.C. McCrudden, A.Z. Alkilani, E. Larrañeta, E. McAlister, A.J. Courtenay, M.C. Kearney, T.R. Raj Singh, H.O. McCarthy, V.L. Kett, E. Caffarel-Salvador, S. Al-Zahrani, A.D. Woolfson, Hydrogel-forming microneedles prepared from “super swelling” polymers combined with lyophilised wafers for transdermal drug delivery, PLoS One. 9 (2014). https://doi.org/10.1371/journal.pone.0111547.

[37] S.S. Huang, H. Liu, S.S. Huang, T. Fu, W. Xue, R. Guo, Dextran methacrylate hydrogel microneedles loaded with doxorubicin and trametinib for continuous transdermal administration of melanoma, Carbohydr. Polym. 246 (2020) 116650. https://doi.org/10.1016/j.carbpol.2020.116650.

[38] Z. Zeng, G. Jiang, T. Liu, G. Song, Y. Sun, X. Zhang, Y. Jing, M. Feng, Y. Shi, Fabrication of gelatin methacryloyl hydrogel microneedles for transdermal delivery of metformin in diabetic rats, Bio-Design Manuf. (2021). https://doi.org/10.1007/s42242-021-00140-9.

[39] S. Fakhraei Lahiji, Y. Jang, Y. Ma, M. Dangol, H. Yang, M. Jang, H. Jung, Effects of dissolving microneedle fabrication parameters on the activity of encapsulated lysozyme, Eur. J. Pharm. Sci. 117 (2018) 290–296. https://doi.org/10.1016/j.ejps.2018.03.003.

[40] D.F.S. Fonseca, P.C. Costa, I.F. Almeida, P. Dias-Pereira, I. Correia-Sá, V. Bastos, H. Oliveira, C. Vilela, A.J.D. Silvestre, C.S.R. Freire, Swellable Gelatin Methacryloyl Microneedles for Extraction of Interstitial Skin Fluid toward Minimally Invasive Monitoring of Urea, Macromol. Biosci. 20 (2020) 1–11. https://doi.org/10.1002/mabi.202000195.

[41] W. Yao, D. Li, Y. Zhao, Z. Zhan, G. Jin, H. Liang, 3D Printed Multi-Functional Hydrogel Microneedles Based on High-Precision Digital Light Processing, (n.d.).

[42] H. Cruz, B. Laycock, E. Strounina, T. Seviour, A. Oehmen, I. Pikaar, Modified Poly(acrylic acid)-Based Hydrogels for Enhanced Mainstream Removal of Ammonium from Domestic Wastewater, Environ. Sci. Technol. 54 (2020) 9573–9583. https://doi.org/10.1021/acs.est.9b07032.

[43] T. Waghule, G. Singhvi, S.K. Dubey, M.M. Pandey, G. Gupta, M. Singh, K. Dua, Microneedles: A smart approach and increasing potential for transdermal drug delivery system, Biomed. Pharmacother. 109 (2019) 1249–1258. https://doi.org/10.1016/j.biopha.2018.10.078.

[44] S. Paik, S. Byun, J. Lim, Y. Park, A. Lee, S. Chung, J. Chang, K. Chun, D. Dan, In-plane single-crystal-silicon microneedles for minimally invasive microfluid systems, 114 (2004) 276–284. https://doi.org/10.1016/j.sna.2003.12.029.

[45] M.A. Lopez-Ramirez, F. Soto, C. Wang, R. Rueda, S. Shukla, C. Silva-Lopez, D. Kupor, D.A. McBride, J.K. Pokorski, A. Nourhani, N.F. Steinmetz, N.J. Shah, J. Wang, Built-In Active Microneedle Patch with Enhanced Autonomous Drug Delivery, Adv. Mater. 32 (2020) 1–10. https://doi.org/10.1002/adma.201905740.

[46] X. Ning, C. Wiraja, D. Chin, S. Lio, C. Xu, A Double-Layered Microneedle Platform Fabricated through Frozen Spray-Coating, 2000147 (2020) 1–9. https://doi.org/10.1002/adhm.202000147.

[47] D. Han, R.S. Morde, S. Mariani, A.A. La Mattina, E. Vignali, C. Yang, G. Barillaro, H. Lee, 4D Printing of a Bioinspired Microneedle Array with Backward-Facing Barbs for Enhanced Tissue Adhesion, Adv. Funct. Mater. 30 (2020). https://doi.org/10.1002/adfm.201909197.

[48] E.M. Saurer, R.M. Flessner, S.P. Sullivan, M.R. Prausnitz, D.M. Lynn, Layer-by-layer assembly of DNA- and protein-containing films on microneedles for drug delivery to the skin, Biomacromolecules. 11 (2010) 3136–3143. https://doi.org/10.1021/bm1009443.

[49] J.S. Kochhar, S. Zou, S.Y. Chan, L. Kang, Protein encapsulation in polymeric microneedles by photolithography, Int. J. Nanomedicine. 7 (2012) 3143–3154. https://doi.org/10.2147/IJN.S32000.

[50] E. Proksch, pH in nature, humans and skin, J. Dermatol. 45 (2018) 1044–1052. https://doi.org/10.1111/1346-8138.14489.

[51] S.M. Ali, G. Yosipovitch, Skin pH: From basic science to basic skin care, Acta Derm. Venereol. 93 (2013) 261–267. https://doi.org/10.2340/00015555-1531.

[52] Y. Marunaka, Roles of interstitial fluid pH in diabetes mellitus: Glycolysis and mitochondrial function, World J. Diabetes. 6 (2015) 125. https://doi.org/10.4239/wjd.v6.i1.125.

[53] H. Takahashi, T. Kan, G. Lee, N. Dönmez, J. Kim, J. Park, D. Kim, Y.J. Heo, Self-focusing 3D lithography with varying refractive index polyethylene glycol diacrylate, Appl. Phys. Express. 13 (2020). https://doi.org/10.35848/1882-0786/ab9ba3.

[54] D. Zhao, R. Rajan, K. Matsumura, Dual Thermo- And pH-Responsive Behavior of Double Zwitterionic Graft Copolymers for Suppression of Protein Aggregation and Protein Release, ACS Appl. Mater. Interfaces. 11 (2019) 39459–39469. https://doi.org/10.1021/acsami.9b12723.

[55] M. Biancalana, S. Koide, Molecular mechanism of Thioflavin-T binding to amyloid fibrils, Biochim. Biophys. Acta - Proteins Proteomics. 1804 (2010) 1405–1412. https://doi.org/10.1016/j.bbapap.2010.04.001.

Chapter 4: General Conclusion

Regarding the objective of this research, the main goal is to make the microneedle suitable for industrial scale, and the microneedle itself performs the high drug loading capacity, high-efficiency drug release, and inhibits protein aggregation. Chapter 2 shows successfully fabricating microneedle by the photolithography method, which overcomes the limitation of other fabrication methods.[1–10] It takes less than 5 minutes for each fabrication process. Furthermore, the microneedle's length and shape can be controlled by very time UV irradiation and the pattern micro-windows on the photomask. Four-point star-shaped microneedles are fabricated via a photolithography process, and sulfobetaine (SPB) monomer is combined with dextran-glycidyl methacrylate/acrylic acid (Dex-GMA/AAc) to form the hydrogel network. The toxicity study shows that the Dex-GMA/AAc/SPB polymer can be considered as extremely biocompatible. The microneedle has a good aspect ratio related to the drug loading capacity. There are covalent bindings between hydrogel microneedle and AESO substrate. Microneedle’s substrate shows a clear and flexible property and non-absorb drug during the drug loading process; when the microneedle patch is applied to the skin, it also curves along the surface, demonstrating its ability to be easy to apply to any body part.

The rhodamine B drug loading and releasing models show that the microneedle can load drug up to 8μg on one microneedle patch and release up to 80% of loading with only 41 needles in 6h. The microneedle has potential for chemotherapeutic agents such as gemcitabine[11], donepezil hydrochloride (DPH) used for the treatment of Alzheimer's disease[12] and doxorubicin[1][2] according to having a greater loading and releasing efficiency in microneedle applications. In chapter 3, the Dextran-FITC drug model represents

that the molecular drug weight lower than 10 kDa can absorb/diffuse into the center of the microneedle. The Dextran-FITC showed a fast release and diffusion into the artificial skin in a short period.

The protein delivery shows some limitation of protein loading and releasing at low pH, but at pH 7.4, protein releases show higher efficiency suitable for transdermal drug delivery, owing to the presence of pH 7.4 in the interstitial fluid.[13] It can increase the drug doses by longer time loading and the number of needles per patch. LDH enzyme activity study illustrates that the poly-SPB side chains in the Dex-GMA/SPB/AAc hydrogel inhibit protein aggregation according to having a higher enzyme kinetic activity than Dex-GMA/AAc hydrogel that do not have the poly-SPB side chains even under external physics stress (45°C for 1 h), releases the proteins in their native state (without activity loss). In addition, ThT assay determining the fibril formation in human insulin indicates that the human insulin-loaded Dex-GMA/AAc and Dex-GMA/SPB/AAc effectively suppress the formation of fibrils in human insulin under the dry condition and high-temperature (45 °C for 3) condition that presented only 25% and 20% aggregation, respectively. The combination of hydrogel microneedle and poly-SPB side chains has a potential for biopharmaceutical transdermal drug delivery, especially protein base drug that increases the efficiency bioavailability.

Further research is warranted to control the incorporation of different monomers in the hydrogel, which would enable greater control over the rate of drug release and may be used to deliver several therapeutic drugs and can even be used to deliver vaccines efficiently.

References

[1] S. Bhatnagar, N.G. Bankar, M.V. Kulkarni, V.V.K. Venuganti, Dissolvable microneedle patch containing doxorubicin and docetaxel is effective in 4T1 xenografted breast cancer mouse model, Int. J. Pharm. 556 (2019) 263–275. https://doi.org/10.1016/j.ijpharm.2018.12.022.

[2] S.S. Huang, H. Liu, S.S. Huang, T. Fu, W. Xue, R. Guo, Dextran methacrylate hydrogel microneedles loaded with doxorubicin and trametinib for continuous transdermal administration of melanoma, Carbohydr. Polym. 246 (2020) 116650. https://doi.org/10.1016/j.carbpol.2020.116650.

[3] M.A. Lopez-Ramirez, F. Soto, C. Wang, R. Rueda, S. Shukla, C. Silva-Lopez, D. Kupor, D.A. McBride, J.K. Pokorski, A. Nourhani, N.F. Steinmetz, N.J. Shah, J. Wang, Built-In Active Microneedle Patch with Enhanced Autonomous Drug Delivery, Adv. Mater. 32 (2020) 1–10. https://doi.org/10.1002/adma.201905740.

[4] M. Wang, L. Hu, C. Xu, Recent advances in the design of polymeric microneedles for transdermal drug delivery and biosensing, Lab Chip. 17 (2017) 1373–1387. https://doi.org/10.1039/C7LC00016B.

[5] K. Lee, H. Jung, Drawing lithography for microneedles: A review of fundamentals and biomedical applications, Biomaterials. 33 (2012) 7309–7326. https://doi.org/10.1016/j.biomaterials.2012.06.065.

[6] J.D. Kim, M. Kim, H. Yang, K. Lee, H. Jung, Droplet-born air blowing: Novel dissolving microneedle fabrication, J. Control. Release. 170 (2013) 430–436. https://doi.org/10.1016/j.jconrel.2013.05.026.

[7] A.R. Johnson, A.T. Procopio, Low cost additive manufacturing of microneedle masters, 3D Print. Med. 5 (2019). https://doi.org/10.1186/s41205-019-0039-x.

[8] H. Takahashi, Y.J. Heo, N. Arakawa, T. Kan, K. Matsumoto, R. Kawano, I. Shimoyama, Scalable fabrication of microneedle arrays via spatially controlled UV exposure, Microsystems Nanoeng. 2 (2016) 1–5. https://doi.org/10.1038/micronano.2016.49.

[9] H. Takahashi, T. Kan, G. Lee, N. Dönmez, J. Kim, J. Park, D. Kim, Y.J. Heo, Self-focusing 3D lithography with varying refractive index polyethylene glycol diacrylate, Appl. Phys. Express. 13 (2020). https://doi.org/10.35848/1882-0786/ab9ba3.

[10] W.G. Bae, H. Ko, J.Y. So, H. Yi, C.H. Lee, D.H. Lee, Y. Ahn, S.H. Lee, K. Lee, J. Jun, H.H. Kim, N.L. Jeon, W. Jung, C.S. Song, T. Kim, Y.C. Kim, H.E. Jeong, Snake fang-inspired stamping patch for transdermal delivery of liquid formulations, Sci. Transl. Med. (2019). https://doi.org/10.1126/scitranslmed.aaw3329.

[11] S. Bhatnagar, P. Kumari, S.P. Pattarabhiran, V.V.K. Venuganti, Zein Microneedles for Localized Delivery of Chemotherapeutic Agents to Treat Breast Cancer: Drug Loading, Release Behavior, and Skin Permeation Studies, AAPS PharmSciTech. 19 (2018) 1818–1826. https://doi.org/10.1208/s12249-018-1004-5.

[12] J.Y. Kim, M.R. Han, Y.H. Kim, S.W. Shin, S.Y. Nam, J.H. Park, Tip-loaded dissolving microneedles for transdermal delivery of donepezil hydrochloride for treatment of Alzheimer's disease, Eur. J. Pharm. Biopharm. 105 (2016) 148–155. https://doi.org/10.1016/j.ejpb.2016.06.006.

[13] Y. Marunaka, Roles of interstitial fluid pH in diabetes mellitus: Glycolysis and mitochondrial function, World J. Diabetes. 6 (2015) 125. https://doi.org/10.4239/wjd.v6.i1.125.

Achievements

Journal publications

1. H. Pitakjakpipop, R. Rajan, K. Tantisantisom, P. Opaprakasit , D. D. Nguyen, V. A. Ho, K. Matsumura, P. Khanchaitit, Facile Photolithographic Fabrication of Zwitterionic Polymer Microneedle with Protein Aggregation Inhibition for Transdermal Drug Delivery, Biomacromolecules, 2022, 23, 1, 365–376

Others Journal publications

1. Golas, H. Pitakjakpipop, M.S. Rahn, C.A. Siedlecki, E.A. Vogler, Enzymes produced by autoactivation of blood factor XII in buffer. A contribution from the Hematology at Biomaterial Interfaces Research Group, Biomaterials.37 (2015)1–12.
2. A. Golas, C.H. Josh Yeh, H. Pitakjakpipop, C.A. Siedlecki, E.A. Vogler, A comparison of blood factor XII autoactivation in buffer, protein cocktail, serum, and plasma solutions, Biomaterials. 34 (2013) 607–620.

Conferences:

1. Poster : "*Degradable oxidation dextran-base hydrogel with Amino-Carrageenan Polydopamine microneedle polymer for Controlling transdermal insulin delivery*" H. Pitakjakpipop, K. Matsumura. 68th symposium on macromolecules 2019 and gel symposium, (SPSJ). Fukui University, Fukui. September 25-28, 2019.
2. Oral : "*A photolithographic fabrication of dextran-based zwitterionic polymer microneedle: protein aggregation inhibition for transdermal drug delivery*." H. Pitakjakpipop, R. Rajan, P. Opaprakasit, K. Tantisantisom, P. Khanchaitit, K. Matsumura, The 10th Japanese Society for Biomaterials Hokuriku Shinetsu (2021).
3. Poster: : " *A protein aggregation inhibition microneedle for transdermal drug delivery via dextran-based zwitterionic polymer.* " H. Pitakjakpipop, R. Rajan, P. Opaprakasit, P. Khanchaitit, K. Matsumura. The 43rd Annual Meeting of the Japanese Society for Biomaterials and the 8th Asian Biomaterials Congress (2021).

Acknowledgment

Firstly, I would like to thank my supervisor, Prof. Kazuaki Matsumura, for all support, education, supervision, guidance, funding, and motivation during my study at JAIST. It is a great honor for me to be a part of Matsumura's laboratory from my heart. I appreciate all his time, academic activity, and non-academics, such as sports, parties, and camping. These experiences fully feel my Ph.D. experience in Japan. Without his supports, I would not have achieved this far, and this thesis would not have been completed.

I would like to thank the Assistant. Prof. Robin Rajan and Dr. Punnida Nonsuwan brought me to the polymer synthesis world. Dr. Rajan, especially, educated me not only on chemical synthesis and characterization techniques.

I would like to thank all my lab members in Matsumura's lab and NANOTEC's lab for encouraging, kindness, and support even though we are in a difficult situation (COVID 19).

I would like to thank dual degree program (SIIT-JAIST) Scholarships for financial support during my doctoral study. Without these facilities and sponsorship, I would not have been able to achieve and complete the program.

Finally, I gratefully thank my family, especially my wife, for always support, encourage, understanding, and cheer me up for all routes to this success.

Harit Pitakjakpipop